



# Towards the next generation of machine learning models in additive manufacturing: A review of process dependent material evolution



Mohammad Parsazadeh <sup>a</sup>, Shashank Sharma <sup>b</sup>, Narendra Dahotre <sup>a,b,\*</sup>

<sup>a</sup> Center for Agile and Adaptive Additive Manufacturing, University of North Texas, 3940 N ELM Street, Denton, TX 76207, USA

<sup>b</sup> Department of Materials Science & Engineering, University of North Texas, 3940 N ELM street, Denton, TX 76207, USA

## ARTICLE INFO

### Keywords:

Additive manufacturing  
Defect detection  
Physics informed machine learning  
Product quality  
Supervised learning  
Unsupervised learning

## ABSTRACT

Additive manufacturing facilitates producing of complex parts due to its design freedom in a wide range of applications. Despite considerable advancements in additive manufacturing techniques, 3D-printed parts are still suffering from durability, repeatability, and reliability. One main reason, which increases the complexity of the problem and causes defects during manufacturing, is the high number of processing parameters. Machine learning approaches seem to be a promising solution to tackle the challenges in the additive manufacturing field. This paper employs a systematic literature review by employing natural language processing and text mining techniques to analyze the recent advancement in the application of machine learning in porosity detection and prediction in 3D-printed parts. Two methods of text analytics are used to evaluate different avenues of research in additive manufacturing. Most frequent machine learning methods employed to evaluate the porosity formed in the 3D-printed parts are introduced and classified based on their applications. Recent advancements in developing hybrid machine learning models reveal the importance of physical domain knowledge (e.g., thermomechanical laws and constraints) in these models and their accuracy. Eventually, challenges and opportunities that exist for the next generation of machine learning techniques in the AM field are identified and summarized.

## 1. Introduction

### 1.1. Additive manufacturing

A group of track-by-track followed by layer-by-layer fabrication processes, which is now called additive manufacturing (AM), has had different names during the past 30 years. AM has evolved from rapid prototyping (RP) [1] and rapid tooling [2] methods to a technique employed for end-use parts. AM was also known as solid freeform fabrication (SFF) [3], 3D printing (3DP) [4], and rapid manufacturing (RM) [1]. AM, which was previously limited to prototype fabrication, is now capable of producing end-use metallic products [5]. AM has unique capabilities for building complex and customized one-of-a-kind parts (particularly in the aerospace [6] and biomedical industries [7]) from computer-aided design (CAD) [8] models. Compared to traditional manufacturing techniques, AM

\* Corresponding author at: Center for Agile and Adaptive Additive Manufacturing, University of North Texas, 3940 N ELM Street, Denton, TX 76207, USA.

E-mail address: [Narendra.Dahotre@unt.edu](mailto:Narendra.Dahotre@unt.edu) (N. Dahotre).

enables fabrication of intricate products with unique microstructure and material properties in a time-efficient and cost-effective way [9].

AM processes can be classified into 7 categories based on ASTM F42 [10]. The articles reviewed here fall into 3 classes of deposition techniques, namely powder bed fusion (PBF), directed energy deposition (DED), and material extrusion, as shown in Fig. 1. In the PBF process, the powder bed uniformly spread over the substrate is selectively melted by a laser or electron beam, which is used as the energy source [11]. In the DED process, the continuous powder stream or wire fed from the deposition nozzle is melted by a focused laser beam to fabricate an object [12]. In the PBF process, the laser speed is approximately one order of magnitude faster than that in DED and the melt pool dimensions are approximately one order of magnitude smaller than that found in the DED process [13]. In the materials extrusion process, the metal powder is mixed with a polymer binder, then the mixture is extruded through the nozzle layer-by-layer to fabricate a part [5,14].

There are many barriers that still restrict the widespread application of metal-based AM as a mainstream manufacturing method. A major challenge in the current additive manufacturing (AM) field is the inconsistency of the printed products (repeatability) [15–17]. Lack of standardization [18], process reliability, and part quality [19] are also other challenges in the AM field, which require more attention. These issues also affect the performance of the product [20,21]. To identify these technological obstacles and desired capabilities of AM, many recent road mapping efforts have been conducted [22,23]. However, a better understanding of AM manufacturing from design to production is still required.

Improving the reliability and part quality needs a deep understanding of defect formation during manufacturing. In one attempt by Qu et al. [24], nanoparticles were employed to eliminate the large spatters by controlling laser powder bed interaction instabilities. The elimination of large spatters led to a significant reduction of defects in the 3D-printed parts, though multiple pores were observed in the samples printed in their study. Pore formation can have two origins in the AM process. One originated from the powders (gas entrapment in powders) and another one could be originated from the AM processing conditions (oxidation during the AM process, hydrodynamics conditions, including capillary and wetting effects, etc. [25,26]) [27]. These processing conditions could be more than 130 parameters [28], which affect the final quality of the 3D-printed parts and make the design challenging [29]. Carefully designed experiments are one way to evaluate various parameters, (e.g., powder quality, beam power, layer thickness, laser speed, and scan speed) affecting the quality of 3D-printed parts.

## 1.2. Research strategy

One major challenge of AM field that is rich with data is to store and analyze the data. Among all the data-driven methods, machine learning (ML) models seem to be promising to predict and optimize the quality of 3D-printed materials. Recent signs of progress in employing ML to analyze the data in the AM field have been reviewed with a focus on introducing the concept of ML and the potential ML algorithms for solving the existing problems in the AM field [30], investigating shallow and deep learning-based methods for monitoring processing parameters [31], predicting quality of 3D-printed parts using supervised learning [32], summarizing the ML algorithms used for defect detection in the metal laser-based AM process [33], predicting fatigue life and fracture of 3D-printed parts [34], optimizing processing parameters and detecting anomalies, and designing for AM, property prediction and material analytics [35–38]. A few of these review papers [39] focused on the studies that implemented the laws of physics in developing ML models, but they are not covering a broad application of ML in the AM field. This review paper aims to conduct a systematic literature review to differentiate various ML approaches implemented to analyze the process-dependent material evolution, categorize the datatypes used to develop ML models in the AM field, summarize the studies that constrained their ML models by laws of physics, and discuss the challenges and opportunities in the AM field.

To review the ongoing research regarding the application of ML in AM, a systematic literature review [40] has been conducted with a focus on recent publications on physics-informed machine learning models. The overall structure of this review paper is indicated in Fig. 2. The methodology used to conduct this literature review is also indicated in Fig. 3. At first, the relevant publications to the scope of this review are selected based on their qualities, publication date, and keywords. The titles, abstracts, and keywords of the selected articles for review are extracted and stored separately to further analyze the selected documents using the natural language processing (NLP) [41] and text mining approaches. To do this, NLP with K-means clustering and text mining techniques of the co-occurrence network were employed to extract the hidden knowledge. Several preprocessing steps should be taken to transform the text data into a more suitable form for text mining machine learning. At first, the text is split into smaller groups called tokens, which form strings. Then, the tokens, having low values archived in the stopwords list [42] or manually identified were removed. The process of

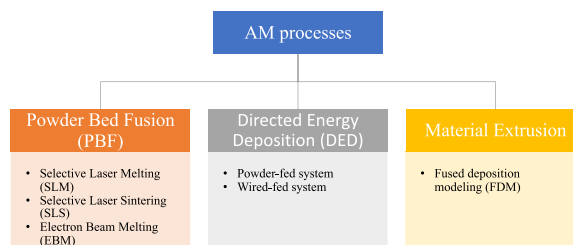


**Fig. 1.** AM processes in machine learning.

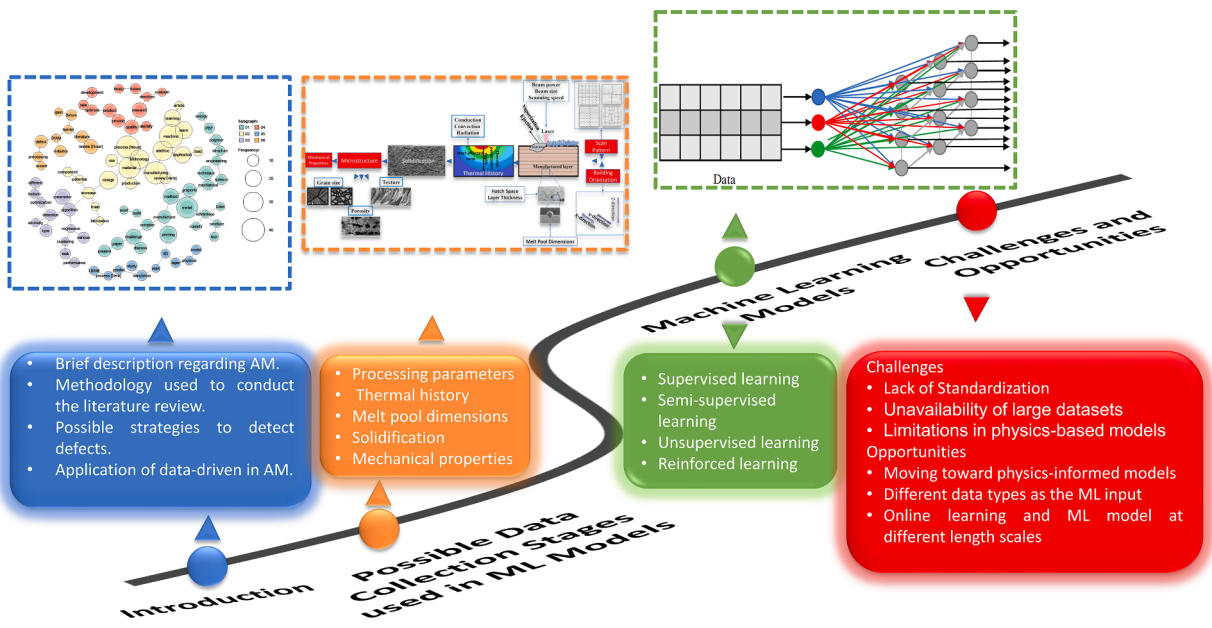


Fig. 2. Overall structure of this review paper.

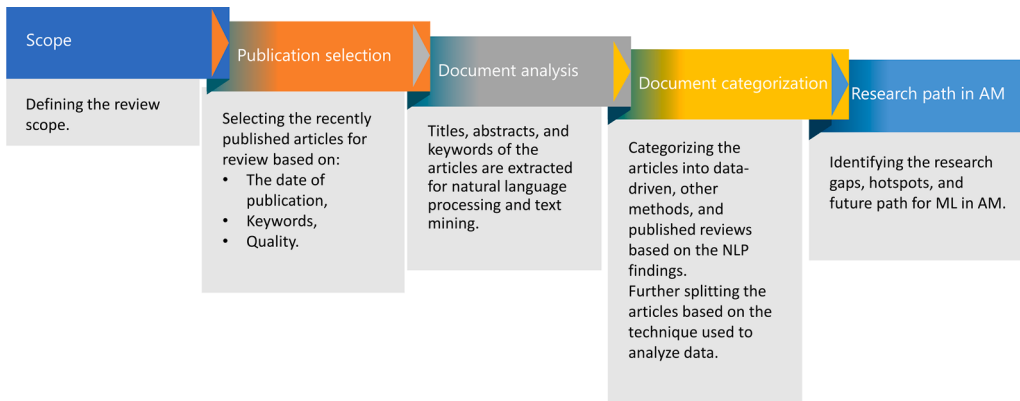
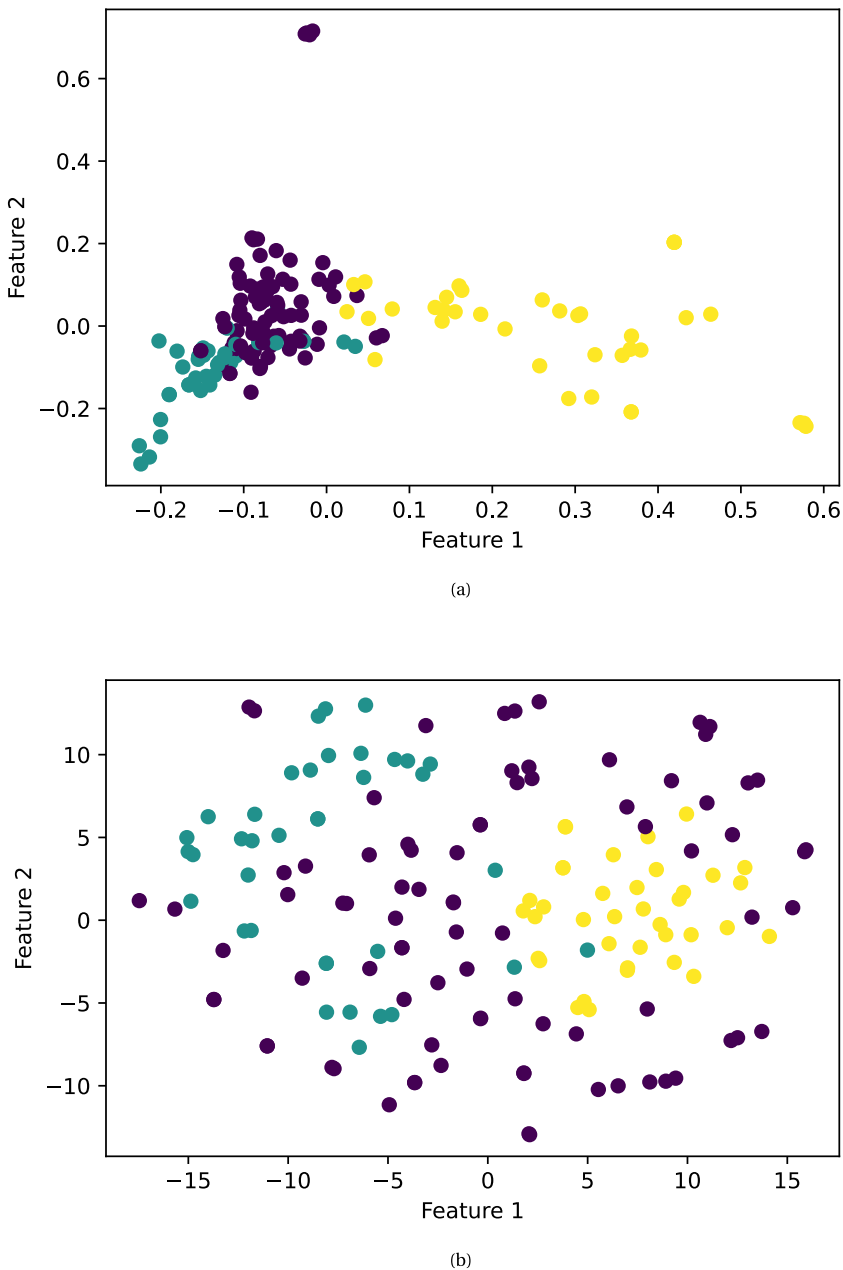


Fig. 3. Methodology used to conduct this literature review.

reducing the word into its base form (lemmatization) and additional filtering were conducted as the last step of preprocessing to improve the performance of text mining and NLP techniques. To convert text into a digestible form for machine learning, the term frequency-inverse document frequency (TF-IDF) [43] method was employed. TF-IDF is a weighting scheme that assigns higher weights to the words that are not commonly observed in a dataset but are repeated frequently in a few documents. The matrix created using the TF-IDF approach is fed into a K-means clustering algorithm. The number of clusters in the K-means algorithm was chosen based on the within-cluster sum of square (WCSS) and average silhouette score criteria [44]. The WCSS and silhouette calculate the compactness of clusters and the separation of the distance between clusters, respectively. The principal component analysis (PCA) and t-distributed Stochastic Neighbor Embedding (t-SNE) were also employed to transform the high-dimensional TF-IDF matrix [43] into two-dimensional representation, and the results of these two transformations are indicated in Fig. 4. The results indicated that PCA performed better than t-SNE regarding visualizing the clusters, as the clusters are not clearly differentiable in t-SNE. The natural language processing analysis indicates that the articles selected to review based on the criteria indicated in Fig. 3 can be classified into three categories, namely the papers employed experimental and physics-based approaches, the papers employed data-driven approaches, and the literature review papers published recently in the AM field. A part of these clusters overlapped, which means that both data-driven and physics-based models were used and discussed in these manuscripts.

As K-means clustering can only reveal the association between clusters of documents and fails to indicate the association between the words within a cluster, co-occurrence network [45] was applied to each cluster identified earlier as illustrated in Fig. 5. In the co-occurrence network, communities (or subgraphs) of words are formed among the words with strong co-occurrence. Dashed lines indicate the co-occurrence of words in different communities. Each community with enough nodes describes a storyline, and the

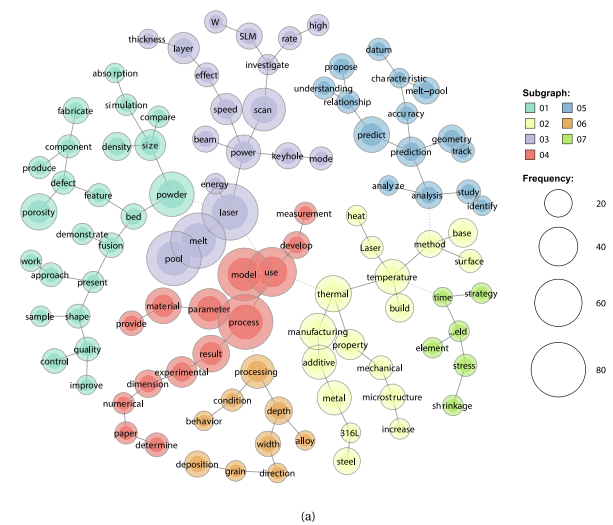


**Fig. 4.** Categorizing the articles reviewed in this paper using (a) PCA, (b) t-SNE.

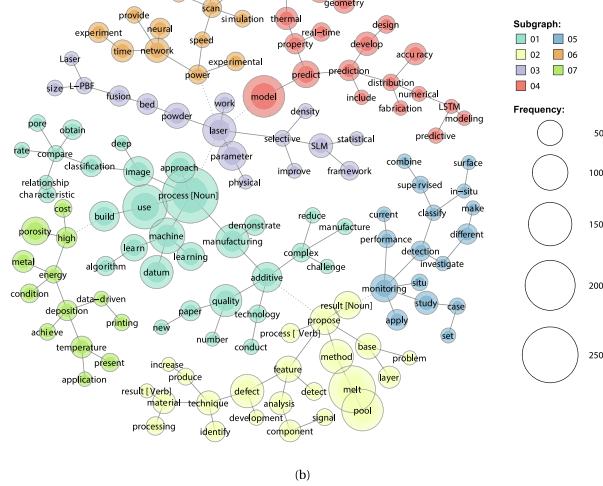
connected communities could be merged into one storyline. In Fig. 5a, the network structure in subgraph No. 1 (in cyan) can construct a field of research related to "defects" "demonstration" and "quality" "improvement" in "powder" "bed" "fusion", while the network structure in subgraph No. 3 (in purple) can construct a field of research related to the "effect" of "scan" "speed", "laser" "power", and "layer" "thickness" on "keyhole" and conduction "modes" in "melt" "pools". Similarly, subgraph 1 (in cyan) anecdotes the application of "machine" "learning" "approaches" in "classification" of "porosity" and "quality" evaluation as depicted in Fig. 5b, and different research areas covered in the recently published review papers are depicted in Fig. 5c. These subgraphs provide brief straightforward storylines regarding the articles reviewed in this paper and research conducted in additive manufacturing.

### 1.3. Defect detection

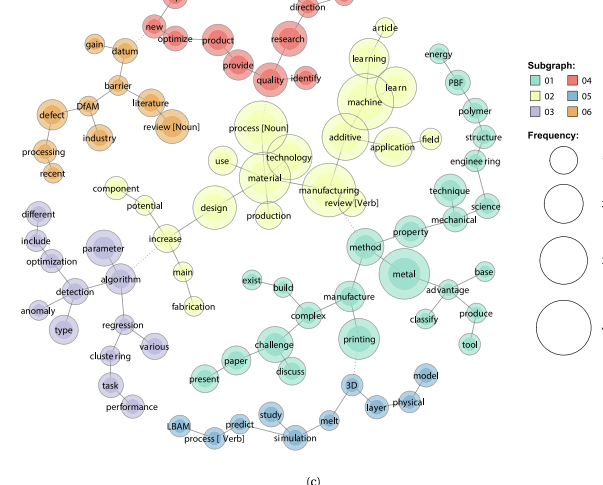
To obtain an optimal processing window for part manufacturing with little to no defects, various experimental monitoring approaches have been employed, which could be categorized into in-situ monitoring techniques conducted during the part



(a)



(b)



(c)

(caption on next page)

**Fig. 5.** Co-current network diagram for three identified clusters, namely (a) the papers employed experimental and physics-based approaches, (b) the papers employed data-driven approaches, and (c) review papers.

manufacturing, and ex-situ monitoring techniques conducted after the part production [46]. For example, computed tomography (CT scan), a nondestructive evaluation technique, can be used for defect detection, geometric analysis, quantitative comparison, structural quantification, and porosity analysis [47,48]. The majority of these monitoring techniques pay particular attention to the characteristics of the melt pool, as the common defects (i.e., keyhole porosity, lack of fusion, balling), happening during the fabrication in the AM field, have an origin in the dynamics of the melt pool [49–53]. These fabrication defects affect the structural performance and fracture behavior of the 3D-printed parts, as discussed in a study by Khosravani and Reinicke [54]. In experimental techniques, usually small cubes are built, and the mechanical properties of these cubes are evaluated [55] or material is printed on a single-track basis at different processing conditions [56,57]. Although the experimental approaches are reliable, they are tedious and expensive [37,35]. Physics-based models [58] could also be an alternative, but they are computationally expensive, and their accuracy depends on the assumptions, element type, boundary conditions, and constitutive models (i.e., finite element (FE) models) employed during the simulation [59,60]. They also require many simplifying assumptions, and the large uncertainty of the underlying thermo-physical process makes the models less reliable (i.e., analytical solutions, FE models) [61–64].

#### 1.4. Application of machine learning in additive manufacturing

To remedy the issues with experimental and physics-based approaches, data-driven approaches are employed. Data-driven approaches seem to be a suitable alternative, as these methods can predict highly non-linear relationships between a variety of parameters. Traditionally, the design of experiment (DOE) scheme has been used to analyze the processing parameters and optimize the output [65]. However, the DOE approaches require many trials and error efforts to find the zone where the response behavior changes. In the AM field, these trials and error efforts are time-consuming and costly [66,67]. ML models are an attractive alternative data-driven approach to optimize the response based on past data or experience [68]. Due to the high capability of the ML models in predicting highly nonlinear problems, these models have been previously used in many nonlinear problems (e.g., corrosion [69], erosion [70], mechanical properties optimization [71,72]), which are out of the scope of this review paper. ML can improve the quality of 3D-printed parts, optimize processing parameters, and reduce cost. Analyzing data using ML is relatively limited in materials science due to a variety of reasons. Developing an ML model requires a large dataset. The lack of a large dataset is a significant reason, limiting the use of ML [73]. Also, current ML models find statistical correlations between the inputs and output of AM problems at the expense of ignoring physical laws, which makes these models inexplicable. The models generated using this approach do not enlighten how they can make the final decision. For example, the melt pool images are widely used as the inputs in the ML-driven models without understanding the complex laws of nature and the physical relationship between the inputs and response. One way to go around these limitations is to link the ML-driven models to physics-based models and experimental data to analyze the process-structure-property of the fabricated part in a timely manner and accurately [59,74–76]. The paradigm developed using this approach uplifts the conventional non-physics-informed ML models, which act as a black box, to physics-informed ML (PIML) models, which are capable to constrain the model based on domain-specific knowledge.

This review paper also introduces the responses studied in the metallic AM field to control and improve the quality of 3D-printed parts. Although the outputs of each of these processing-structure-property-performance (PSPP) stages affect the quality of the part [77–79], this review paper focuses mostly on the recent application of ML in analyzing and optimizing the metallic AM processing parameters and their effects on the processing and structure stages with specific attention to the PIML models. A detailed review is available elsewhere regarding the application of ML in other stages of 3D printing [21,35,37,30,80] and more specific to polymeric materials [81]. The ML approaches implemented in the AM field were categorized, and the way that these data-driven approaches

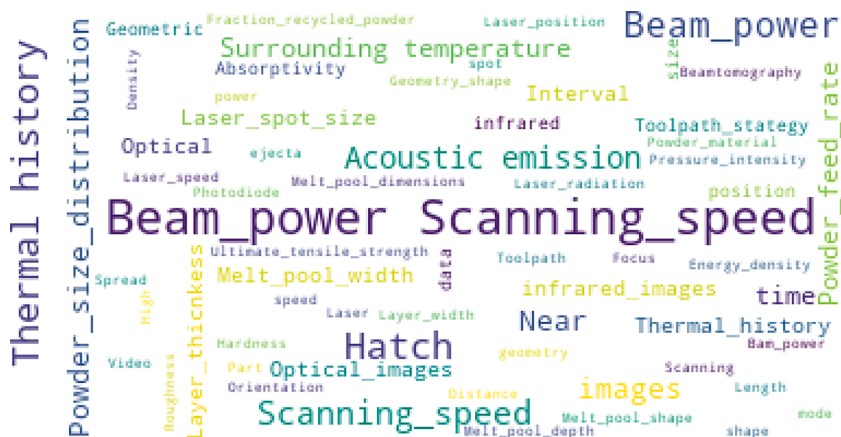


**Fig. 6.** Word cloud of the input parameters studied in the articles reviewed.

accelerate the discovery of the most suited processing conditions in the AM processes was discussed. Eventually, this review paper provides concluding remarks and future research directions toward the next generation of machine learning in AM.

## 2. Types of data in AM

The final quality of 3D-printed parts depends on more than 130 processing parameters, which make the prediction of the quality of the parts very complex. The effects of many of these processing parameters on the quality of the 3D-printed parts have been evaluated in different studies. The processing parameters evaluated in the articles reviewed in this paper have been collected and the frequency of evaluating these input parameters was obtained using the wordCloud library in Python and indicated in Fig. 6. As indicated, the beam power and scan speed are the two most frequent processing parameters widely analyzed in different studies.

The processing parameters have a relationship with the parameters in other stages of manufacturing, which are directly or indirectly linked to the quality of 3D-printed parts. The interrelationships between the processing parameters, thermal history, solidification, microstructure, and mechanical properties of the AM parts were illuminated in Fig. 7. A better understanding of these interrelationships could improve the quality of the 3D-printed parts.

### 2.1. Porosity formation

Porosity, a common defect in 3D-printed parts, significantly affects the quality of parts and repeatability. Porosity formation could be due to the keyhole effect, gas entrapment, lack of fusion, and rapid solidification of the AM part [82,63,83,84]. The porosity size and shape formed by each of these phenomena could be different, as depicted in Fig. 8. Microscopic pores are usually formed due to gas entrapment (gas is sometimes trapped and remained inside the vapor cavity, as the vapor cavity is solidified and closed up before the gas can escape) [85], while the size of process-induced pores (i.e., lack-of-fusion porosity [86,87] and shrinkage porosity [88]) varies from sub-microns to macroscopic scales[89].

When laser irradiation strikes the powder and substrate, two melting modes may occur. At low to moderate laser energy intensity, the material is locally melted without clear material vaporization. Conduction is the main mechanism of heat transfer inside the melt pool, which is expressed as conduction mode [83]. Insufficient penetration of the melt pool of a succeeding layer into the substrate or previous layer leads to lack-of-fusion and un-melted powders [90]. This un-melted particle causes high porosities and poor mechanical properties [91]. High melting rates may also cause keyhole porosity [92,25] and lack-of-fusion [27] as depicted in Fig. 9 due to Marangoni convection and recoil pressure [93]. At high laser energy intensity, the material vaporizes on the surface and forms a dense vapor plume, consisting of a cluster of molecules, atoms, ions, and electrons that creates a recoil momentum on the melt pool and forms a cavity [83] in the keyhole mode. In one definition, keyhole mode occurs when power density is higher than  $10^6 W/cm^2$ , otherwise, conduction mode is dominant [94,95]. In another definition, if the aspect ratio of the melt pool is larger than unity, the melting occurs in the keyhole mode otherwise the conduction mode is dominant [96]. It is worth mentioning that the presence of keyhole mode does not necessarily lead to keyhole porosity [92].

The effects of scan speed and beam power, which determine the dominant melting mode, on the porosity formation were evaluated in a study by Jadhav et al. [97], and an L-PBF-based process map, revealing the threshold line between these modes were plotted in

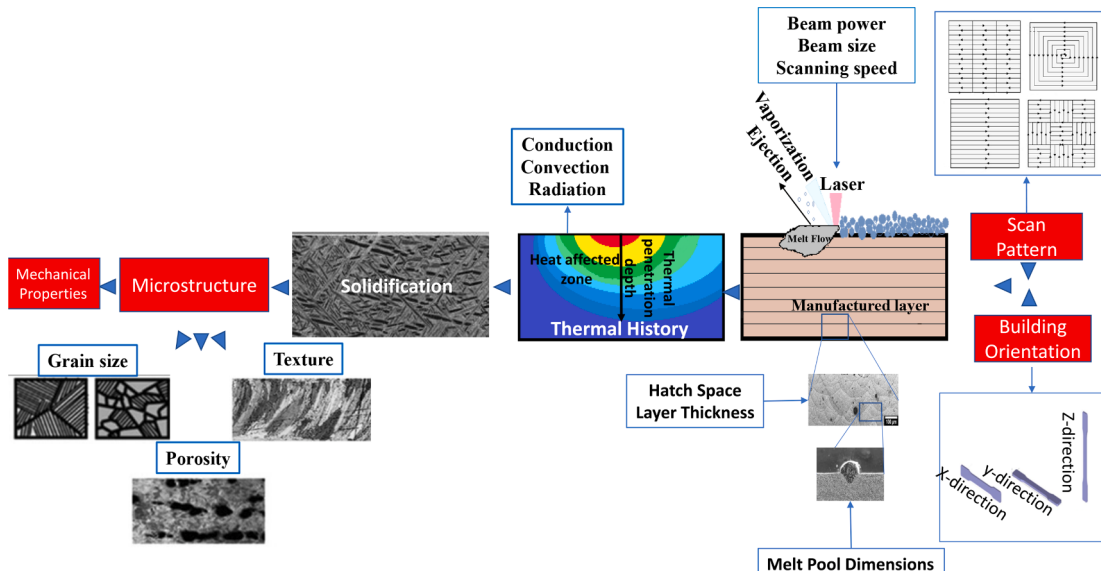


**Fig. 7.** Relationship between manufacturing processing parameters, thermal history, solidification, microstructure, and mechanical behavior of AM parts.

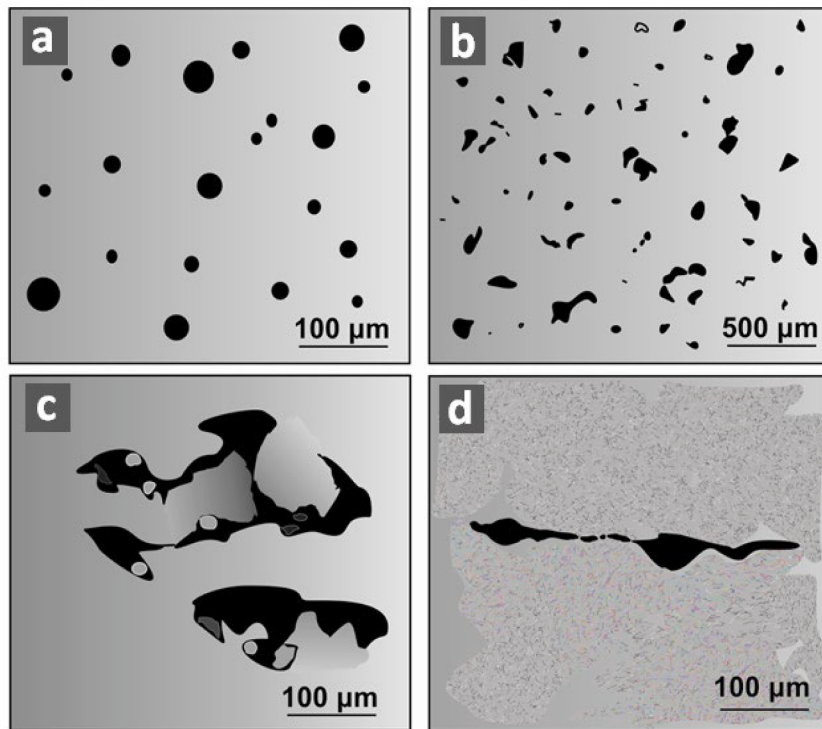


**Fig. 8.** Charachteristic pores in SLM (a) entrapped gas porosity, (b) incomplete melting-induced porosity, (c) lack of fusion with unmelted particles inside large irregular pores, and (d) cracks [104].

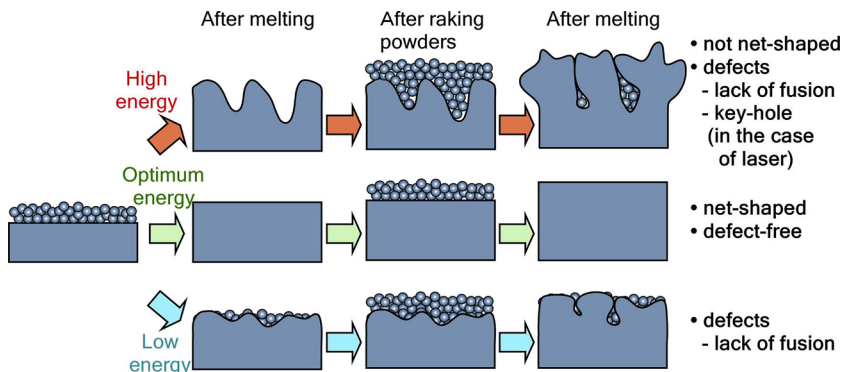


**Fig. 9.** Schematics of the relationships between surface morphology and defect formation in a powder-bed fusion type AM process [27].

**Fig. 10.** Also, the transition mode observed in between the conduction and keyhole modes results in oscillatory melt surface wave, melt spatter, and denudation, negatively affecting the surface roughness and mechanical properties [98]. Transition conditions can also be identified using the normalized enthalpy, which combines the effects of laser speed, power, and beam size during the LPBF process [92]. No method is capable of fully considering all processing parameters to predict the dominant melting mode and quality of the 3D-printed parts.

Pores can also form due to balling effect, resulting in an uneven powder layer [99]. Balling effect depends on the wettability, capillary forces, and surface tension of the melt pool [100]. Balling phenomenon could also occur in high beam powers and scan speeds or in high scan speeds and low beam powers, causing weak bonding to the substrate [101]. Porosity can also be formed between grains and follow the shape of grain boundaries during solidification [102]. Predicting the nonlinear relationship between processing parameters and porosity is very difficult using conventional approaches. Density measurement and image processing methods are two common ways to identify the porosity percentage in a product. Wang et al. [103] recently reviewed the role of porosity defect in the 3D-printed parts, including the defect characterizations, formation and migration mechanisms, and their effects on the quality of 3D-printed parts. To evaluate the porosity percentage in the 3D-printed parts and develop a predictive model, data-driven techniques are employed due to the previously mentioned benefits of these techniques compared to other techniques.

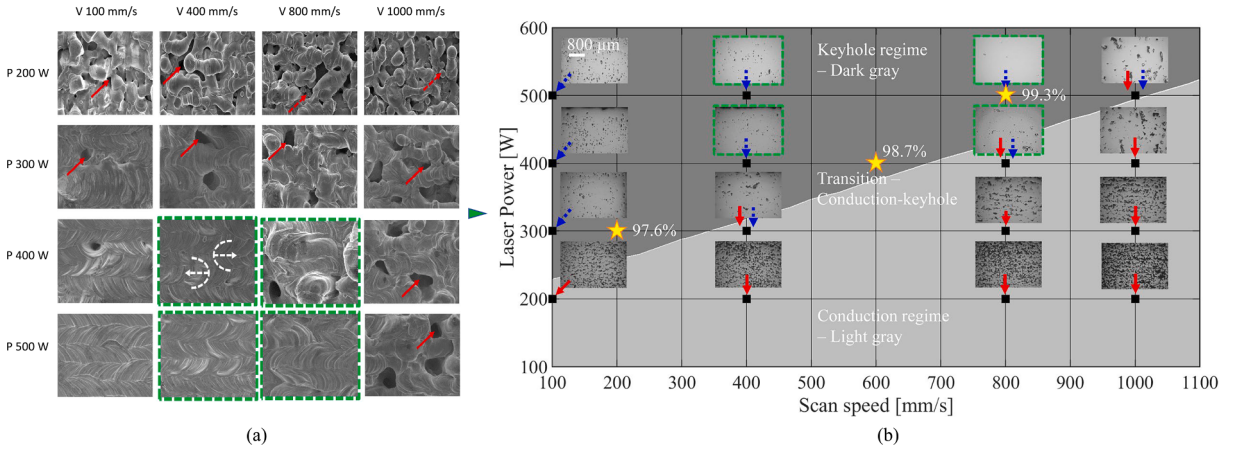


**Fig. 10.** (a) Morphology of melt tracks present on the top surface of the sample built, (b) L-PBF process map of pure copper, indicating a threshold line between the conduction and keyhole melting regimes [97].

## 2.2. Dimensional inaccuracies

One main contributor to dimensional inaccuracies produced by the AM approaches is material shrinkage (MS) [105], which is related to the powder properties and processing parameters [106]. Sintering shrinkage and thermal shrinkage are two common kinds of material shrinkage. The former is generally formed by densification, while the latter is mainly caused by cyclic heating and cooling, leading to significant residual stress and local plastic deformation [107]. To evaluate the material shrinkage, the shrinkage ratio, which is defined as the difference between the desired value and the actual value over the desired value, is employed. When the heated zone starts cooling down, along with changes in the microstructure, the material shrinkage occurs, but this deformation is restrained by the plastic strain formed during the heating step [108] and previously solidified layers underneath [109]. Thus, strong tensile stresses are formed at the interlayer zone [110]. These variations during the cooling step result in a significant deviation from the expected nominal geometry [111]. Zhu et al. [112] attributed the shrinkage of metallic powder to the scan speed and beam power during the SLM process. Wang et al. [113] simulated a multi-layer deposition process to analyze the surface unevenness and excessive build-ups, which always occur in the DED process and reported unstable linear powder feed rate, laser/powder defocusing, accumulated heat, and powder positive defocusing as the reasons of these dimensional inaccuracies in the 3D-printed parts. Raghunath and Pandey [114] used the Taguchi method [115] to design experiments and evaluate the importance of the processing parameters using the analysis of variance [65] between the processing parameters and shrinkage of 12 samples produced using the SLS technology. They concluded that hatch spacing and beam power significantly affect dimensional accuracy.

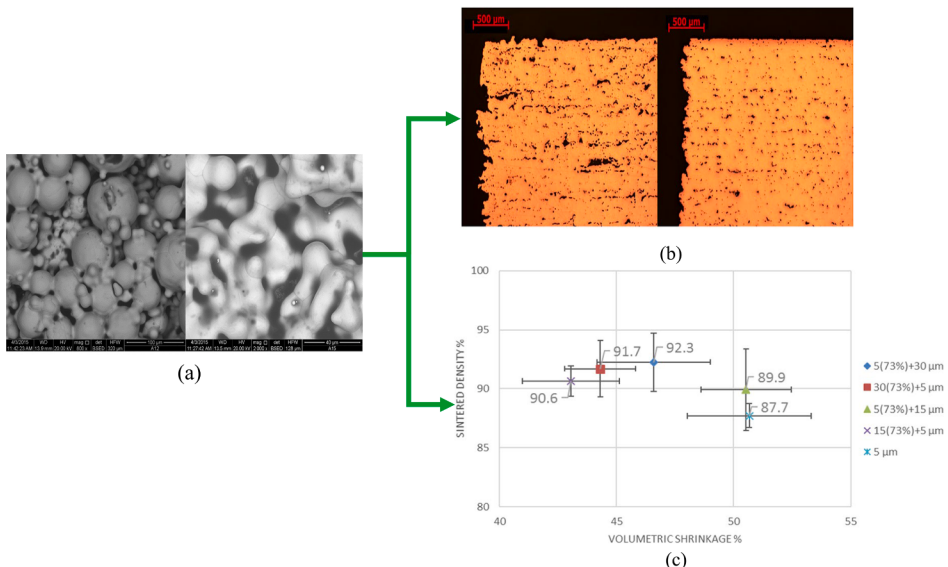


**Fig. 11.** (a) Surface microstructure of two different sizes of powders, (b) Optical microscopy of 5 $\mu\text{m}$  powder (left) and 30 + 5 $\mu\text{m}$  (right), and (c) sintered density and volumetric shrinkage relationship of 5 $\mu\text{m}$  powder and its bimodal mixtures [121].

Material shrinkage during the sintering process could also contribute to porosity in 3D-printed parts and lead to part defects [116], as material shrinkage causes non-uniform internal stresses [117,118]. These non-uniform internal stresses result in the deformation of 3D-printed products [119]. This materials shrinkage could be controlled by correlating the material shrinkage with the processing parameters [119,120]. Bai et al. [121] evaluated the effect of powder size on the material shrinkage and porosity, as depicted in Fig. 11. They concluded that there is a relationship between material shrinkage and density as indicated in Fig. 11c. It is worth mentioning that the relationship depicted between the powder size and material shrinkage is highly dependent on other processing parameters, which require a large dataset to further investigate.

### 2.3. Melt pool dimensions

One significant response parameter in the processing stage, which has been heavily employed to analyze the quality of the 3D-printed parts, is the melt pool dimensions. Melt pools are mainly defined as deposited, remelted, and heat-affected zones[83]. Melt pool geometry is indirect evidence of interactions between the processing parameters and microstructure of the materials (i.e., intrinsic materials properties) [122]. Keyhole formation, balling effect, and lack of fusion can be distinguished based on the melt pool geometry [123]. More importantly, melt pool depth has been measured and analyzed in many studies [124–126,122], as the melt pool depth is of great interest compared to melt width and length. Melt pool depth reveals if the energy is sufficient to melt through the powder and substrate at a certain beam power and speed [29]. High energy deposition on powder layers causes metals to vaporize [91]. The reaction force of evaporation of liquid metals causes the formation of a vapor cavity in the melted region and causes a deeper melt pool. Several physics-based models have also been developed to predict the melt pool depth and width [127–131], however, more physical phenomena should be considered in these models to make the model more reliable.

As considering all physical phenomena occurring during the melt pool is difficult, the design of experiment scheme is used to develop regression models based on the processing parameters. In one attempt, Zhuang et al. [132] employed response surface methodology [65] to correlate the processing parameters with the dimensions of the melt pool produced in the SLM process. Melt pool dimensions and shape were also predicted using a coaxial imaging system in a study conducted by Sun et al. [133]. Melt pool dimensions could be used as a key feature to characterize the microstructure and predict the mechanical properties of the parts additively manufactured [50]. To do this, data-driven models could be assisting physics-based models to better identify the relationship between the processing parameters, melt pool dimensions, defect formation, and mechanical properties.

### 2.4. Remelted depth

Carefully controlling the microstructure and homogeneity is one way to improve the quality of 3D-printed parts. The heat-affected zone [134] and the remelted depth are the parameters evaluated to enhance the quality of the 3D-printed parts through improving the material homogeneity [135], degassing and deoxidation [136], and reducing porosity [137]. Small remelted depth may result in incomplete fusion [138], poor metallurgical bonding between the previously solidified layer and the melted powder [139,140], uneven microstructure distribution [141], and poor wetting [142]. On the other hand, large remelted depth causes geometrical inaccuracy in the 3D-printed parts [143] and deteriorated interlayer metallurgical bonding [144].

To analyze the quality of the 3D-printed parts, many studies tried to find the relationship between the processing parameters and remelted depth. Vastola et al. [145] evaluated the effect of beam size, shape, and scan speed on the size of the remelted pool for an AISI 316L stainless steel. Zhang et al. [146] evaluated the relationship between the remelted depth and linear energy density defined as the beam power over scan speed for Ti6Al4V. Predicting the remelted depth requires identifying the dominant parameters and developing a correlation based on these parameters. Developing a correlation between the processing parameters and remelted depth requires employing appropriate data-driven techniques and a large dataset, which are further discussed in the next sections.

### 2.5. Thermal history

Another way to evaluate the microstructure of the AD-fabricated parts is to evaluate the real-time melt pool temperature distribution. Analyzing the heat transfer mechanisms, thermal accumulation, transient temperature distribution, and their relationship helps reduce residual stresses, distortion [147], micro-voids, and cracks formation in 3D-printed parts [148,149]. This thermal distribution in the material is related to scan strategies [150]. A small melt pool at low temperature implies insufficient overlaps between the current melt pool with the next melt pool and lack-of-fusion porosity in the built part [151]. In a melt pool, the cooling rate increases with the increase of the beam power and scan speed [152]. The creation of large thermal gradients is more probable at high cooling rates, which result in an increase of residual stresses, cracking [152], instability, and porosity formation [111,153]. On the other hand, low cooling rates and high temperatures may negatively affect the microstructure refinement and mechanical properties of the 3D-printed parts [152]. The desired uniform operating temperature helps melted material to flow within the melt pool moderately. However, non-uniform temperature gradients and repeated thermal cycles, occurring mainly in the DED process lead to porous and anisotropic microstructures [154] within the 3D-printed parts due to the rapid solidification [155]. This heterogeneous behavior in the microstructure due to the variation in the thermal history affects the mechanical properties, such as fatigue resistance and tensile strength [156]. To homogenize temperature distribution and reduce local heat accumulation, the scanning pattern, one influential parameter on the temperature distribution, needs to be optimized, which leads to minimum distortion [157]. The relationship between the processing parameters and the temperature of the melt pool has been analyzed by Hua et al. [158]. Balling can also be detected via observation of the temperature distribution of the melt pool and its surrounding area [159]. Non-uniform grains and porosity observed

in the resultant microstructures affect the mechanical properties of the 3D-printed parts [160]. As indicated in Fig. 12, thermal history could also be used as an input parameter [161,162] along with the processing parameters to evaluate the quality of the part, as developing a model using beam parameters (e.g., power, speed, and size) and build parameters (e.g., hatch spacing) may not account for the complex heat distribution in a real part.

## 2.6. Acoustic and spectra signals

Acoustic and spectra emissions are two common data types that have been used to evaluate the quality of the 3D-printed parts. These acoustic emissions could be used as the input of an ML model, which are correlated to the possible defects, or could be used as the output of an ML model, which is linked to the processing parameters. Acoustic signals acquired during the AM processes are converted into electrical signals, and the signal features are extracted and employed to form clusters used to distinguish different defect mechanisms.

Also, the spectra emissions produced during the process are collected to extract information about the physics of the problem [164]. When the powder is melted by the laser, a part of the metal is evaporated, which forms plasma above the melt pool. Photons emitted as line emissions have specific wavelengths, and thermal radiation is collected in the spectra. The constitutive elements of the plasma are identified by these wavelengths of the line emissions in the spectra [165]. The intensity and shape of spectra indicate the concentration and plasma condition, including the plasma temperature [165], and are directly related to the process parameters and quality of the 3D-printed parts.

## 3. Machine learning

Machine learning approaches have gained increasing attention due to their great performance in data tasks, such as regression, classification, and clustering. They can be categorized according to the amount and type of supervision required during training [166] into supervised learning, unsupervised learning, semi-supervised learning, and reinforcement learning [166], as shown in Fig. 13. In supervised learning, the data are labeled, and the data are split into training data and testing data [55]. In unsupervised learning, the data are not labeled, and no training data are required to create the model. In semi-supervised learning, a small part of the datasets are labeled, and then the system learns from these labeled data and classifies a large amount of data. Reinforcement learning, however, is dissimilar from other ML approaches, because this approach uses a reward-and-penalty mechanism to train the algorithm. Favorable actions are rewarded and unfavorable actions are punished, leading to reinforcing good behavior [167]. Reinforced learning (RL) is a suitable approach for real-time metal AM process control in which it is adjusted through machine setting, as RL authorizes goal-seeking sequential decision-making, which was previously used in different AM applications, including controlling melt pool depth and

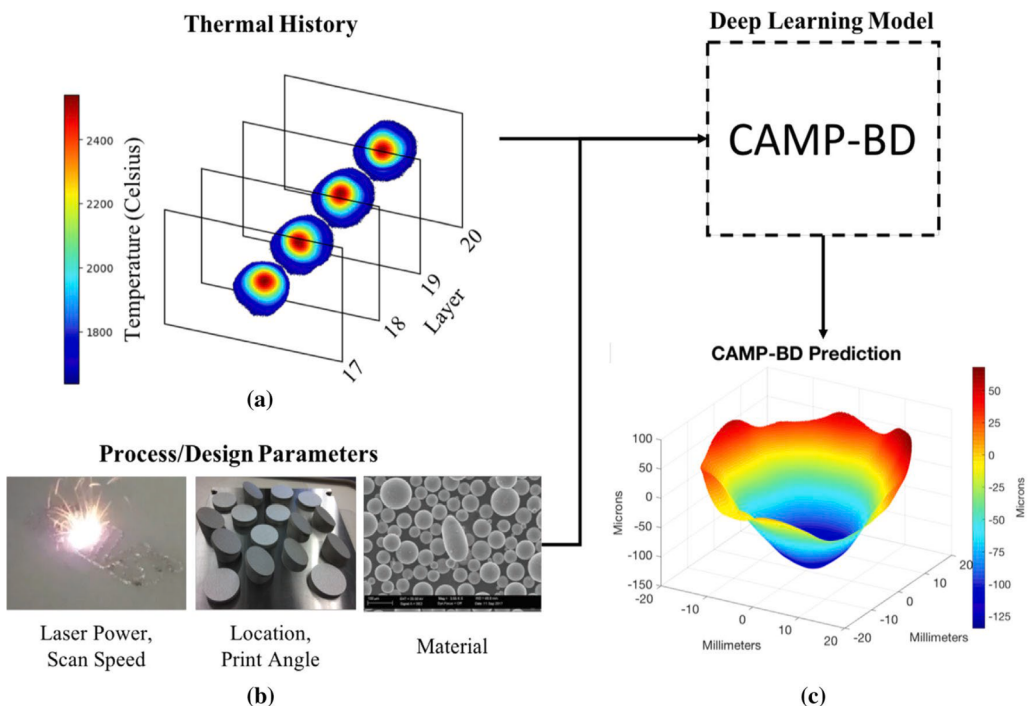


**Fig. 12.** Geometric error compensation of Ti-6Al-4 V in the L-PBF process. The input parameters are (a) the thermal history and (b) processing parameters. The output is (c) the predicted distortion using an ML model [163].

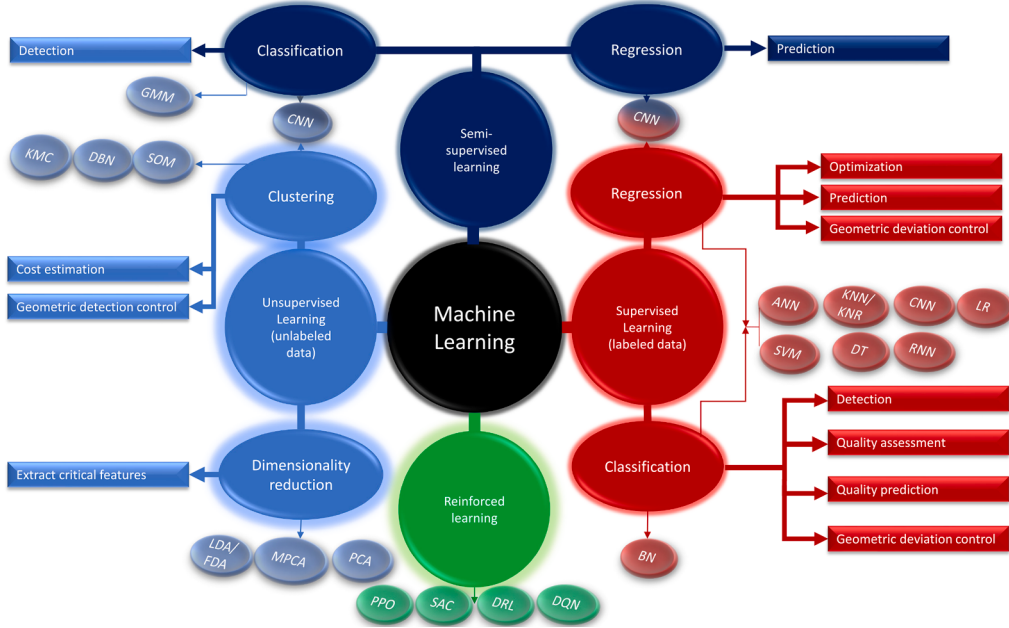


**Fig. 13.** Applications of machine learning in the AM field.

improving mechanical properties consistency throughout the AM parts [168].

Developing a machine learning model starts with data preparation and data organization. Several different mathematical tools could be employed to represent scalar values. Typically, observations are stored in rows and each column represents a feature. These observations form a matrix as follows [169]:

$$X = \begin{bmatrix} x_{1,1} & x_{1,2} & \cdots & x_{1,m} \\ x_{2,1} & x_{2,2} & \cdots & x_{2,m} \\ \vdots & \vdots & \ddots & \vdots \\ x_{n,1} & x_{n,2} & \cdots & x_{n,m} \end{bmatrix}, \quad (1)$$

where the columns of  $X$  represent each feature (i.e., processing parameters) and the rows of  $X$  represent observations. Similarly, the output (i.e., resulting properties) can be stored in a separate vector as follows:

$$Y = \begin{bmatrix} y_1 \\ y_2 \\ \vdots \\ y_n \end{bmatrix}, \quad (2)$$

which is also called labeled data and employed mostly in supervised machine learning approaches.

Two hypotheses exist in machine learning; (1) A correlation exists between the input data and output (the relational hypothesis), (2) similar inputs in the design space will reach similar outputs (the similarity hypothesis). In supervised machine learning, the goal is to determine a relationship between  $x$  and  $y$  based on the previous observations of  $x$  and  $y$  as follows:

$$f(x) = y. \quad (3)$$

This functional mapping can take either the form of regression or classification. Functional relationships can have many forms, depending on the type of supervised machine learning model employed. One way to form this relationship is:

$$X\beta = Y, \quad (4)$$

where  $\beta$  is a vector of coefficient, which defines the weight of inputs to predict  $Y$ . Least square regression is a common method to measure  $\beta$ , which is based on the minimization of the difference as follows:

$$\min ||X\beta - Y||_2^2 \quad (5)$$

Similarly, Eq. 5 could be applied in an unsupervised approach, the closer  $X\beta - Y$  is to 0, the more similar  $X\beta$  is to  $f(x)$ , as unsupervised machine learning approaches are employed to detect similarities and conclude based on the similarity hypothesis. In unsupervised learning, a distance parameter can be defined between the data points in the design space as follows [170]:

$$\|a - b\|_2 = d, \quad (6)$$

where  $a$  and  $b$  are the data at two specific conditions of the input values (features), and the value of  $d$  represents how close or similar  $a$  and  $b$  are. In general form, the distance function can be written in the form of [170]:

$$d(a, b) = \|a - b\| = \sqrt{\sum_{s=1}^D (a_s - b_s)^2}, \quad (7)$$

where  $D$  represents the dimensions or the number of features. Further details regarding the mathematics of ML models can be found in [169,170] for interested readers.

The machine learning models can also be categorized into batch/offline learning and online learning [166]. In offline learning, the model is incapable of learning incrementally and must be trained using all available data. The model requires a lot of time and computing resources. When the model is trained and is ready for production, it runs without learning anymore [166]. In online learning, the model can learn incrementally on the fly [166], as shown in Fig. 14. This approach is suitable when one is dealing with an extremely large dataset, which is updated and getting larger with time. Although online monitoring of the live AM process linked with a feedback control adjusting experimental parameters on the fly could be a major research thrust in AM, online learning has not been tested enough in the AM field. Similarly, ML methods can be classified into instance-based and model-based learning [166]. In instance-based models, the model identifies new cases by using a similarity measure, while a model is built and then used to make predictions in model-based learning [166]. The most common machine learning approaches used in the AM field are either offline instance-based or model-based, supervised, or unsupervised learning models, while other machine learning approaches have been less frequently employed in additive manufacturing. The ML models employed in the AM field and discussed here in this review are briefly summarized in Table 1.

### 3.1. Supervised learning

In the AM field, many studies [78,35,30,199] employed ML models to evaluate the response at each PSPP stage. For example, the roadmap of a potential approach [199], which utilizes a combination of a large amount of data collected from a large number of miniature specimens to train a machine learning model for evaluation of fatigue performance of AM parts, is illustrated in Fig. 15. This approach has the capacity of predicting fatigue crack growth of materials, analyzing the cause and effect flow to save time for experiments and simulations by developing ML forward models (PSPP left to right relationship), and optimizing the performance of AM parts by building ML inverse models (PSPP right to left relationship). In the AM processing stage, the input parameters indirectly affect the performance [77]. Depending on the type of the problem in AM, regression, classification, or clustering approach is employed, as indicated in Fig. 13. Tuning processing parameters is difficult [200]. Conventional ML approaches could be a suitable solution to link the processing parameters to the microstructure of the 3D-printed part and its performance. In contrast to experimental techniques, which are only designed and applicable for a particular subject, ML approaches are highly flexible and can be easily applied from one application to another [46]. However, these ML approaches sacrifice the complex physical relationships between the inputs and outputs in the AM field, which encourage practitioners toward developing the next generation of machine learning approaches by considering the laws of physics in the ML model. A recent review paper [39] listed five main ways to integrate physics into ML and develop physics-informed machine learning models (PIML), namely model input, model training, model components, model architecture, and model output.

In physics-informed model input (PIMI), hidden physical information is extracted from in-situ production data and linked to the processing parameters and/or simulation data to develop an ML model and create a meaningful relationship between the inputs and response. Projecting the time-temperature series into the time-frequency domain using wavelet transforms is an example of this method described in a study by Xie et al. [201]. Physics-informed model training (PIMT) and physics-informed model components (PIMC) are other types of PIML models, which have been employed in the AM field. The latter is based on physical consistency between inputs and outputs by punishing nonsense outputs through loss function [202], while the former is based on physics-informed activation functions and/or physics-informed initialization procedures. For instance, Inyang-Udoh and Mishra [203] developed a PIMC model, termed constrained-flow model, to analyze the spatial effect of droplet deposition in inkjet 3-D printing and proposed an

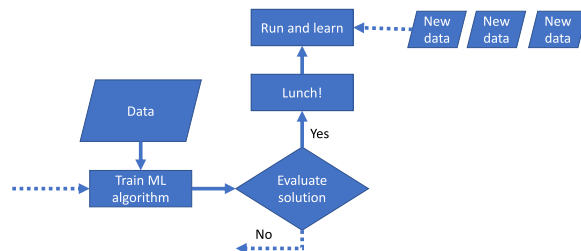


Fig. 14. Online learning flowchart.

**Table 1**  
Machine learning models.

Model	Description	Application in AM	Feature
Random forest (RF)[171]	Consisting of several decision trees trained on random sub-samples. Returning the average outputs of the decision trees (regression). Returning the highest vote of the decision trees (classification).	Reg., Clas.	
Support vector machine (SVM) [172]	Predicting based on finding hyperplane, separating data points of different categories (regression).	Reg., Clas.	
Gaussian process regression model (GPR) [173]	Probabilistic algorithms, returning a probability distribution over output values.	Reg., Clas.	Predict fairly well on small datasets.
Ridge linear regression (Ridge) [174]	A regularized linear regression.	Reg.	Reduce the model complexity and overfitting.
Artificial neural network (ANN) [175]	Mimics human brain with individual networks exchanging information.  Includes an input layer, hidden layer(s), and an output layer.	Reg., Clas.	Large dataset required.  Perform better with more than 1 hidden layer.
Convolution neural network (CNN) [176]	Consisting of multiple convolutional kernels to compute feature maps.	Clas.	Widely used for image recognition in AM.
XGBoost [177]	Implements gradient boosted trees to generate predictions.	Reg., Clas.	
Logistic regression (LR) [178]	Probability values and logistic function outputs are used in classification.	Reg., Clas.	
Gradient Boosting trees (GB) [179]	It builds one tree at a time, which tries to improve errors produced by the previous tree.	Reg., Clas.	
Lasso linear regression (Lasso) [180]	A regularization method, optimizing the weights of linear regression.	Reg.	More accurate prediction with less overfitting compared to linear regression.
K-neighbours regression (KNN/ KNR) [181]	A nonlinear regression algorithm.	Reg.	The larger k, the more accurate interpolation, and the higher computational cost.
Dense convolutional networks (DenseNet)[182]	Connecting each layer to every other layer in a feed-forward fashion.	Clas.	Effective for handling overfitting, and huge computation. Suitable for classifying melt pool images.
Self-organizing map (SOM)[183]	An artificial neural networks-based model that employs competitive learning to discern patterns.	Clus.	Perform well in unsupervised tasks.
Self-organized and error driven (SOEDNN) [184]	A hybridized SOM and ANN method.	Clas.	Highly capable of visualizing data. Improved version of ANNs.
Principal component analysis (PCA) [185]	A statistical technique, converting a set of correlated variables into a set of values linearly uncorrelated.	Dim. reduction	In AM field, help to visualize data.
Multilinear principal component analysis (MPCA) [186]	A method to extract features of multidimensional data expressed as a tensor.	Dim. reduction	Tensor based algorithm
Linear discriminant analysis (LDA) [187]	A method to find a linear combination of features, which characterizes or separates two or more classes.	Dim. reduction	LDA is closely related to PCA.
Bayesian network classifier (BN) [188]	A probabilistic classifier, providing probability information about the examined product.	Clas.	Useful in defect detection.
Spectral convolutional neural networks (SCNN) [189]	A recent extension of CNNs with improved efficiency in classification/regression tasks.	Reg., Clas.	Operating well on irregular data grids.
Support vector regression (SVR) [190]	A method to find the best fit line.	Reg.	Uses the same principles as SVM.
Locally linear embedding (LLE) [191]	It computes low dimensional neighborhood preserving embeddings of high dimensional data.	Clus.	Discover nonlinear structure in high dimensional data
Bag-of -Words (BoW) [192]	It works based on quantization of affine invariant descriptors of image patches.	Clus.	Simple computationally efficient and intrinsically invariant method
K-means clustering algorithm (KMC) [193]	A simple method to classify dataset using a pre-defined number of clusters (k).	Clus.	Widely used image and acoustic emission analysis.
Deep belief network (DBN) [194]	A probabilistic graphical model that contains numerous layers for deep learning.	Clus.	Layer-by-layer training repeated to learn a deep model.
Gaussian mixture model (GMM) [195]	A function comprised of several Gaussians.	Clas.	Relatively time efficient model.
Deep reinforcement learning (DRL) [167]	A combination of deep learning and reinforcement learning.	Clas., Reg.	Automatically learning a policy with minimal manual training.
Proximal policy optimization (PPO) [196]	A widely successful actor-critic method.	Clas., Reg.	Simple to use and tune.
Deep Q-network (DQN) [197]	A combination of deep learning and reinforcement learning.	Clas., Reg.	Fast convergence.
Soft actor critic (SAC) [198]	An off-policy actor-critic method.	Clas., Reg.	One of the most efficient RL algorithms used in real-world robotics.

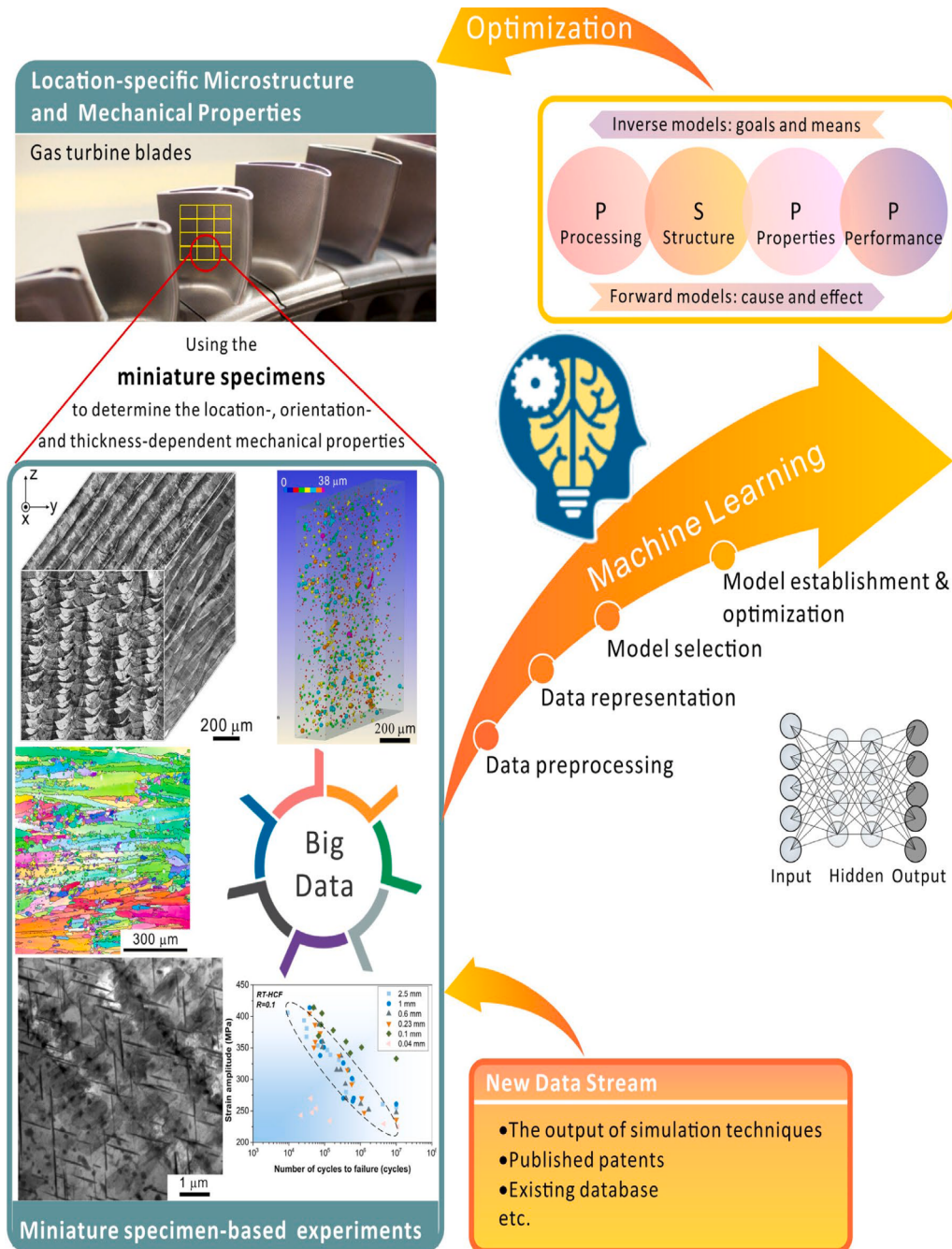


Fig. 15. Roadmap of a data-driven approach to analyze fatigue performance of AM parts using miniature specimens [199].

activation function to analyze the spatiotemporal evolution of the height profile. In another study [204], the same authors built on their previous work [203] by establishing a PIMT for the stability of training the model and translating this model to the physical stability of the height evolution in the inkjet 3-D printing.

Other pillars of PIML are physics-informed model architecture (PIMA) and physics-informed model output (PIMO). In PIMA, the model, representing input information is trained during model optimization to perform physics-based analysis. Using the PIMA concept, Li et al. [205] presented a novel wavelet-driven deep neural network by replacing the first convolutional layer of the standard convolutional neural network (CNN) with a continuous wavelet convolutional (CWConv) layer to make more meaningful kernels employed for extracting defect-related impact component embedded in the vibration signal. Also, PIMO is based on the idea of considering physical consistency in the model while reaching the final decision. Grezma et al. [206] employed this approach and presented an explainable CNN for gearbox fault diagnosis using Layer-wise Relevance Propagation (LRP) [207], which clarifies the

rationale behind the most time–frequency contributors to fault type and severity identification. With that in mind, direct use of physical parameters (e.g., temperature, beam power, scan speed, etc.) as the inputs to the ML models do not meet the PIML definition and should not be mistakenly considered as a PIML approach. In other words, any ML models with physically meaningful inputs or outputs are not necessarily called physics informed, as ML models should be constrained by the laws of physics to become a PIML model. Although PIMI has been employed in some AM-related studies, other types of PIML methods (i.e., PIMC, PIMO, and PIMA) have been barely used in the AM field. This gap can be addressed by developing more PIMC-, PIMA-, and PIMO-based models and evaluating the accuracy of these models and the data size required to develop such a model in the AM field. This review paper refers interested readers to Ref. [39] for more details regarding these types of PIML methods, and the details are not repeated here. In supervised learning ML algorithms, the data are labeled, and the problems are categorized into classification and regression [166] methods. In the classification method, a model is trained to identify to which category the new data belong (categorical variables), while the regression approach is used to predict the numeric value of a target. Depending on the type of the problem (i.e., classification or regression), a supervised learning model is employed. However, there is no rule, specifying which model performs better in a certain problem, as each of these models may perform differently from one problem to another. The application of these methods in machine learning is discussed in the following sections.

### 3.1.1. Regression

**3.1.1.1. Conventional models.** ML-driven regression models seek to predict the variables of interest by finding statistical correlations between these variables and the input parameters at the expense of the laws of nature. These non-mechanistic ML-driven regression models are not constrained by the laws of physics. They do not require a large computational cost imposed by complex physics, such as the laser-powder interaction, fluid dynamics, heat transfer, laser energy distribution, etc. Also, oversimplified assumptions (e.g., neglecting the heat loss caused by substrate and powder reflection) introduced in the FEM models [58] are not reflected in the ML-driven regression models. More importantly, all physical phenomena that occurred during data gathering are translated to the ML model, which increase the prediction accuracy regardless of throwing light on these laws of nature.

To improve the accuracy of these ML-driven regression models, the number of input parameters is significant. The more relevant input parameters are entered into the model, the more accurate the model would be. However, covering more input parameters requires a larger dataset, which is hardly obtainable in the AM field. Selecting the most significant input parameters is one way to reduce the data size required for developing an ML-driven regression model, which was employed by Ye et al. [208]. They implemented Spearman's rank correlation [209] to select the most significant input parameters, consisting of the processing parameters (static) with the features extracted from the in-situ melt pool images to develop a semi-dynamic ML model with a small data size to predict the melt pool depth and height as summarized in Fig. 16.

Accessing a large dataset is a key parameter in accurately predicting the response in ML. In a study by Akbari et al. [101] a quite large experimental dataset has been collected from over 80 AM articles, including several processing conditions, material properties,

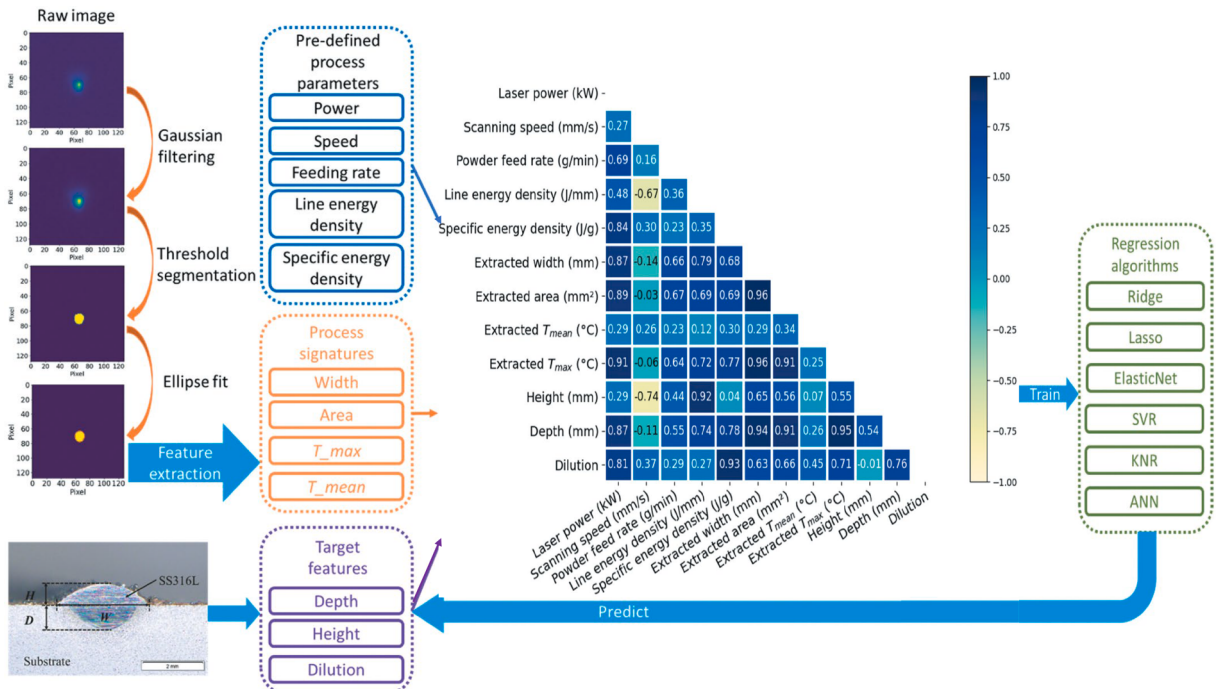


Fig. 16. Schematic description of workflow applied in a study by Ye et al. [208].

melt pool dimensions, and flaw types. This benchmark was then used to develop several ML-driven regression and ML-driven classification models to predict the melt pool dimensions and flaw type, respectively, as indicated in Fig. 17. They also compared the performance of these models and the sensitivity of the models to the data size. Using the random forest, logistic regression, and neural network models, they visualized the decision boundaries for the dataset obtained from printing parts using Ti-6Al-4 V powder at different power and velocity values. They also used the confusion matrix to visualize the performance of the random forest model for different baseline plus absorptivity coefficients in Fig. 18. Although this large dataset could help cover several input parameters, many other input parameters are still missing, and also a limited range could be covered for each parameter compared to the big picture of AM. Generating a large dataset is not the only issue for developing an ML model, labeling this large dataset is also time-consuming and laborious. To obviate the labeling problem, in-situ data could be labeled using the ex-situ data in some cases, and then in-situ data could be employed to train a supervised machine learning model that can predict the final properties of the 3D-printed part on-the-fly. This approach was tested by Yuan et al. [210] to label in-situ video clips using the ex-situ height map analysis algorithm. The labeled in-situ data were then used to train a CNN model employed to predict the melt pool width, standard deviation, and track continuity.

Chowdhury and Anand [211] simulated the deformation of a 3D-printed part for a defined set of process parameters using a thermo-mechanical FEA model. The deformation and preprocessing data were used from the CAD model to create a dataset for training an ANN model. The ANN model learned the direction and magnitude of thermal deformation in each region of a 3D-printed part and was later used to generate a modified geometry, which is capable of compensating for the thermal effects induced in the part during the AM process. The model developed in their study was not validated by experimental data. Developing a more comprehensive FEA model validated by experimental data to predict and modify the thermal shrinkage and thermal deformation could be a good continuation of this work. With all issues mentioned here regarding preparing a dataset suitable for developing an ML model in mind, it seems that developing a PIML model is more important than preparing a large dataset due to the many benefits of the PIML models mentioned earlier.

**3.1.1.2. Physics-informed models.** To make the ML-driven regression models physics-informed, domain-specific knowledge and/or domain-specific constraints are required. Employing physics-based models that are iterative in nature (e.g., finite element methods) could be one alternative combined with data-driven ML models to generate PIML models. Employing a finite element model validated by experimental data to predict the temperature field and produce the data required to train an ML model is an example of a physics-informed ML-driven regression model employed by Pham et al. [212] and Fetni et al. [213] for a two-dimensional simulation and Roy et al. [214] for a three-dimensional fused filament fabrication (FFF) simulation indicated in Fig. 19. These models proposed a set of distance-based features by considering the characteristics of the thermal processes and built a PIML model, which requires a smaller data size or is capable of covering a larger domain compared with previously proposed conventional ML models [64,58,215] based on temporal information that is critical in making the model PIML-driven, as this information cannot be captured from in-situ temperature data alone. It is worth mentioning that laws of physics are employed in the PIML models to cover the missing information, which cannot be captured using experiments, and experiments are employed along with laws of physics to justify and cover the assumptions that simplify the physics-informed models (e.g., constant thermophysical properties, sophisticated effects of microstructure, etc.). An ML model cannot be called physics-informed in the absence of one of these main components. For instance, the proposed data-driven methods by Mozaffar et al. [64] and Ren et al. [216] were not demonstrated on real-time experimental data and were hardly

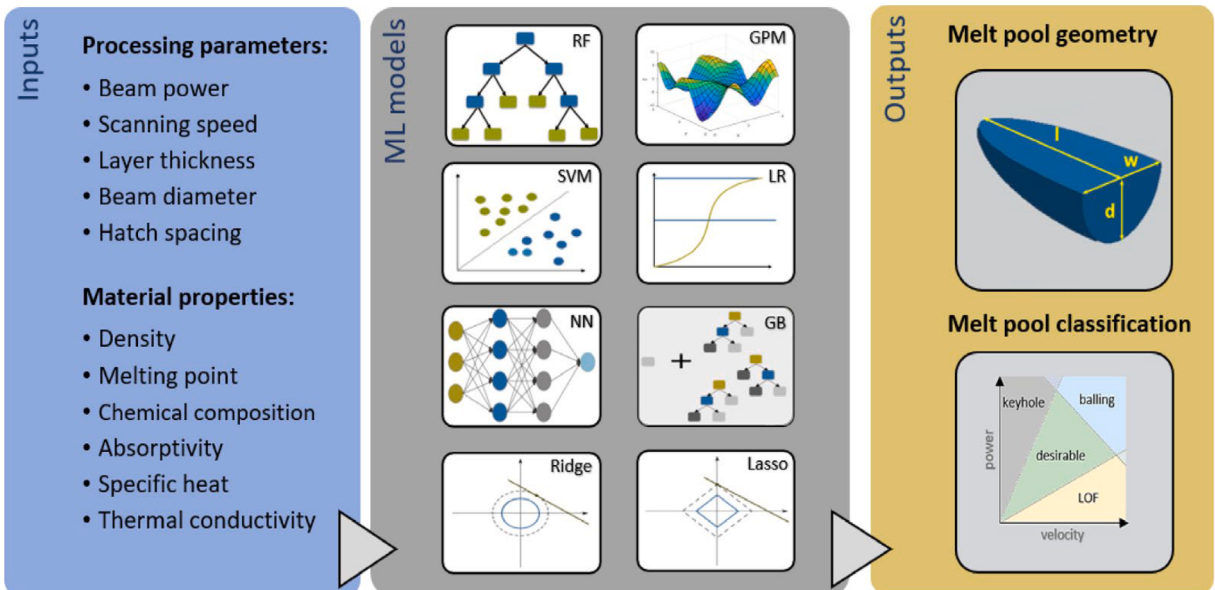
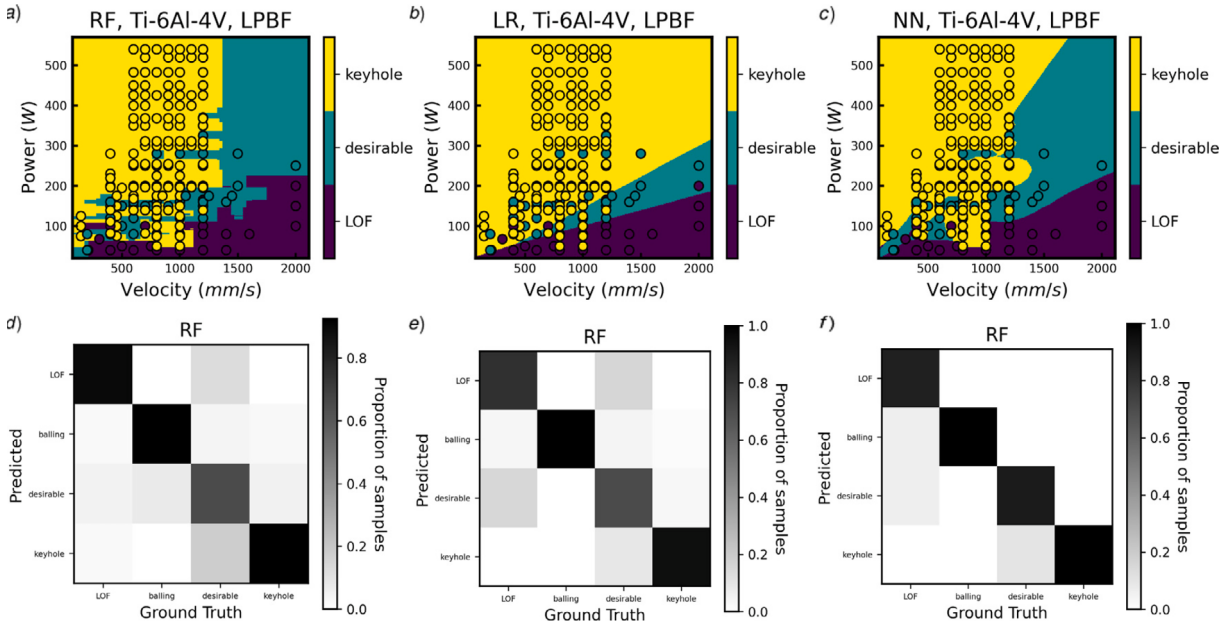
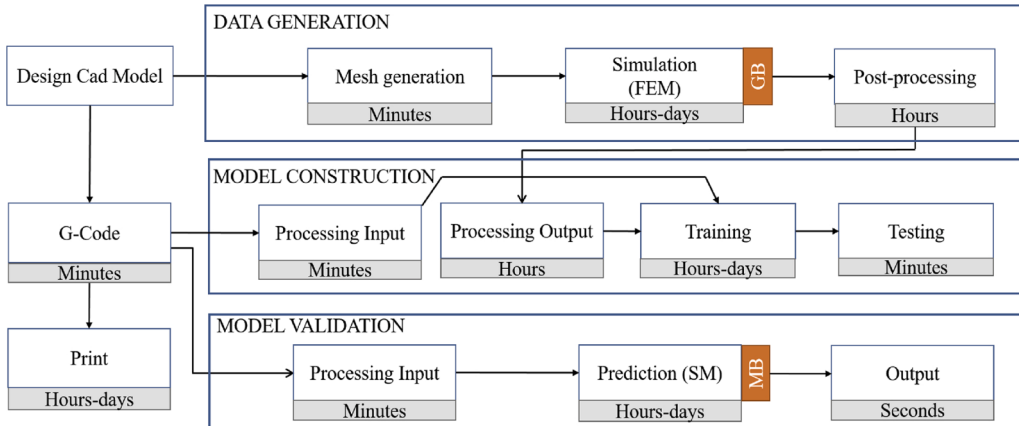


Fig. 17. Schematic description of workflow applied in a study by Akbari et al. [101].



**Fig. 18.** Classification decision boundaries of the dataset based on power and velocity for (a) random forest model, (b) logistic regression model, (c) Neural Network model. Confusion matrix for the classification task for random forest classifier with baseline plus absorptivity coefficient (d) 1, (e) 2, (f) with baseline plus both absorptivity coefficients and hatch spacing as features in a study by Akbari et al. [101].



**Fig. 19.** Workflow of surrogate model construction [214].

convinceable to consider them as physics-informed ML models, as laws of physics should be an assistive tool, constraining the domain under study. This point was clearly indicated in a study by Ren and Wang [217] by developing Gaussian process regression models to predict the melt pool volume using a simulated dataset, an experimental dataset, and a mix of the simulated and experimental datasets. They indicated that the melt pool volume suddenly had a large overshoot due to heat accumulation as depicted in Fig. 20. This large melt pool overshoot was controlled by significantly reducing the laser power of the second and the subsequent tracks. Then, the physics-informed Gaussian process regression model was used to predict this dynamic evolution of the melt pool, as depicted in Fig. 20. It was also found that the model performance can be improved by mixing the numerical and experimental datasets when the experimental data size is not large enough, as the high-fidelity simulated dataset, even though subject to errors, at least can catch the trend of the real-time experimental data. This helps achieve a PIML model with a limited number of experimental data, which could be employed to accurately predict the melt pool size.

To reduce the dependency on a large number of datasets, Zhu et al. [218] introduced a PIMT model, a physics-informed neural network (PINN) model, that incorporates both data and fundamental principles of physics (i.e., continuity, momentum, and energy governing equations) into a deep neural network to inform the training processes. To do this, the loss function used in conventional deep neural networks to measure the model performance against ground truth values was modified by these laws of physics, which were often expressed as a set of PDEs with appropriate initial and boundary conditions, and was penalized by the residuals of the

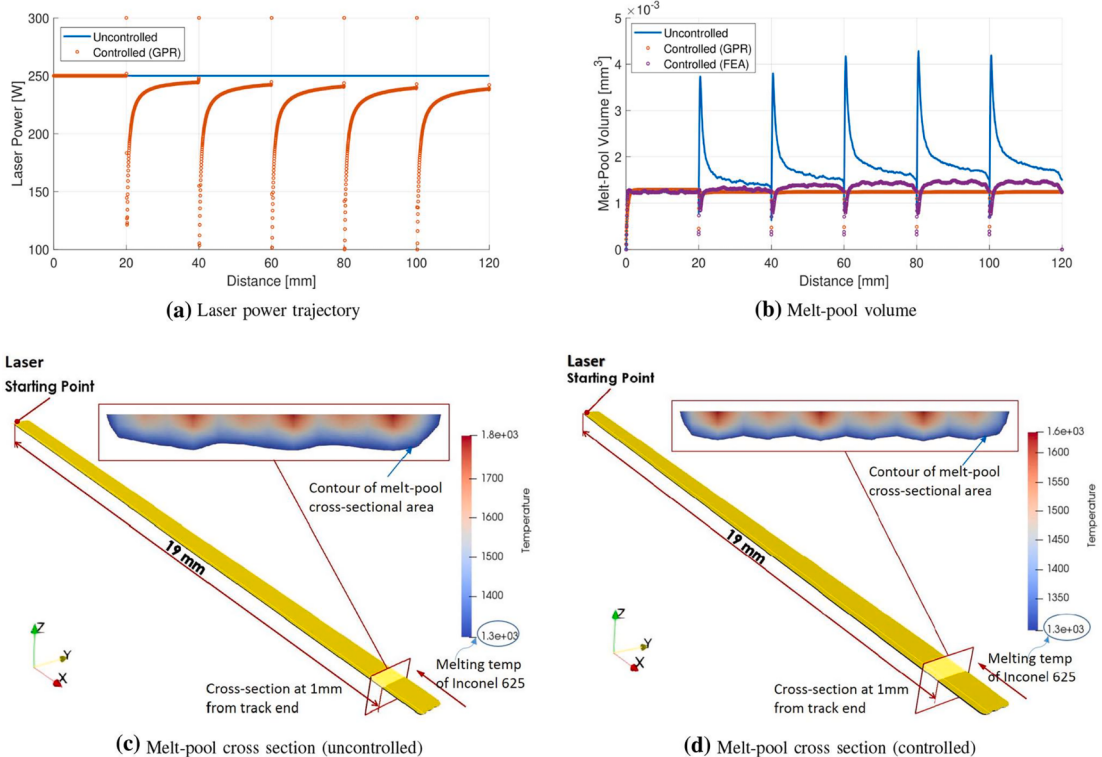


**Fig. 20.** Control performance for a six-track with length = 20mm under the laser scan speed of 600mm/s [217].

Navier–Stokes and energy conservation equations on a set of collocation points. They demonstrated that their PINN model is capable of predicting temperature and melt pool dynamics using a moderate number of labeled datasets, as depicted in Fig. 21. However, the model developed in their study was oversimplified and did not reflect the complexity of metal AM processes, as free-surface deformation of the melt pool, evaporation phenomenon, and ambient gas phase were not considered in the developed PIMT model. Employing multi-phase Navier–Stokes equations modified by missing phenomena (e.g., evaporation) to capture the heat loss, liquid fraction change, and fluid motion and applying additional PDEs (e.g., convection equation of level set and volume of fluid approach) used in the previous studies [219,220] could be a great continuation of Zhu et al. study [218].

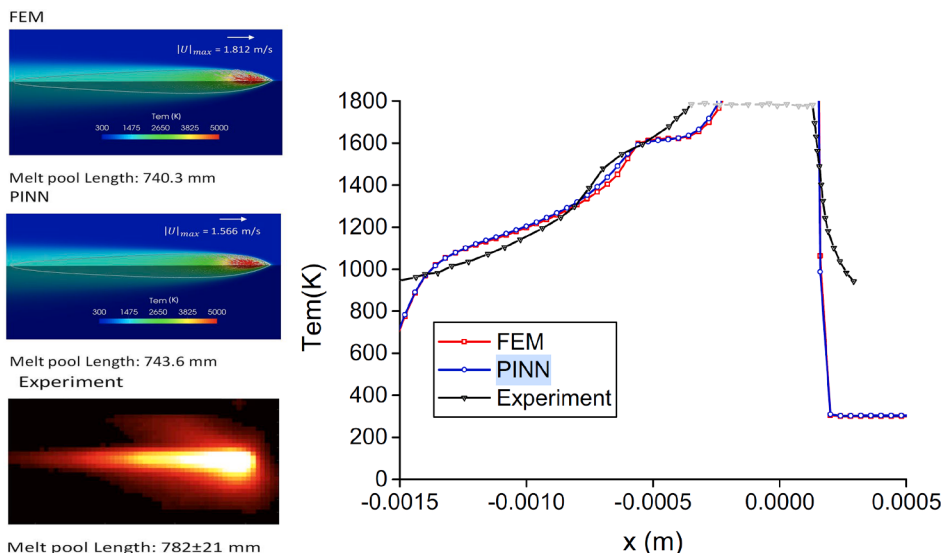


**Fig. 21.** Comparison of the predictions of the temperature and melt pool fluid dynamics of FEM, physics-informed neural network, and experiment (laser power of 195W and scanning speed of 0.8m/s at quasi-steady state. [218].

Selecting the scanning strategy based on the previous thermal history may not be practical from in-situ data alone. However, physics-informed models could assist to make it possible. Ren et al. [221] developed a PIMI model using an FE model to map the temperature field and scanning pattern traced for material deposition for every unit of the simulation step, as depicted in Fig. 22. Extracting this time-sensitive deposition information was critical in making a PIMI model, as this model is not easily achievable from in-situ temperature data alone. In another study [162], the same authors employed an RNN approach for developing a PIMI model to predict the thermal distribution of the next layer using the thermal field of two previous deposited layers and the candidate scan strategy. The temperature distribution predicted using the PIMI model is further employed to select the most suitable scan strategy for the next layer, which minimizes the local heat accumulation during the deposition. The process continues until the fabrication is complete.

### 3.1.2. Classification

**3.1.2.1. Conventional models.** ML classification approaches have been mainly used to detect defects and anomalies in the AM field. Mahmoudi et al. [222] developed a system to detect printing process deviations by capturing the in-situ thermal field of melt pools during fabrication. As depicted in Fig. 23, a similar approach was taken in a study by Seifi et al. [223] to detect the thermal-defect relationship in real-time manufacturing, as there is a direct relationship between the thermal history of the 3D-printed part and its microstructure. To identify this relationship, the highly dynamic thermophysical AM process captured by a pyrometer camera during manufacturing was characterized by developing a tensor-based modeling approach. The key layerwise signature features were extracted from the melt pool images by multilinear principal component analysis (MPCA) and these features were employed to predict the overall quality of the deposited layers using an SVM classifier.

Acoustic emission was also used as the input of an LR model to detect two types of primary defects (i.e., crack and porosity) in a study by Gaja et al. [224]. The results showed the high potential capability of acoustic emission for assessing the overall deposition quality and identifying defects, as indicated in Fig. 24. Although the models developed in Gaja et al. study [224] revealed a promising accuracy in detecting defects, their model should be further extended to cover other types of defects, such as balling, lack-of-fusion, etc. To do this, the LR model employed by Gaja et al. [224] may not be capable to be used in non-binary classification tasks with more than two labels. Thus, this model is not suggested for classification problems. CNN model could be a proper alternative employed in a study by Shevchik et al. [225] to classify the quality of 3D-printed parts into poor, medium, and high through linking acoustic emission of the parts printed at different processing parameters to their qualities. They also used spectral convolutional neural networks (SCNN) [189,226], a recent extension of CNN, to develop a model and compared the accuracy of their CNNs and SCNNs models together. These efforts were also further extended by Ye et al. [227] to link acoustic emission to five different melt states (i.e., underheating, medium

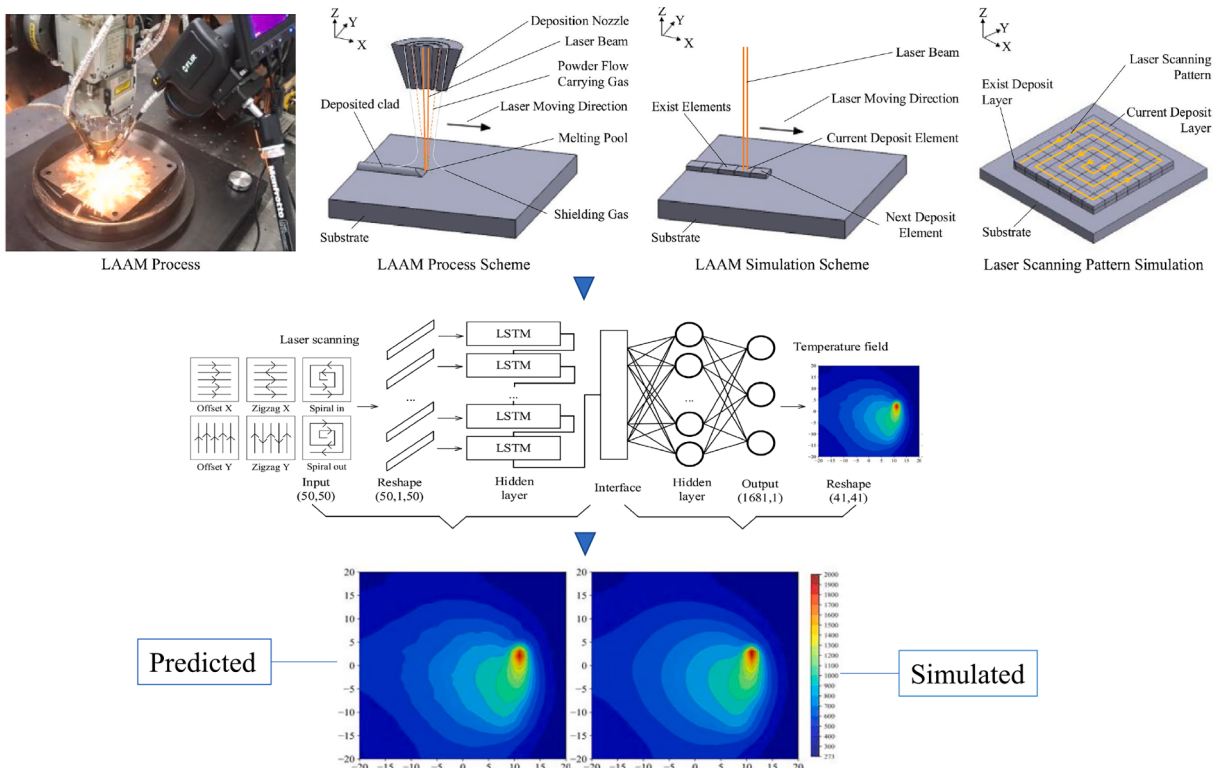
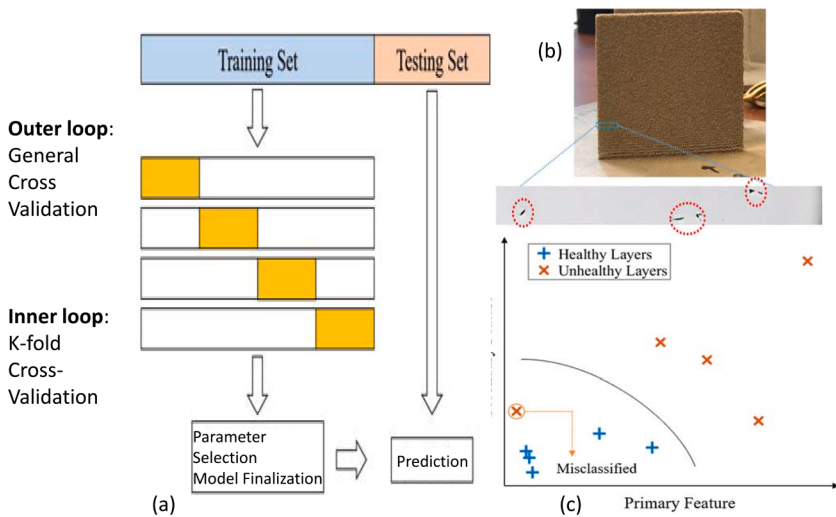
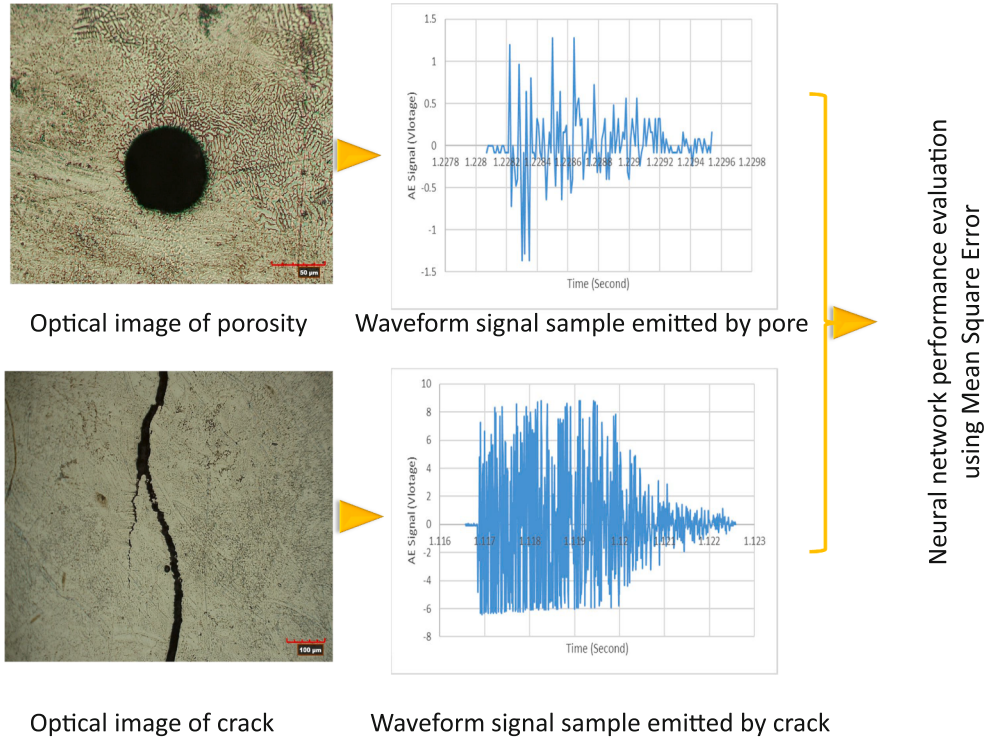


Fig. 22. Applying RNN-DNN model to predict thermal history [221].



**Fig. 23.** (a) A general overview of parameter selection using cross-validation (b) the part with an unhealthy layer, which includes pores, and (c) one iteration of cross-validation in a study by Seifi et al. [223].



**Fig. 24.** Developing ANN model using acoustic emissions in a study by Gaja et al. [224].

underheating, normal, medium overheating, and overheating) formed at different processing parameters using an SVM model. The results showed a fairly high accuracy if all the acoustic emission features are used, and no PCA or FDA dimensionality reduction is conducted for data dimensionality reduction, as these dimensionality reduction methods worked more like a feature extraction method rather than real feature selection in their study.

Linking the morphology of the 3D-printed parts to the defect formation is another way to evaluate the overall quality of deposited layers. Gobert et al. [228] used SVM to detect defects on a staircase cylinder by labeling different defects (i.e., porosity, incomplete fusion, crack, or inclusion). To develop such a model, multiple images were collected at each printed layer and multi-dimensional visual features were extracted and evaluated using a binary classification technique. The regions were then categorized as either a

defect or a nominal build condition. The true location of the defects and nominal build areas were then obtained using a CT scan [47], which was then transferred into a layerwise image domain and fed into the classifiers. These steps are indicated in a flowchart in Fig. 25. Khanzadeh et al. [16] developed an ML framework to establish a relationship between the melt pool morphological characteristics and defects in the microstructure, as indicated in Fig. 26. They employed thermal images to find the melt pool profile and functional principal component analysis to extract the critical features of the melt pools, which are responsible for the majority of the variations in the melt pool. They then used this information to train different ML models (i.e., KNN, SVM, DT, DA), predict defects in the AM parts, and compare the accuracy of these models using the highest rate of accurately classifying melt pools ( $M_1$ ) and lowest rate for incorrectly identifying normal melt pools as pores ( $M_2$ ) as listed in Table 2. Similarly, the type and severity of porosity have been linked to physically intuitive process signatures (i.e., melt pool length, temperature gradient, and ejecta or spatter characteristics), which were extracted from melt pool images, using relatively simple ML models (KNN, LR, and SVM) in a study by Smoqi et al. [229]. The accuracy of these models was then compared with a more complex ML model (i.e., CNN), which directly used raw melt pool images. This procedure was indicated in Fig. 27. The results indicated that the relatively simple ML models trained with pragmatic physically informed melt pool shapes are as effective for defect prediction as using a complex CNN model. In another study [230], a dense convolution network (DenseNet) model was selected among four different models (i.e., AlexNet, GoogLeNet, ResNet, DenseNet) due to better distinguishing information than other models to predict the relationship between the melt pool shape and melt pool states (i.e., normal melting, incomplete melting, and discontinuity melting states) as depicted in Fig. 28. CNN was also employed to classify the melt pool size, which helps detect irregular melt pool formation, without considering spattering using in-situ melt pool monitoring in a study by Yang et al. [231] and detected defects in 3D-printed parts by processing the geometrical anomalies in a study by Khan et al. [232]. The model developed in the latter study integrated the concepts of image processing-computer vision and machine learning and evaluated the effect of various parameters (i.e., input size, batch size, validation split, class mode, activation function, optimizer, steps per epoch, number of epochs), affecting the accuracy of the model as depicted in Fig. 29. Similar to all other conventional data-driven methods, their model requires a large dataset and can be further optimized by enabling defect detection in the vertical plane and by classifying the cause of the defects. In detection and classification problems, CNN is the most common approach widely used in the AM field [233].

In another attempt [234], the layerwise optical images of the powder bed fusion were obtained during manufacturing. Theoretical and multifractal features were extracted during layer-by-layer deposition from each image and linked to the process parameters using several ML classifiers (i.e., SVM, complex tree, LDA, KNN, bagged trees, and ANN) to identify the effect of these parameters on the porosity formation. Also, the ANNs approach was used to find the relationship between the beam power, melt pool shapes, and flaws [235]. Similar to regression problems, linking processing parameters to the parameters, determining the quality of the 3D-printed parts requires a large dataset. Preparing a large dataset mined from a large number of publications is one solution, which was employed by Hertlein et al. [236]. They employed a Bayesian network to link laser power, scan speed, hatch space, and layer thickness to relative

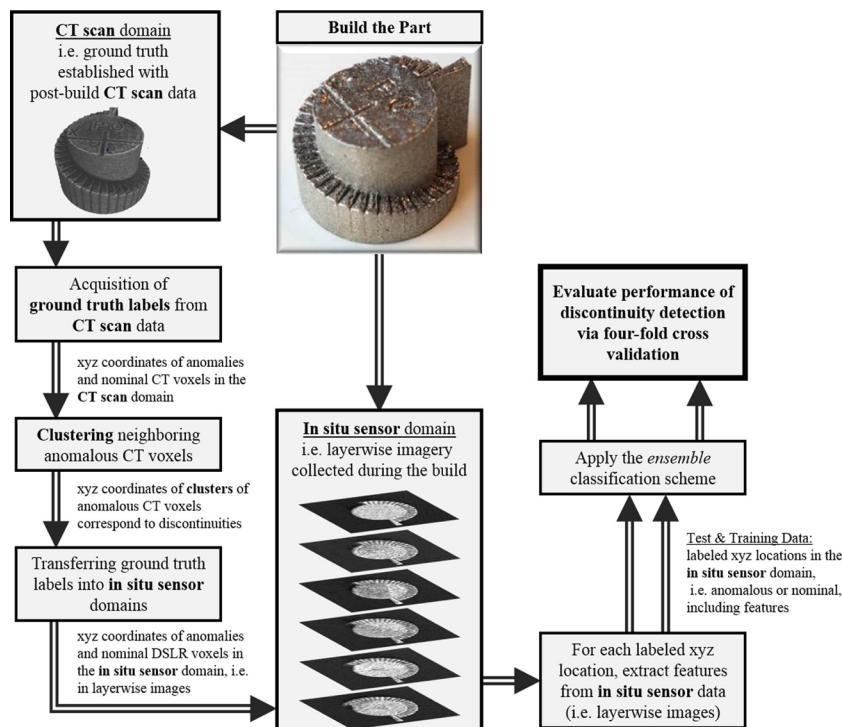


Fig. 25. Flowchart of the steps taken for discontinuity detection in a study by Gobert et al. [228].

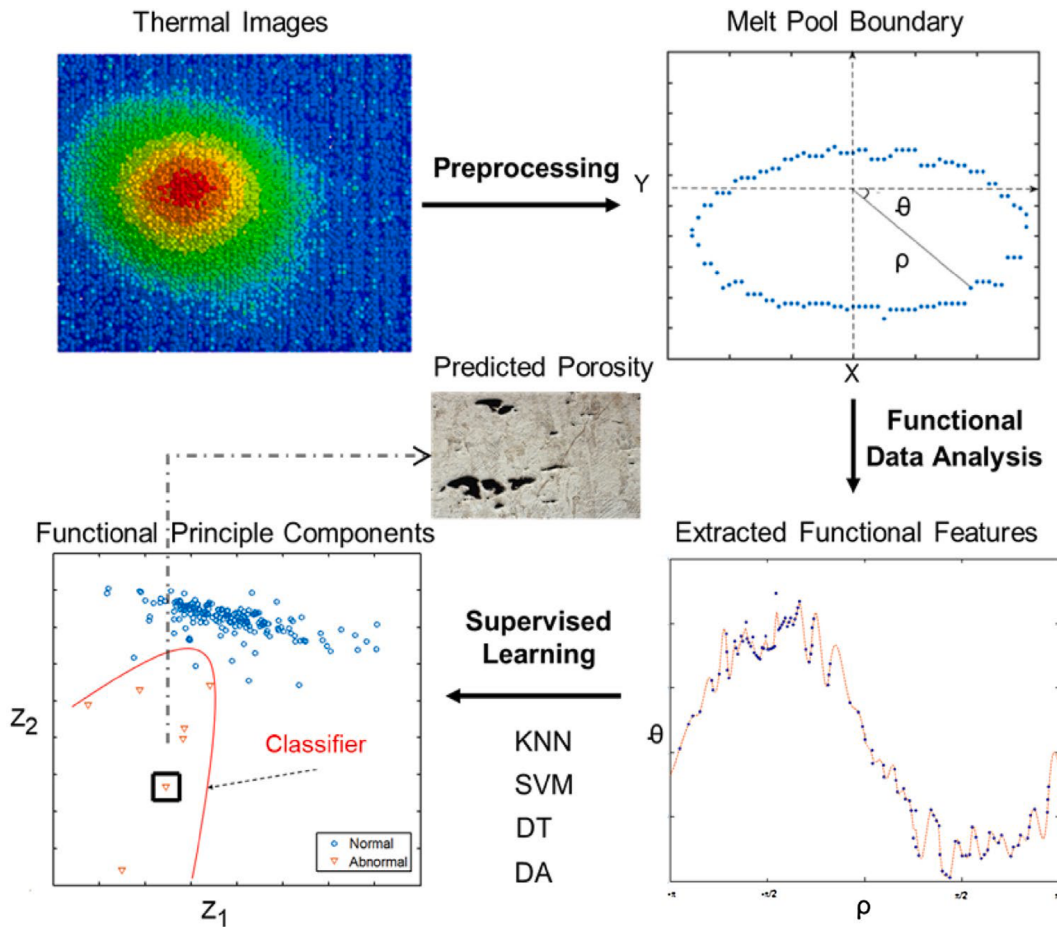


Fig. 26. Demonstration of porosity prediction procedure using supervised ML [16].

density, hardness, ultimate tensile strength in two directions, and surface roughness. Creating a large dataset may help to cover more input parameters, but many other significant input parameters (e.g., laser type, spot size, powder diameter, preheating, etc.) are still missing.

In defect detection problems, linking process conditions to defects, the first step toward in-process quality assurance, is significant. The model trained with melt pool dimensions may be able to accurately classify the melt pool state. However, considering the melt pool images as the input parameters rather than the processing parameters is quite time-consuming and costly, as extra steps are added to prepare these micrographs. It is also worth mentioning that although physically meaningful inputs (e.g., temperature distribution, the morphology of melt pool) are used as the inputs of these relatively simple ML models, the temptation of calling these models PIML should be rejected, as these models reviewed above are not constrained by laws of physics.

**3.1.2.2. Physics-informed Models.** The ML models developed earlier for classification problems are well known for their exemplary performance to learn complex process-property correlations. However, these models are limited to machine settings and ignore the physical laws of the problem. If the machine, components, or range of processing parameters change, the dominant laws of physics may change due to these changes, and consequently, these models fail. In classification problems, developing PIML models is an appropriate solution to obviate such a problem using ML models, which are employed more often in recent publications. In a study by Liu et al. [237], porosity sizes categorized into three levels (i.e., pass, flag, and fail) were correlated with the laser-related physical effects instead of machine setting parameters using six different ML models. The accuracy of the PIML model developed in their study was compared with the accuracy of an ML model that directly used machine setting parameters. They concluded that the ML model developed using the machine setting parameters has nearly the same performance as the PIML model, as depicted in Fig. 30. However, the PIML model does not rely on the machine setting and can be applied to predict quality in different machines and settings.

Mechanistic input parameters predicting balling defect [238,239] using 6 out of 10 most important processing parameters and material properties is a good example of the PIML model employed by Du et al. [240] summarized in Fig. 31. Also, the thermal history of an AM part was predicted from the datasets containing generic and engineered features constructed based on the physics of the underlying thermal process using an extremely randomized tree model in a study conducted by Ness et al. [241]. In their work, the

**Table 2**

The relationship between the model, data, and accuracy.

Reference	Model	Data size	Accuracy
Ren et al.[221]	DNN	47152	94.15%
	CNN		75.4%
	RNN		94.84%
	DNN-RNN		98.09%
Ren et al.[162]	RNN	340	95.05%
Khanzadeh et al. [62]	SOM	1564	96 %
Khanzadeh et al.[16]	QDA	2800	$M_1 = 98.21, M_2 = 1.79\%$
	LDA		$M_1 = 71.15\%, M_2 = 0.1\%$
	DT		$M_1 = 90.74\%, M_2 = 0.3\%$
	SVM		$M_1 = 90.96\%, M_2 = 0.35\%$
	KNN		$M_1 = 98.44\%, M_2 = 0.19\%$
	KNN		$F1-score = 0.97$
	SVM		$F1-score = 0.85$
Smoqi et al.[229]	LR	22400	$F1-score = 0.83$
	CNN		$F1-score = 0.94$
	Genetic algorithm	166	90%
	FFNN	19.9 million	99%
Fetni et al.[213]	ANN	4 million	99%
Roy et al.[214]	ANN	26000 (training)	Error < 5%
Ren et al.[217]	GPR	$data_{numerical} = 8010$ $data_{experimental} = 64$	$RMSE_{largest} = 0.006mm^2$ $RMSE_{largest} = 0.0095mm^2$
Yang et al.[231]	CNN	5689	91%
Kwon et al.[235]	ANN	13200	Error = 1.1%
Akbari et al.[101]	RF	2200	88.41%, AUC-ROC = 98%
	XGBoost		$R^2 = 99.62\%$ , MAE = 10.92
	NN		$R^2 = 95.8\%$ , MAE = 20.54
	GPR, SVM, LR, GB, Lasso, Ridge		
	Lasso		Average Rank = 7
	Ridge		Average Rank = 8
	ElasticNet		Average Rank = 7
	SVR		Average Rank = 3.7
	KNR		Average Rank = 6
	ANN		Average Rank = 2
Yuan et al.[230]	DenseNet	80	99.3%
Gaja et al.[224]	LR	37	MSE = 1.72
	ANN		MSE = 1.70
Ye et al.[227]	SVM	34	77.99%
Hertlein et al.[236]	BN	349	-
Liu et al.[237]	LR, GPR, SVR	549	Error = 10–26%
Ren et al.[247]	KMC, LSTM-Autoencoder	4290	$MSE_{LSTM\_encoder}=6.9 \times 10^{-4}$
Ye et al.[248]	DBN	+ 18000	95.93%
Ye et al.[249]	DBN	-	83.4%
Okaro et al.[250]	GMM	49	77%
Yuan et al.[251]	SLM	1000	Classification: 92% Regression: 93%

domain knowledge provided the laws of physics and made the model PIMI that corrects, enriches, and enhances the data. They demonstrated that simulation-to-simulation predictions are possible with high accuracy for the transferability of thermal histories between a variety of patterns, geometries, meshes, and power intensities, which proves the potential of PIMI in AM. A summary of the supervised models reviewed here is listed in Table 3.

In addition to the resource-intensive nature of conventional ML models, the latency of detection and poor generalizability are common drawbacks of applying these models in the AM field [242–244]. The data recorded continuously using heterogeneous sensors need to be transferred to a data analysis procedure, which causes an inherent latency during data analysis. Also, data-driven approaches developed using simple geometries (e.g., cubes and cylinders) may not be generalizable to complex, practical AM parts. One way to resolve these issues in the classification problem is to employ a PIML approach. A PIMI model was developed by twinning in-situ melt pool temperature measurements with a mechanistic-based thermal model, predicting the thermal history of the part updated layer-by-layer to detect flaw formation in a study conducted by Yavari et al. [245]. Facilitating precise and interpretable detection of flaws and obviating the need of transferring sensor signatures to a separate data analysis algorithm, which leads to precluding the inherent latency in data-driven flaw detection, are the key outcome of employing the PIMI model.

Another significant research thrust in AM is to develop online ML methods for in-situ monitoring of the AM processes and link these data to a feedback control system that adjusts experimental parameters on the fly. Developing models capturing the complexity of AM processes is now achievable through the use of high-performance computers. However, taking these data into the production environment is still a challenge, which can be achieved by leveraging both numerical and experimental data from a structured database. Developing online PIML models by a combination of numerical and experimental data suggested by Yan et al. [220] may be a great

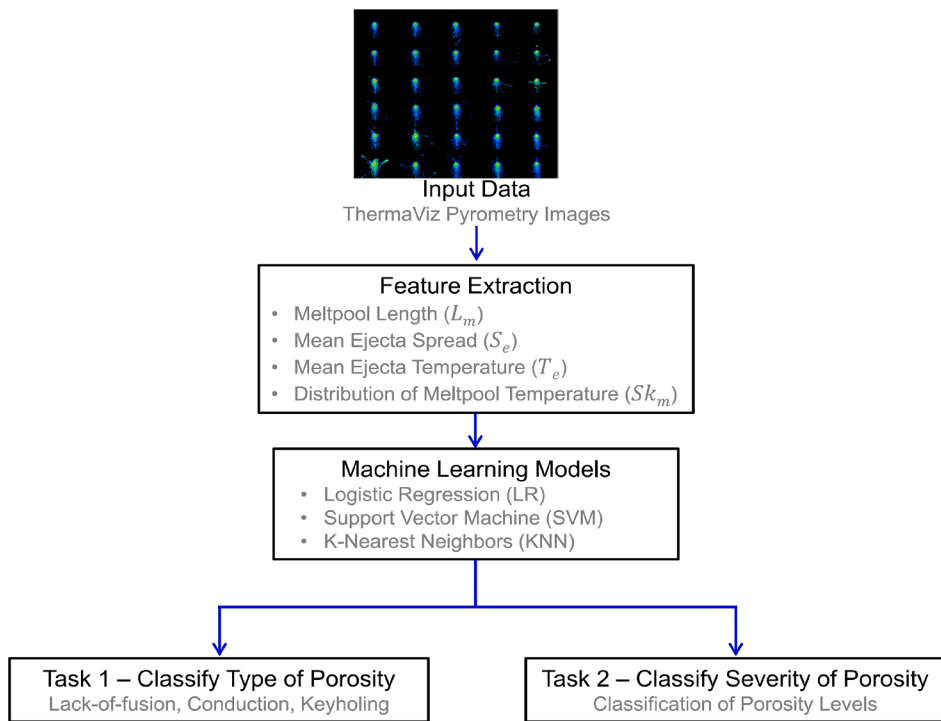


**Fig. 27.** Schematic representation of data processing and machine learning approach used in Smoqi et al. [229] work.

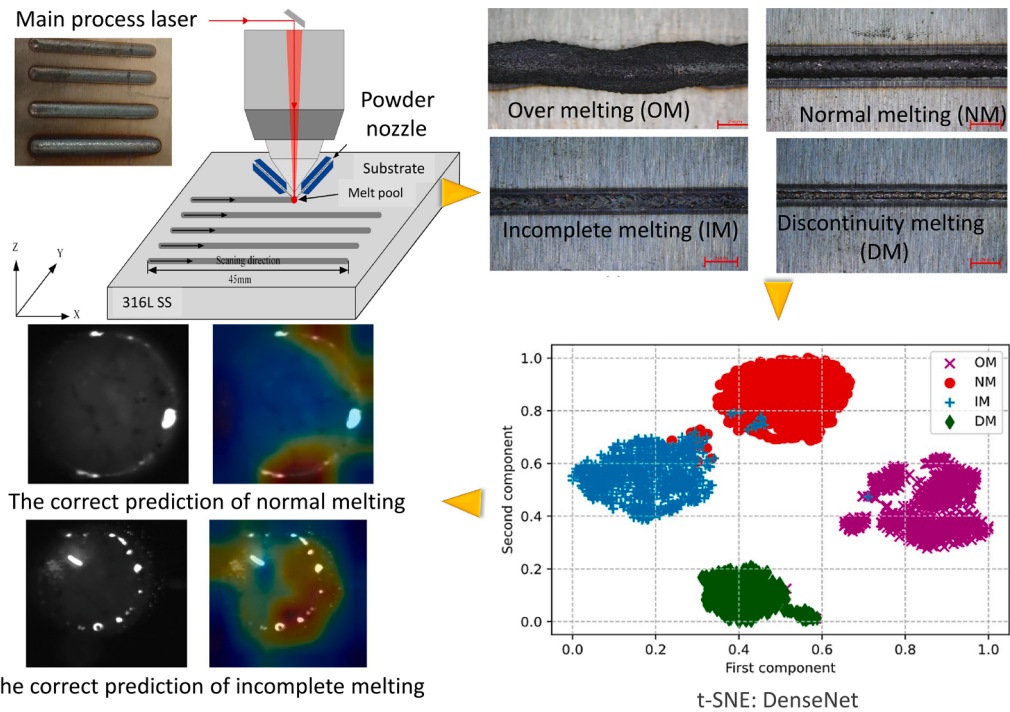


**Fig. 28.** The proposed in-situ monitoring method by Yuan et al. [230].

solution to online monitoring of the AM processes and modifying them based on the live feedback collected during the process, as indicated in Fig. 32. Towards developing such a framework, online ML models have been developed to rapidly detect surface defects by developing an in-situ point cloud processing that enables live surface monitoring with no need for sensor intermittence [246].

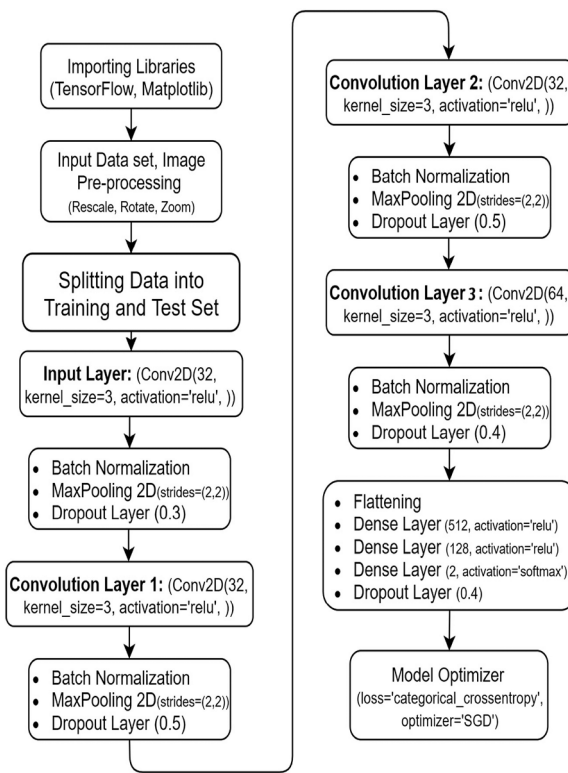


Fig. 29. Structure of CNN code employed in a study by Khan et al. [232].

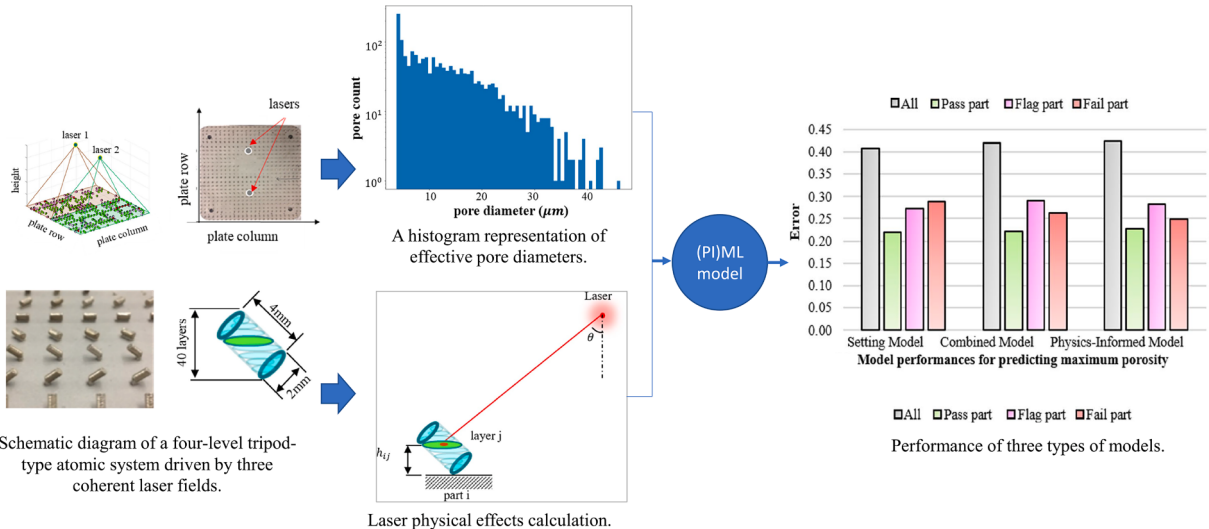


Fig. 30. Summary of developing ML and PIML models in a study by Liu et al. [237] work.

However, involving more physical phenomena in the problem by including micro-scale models (e.g., electron or photon material interactions causing heat generation), mesoscale models (e.g., individual power particle evolution driven by fluid flow and thermal diffusion, surface tension force, Marangoni effect), and macro-scale models (e.g., FEA codes to resolve the fabrication process of a complex product) could further improve the performance of the model toward developing online PIML models.

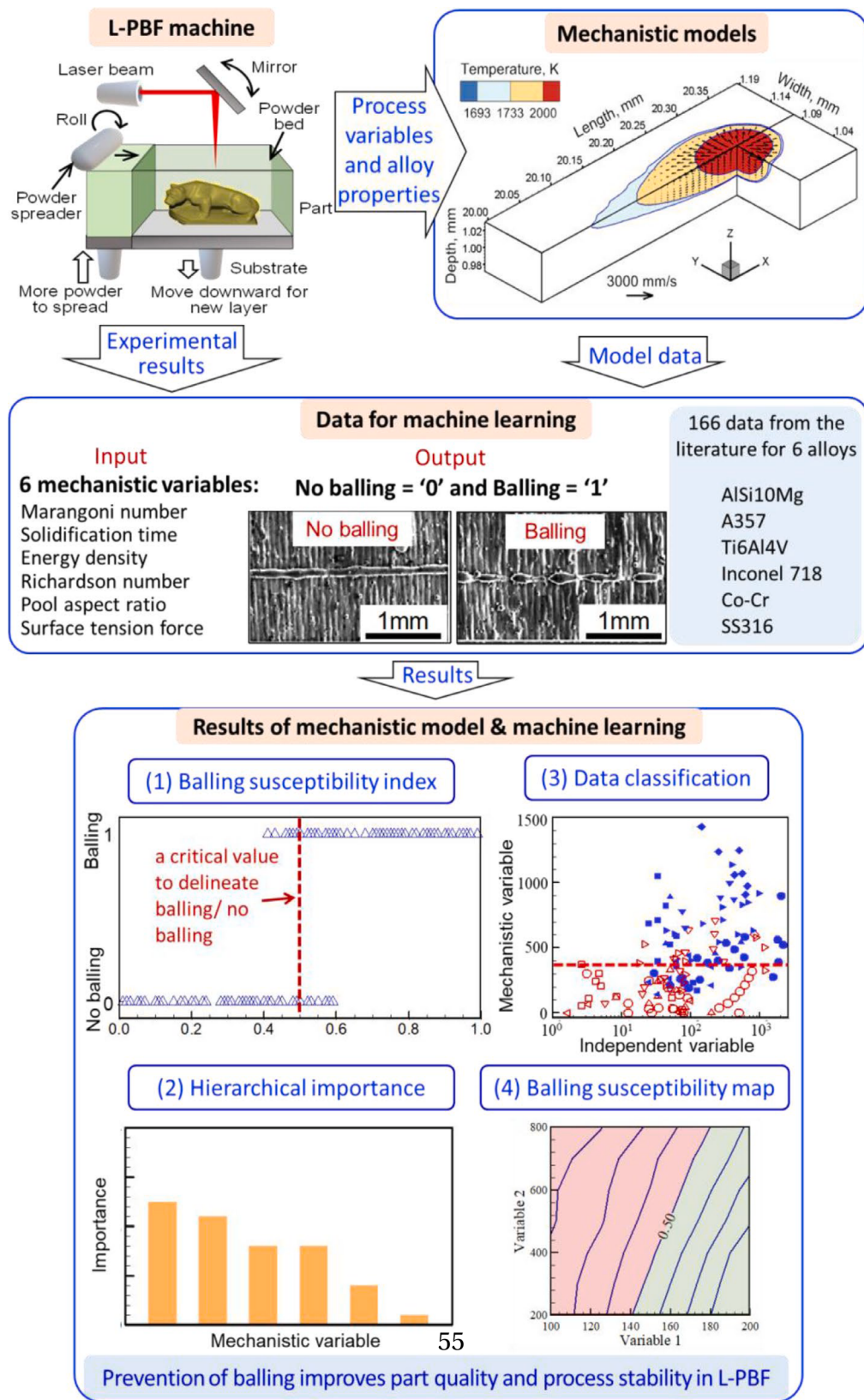


Fig. 31. Schematic representation of the approach proposed and used in Du et al. [240] work.

**Table 3**

Supervised learning.

Reference	AM process	Materials	Input	Output	ML method
Rong-Ji et al. [119]	SLS	-	$L_t$ , BP, $h$ , $v$ , $t_s$ , $T_s$ , $F$	Material shrinkage	ANNs
Tran et al. [252]	SLM	SS316L	BP, $v$ , LSS, $l_t$ , PM, PSD	Depth of melt pool	ANNs
Lee et al. [122]	SLM	alloy 625, 718	BP, $v$ , LSS, $l_t$ , PSD	MP dimensions	Br, Kr, LR, NN, RF SVM
Schmid et al. [253]	SLM	AlSi10Mg	BP, $v$ , $h$	MP dimensions	CNNs
Chen et al. [254]	SLM	TiB <sub>2</sub> , AlSi10Mg	BP, $v$	MP dimensions	ANNs
Meng and Zhang [255]	SLM	SS316L	BP, $v$	Remelted depth	GP
Tapia [100]	SLM	SS17-4 PH	BP, $v$	Porosity, $\rho$	GP
Olleak and Xi [59]	SLM	Ti-6Al- 4v Alloy	BP, $v$ , $\eta$ , LSS	MP	
dimensions	GP, FEM				
Kamath [29]	SLM	SS316L	BP, $v$ , $\eta$ , LSS	Depth of MP	GP, MT
Mozaffar [64]	DED	SS316L	BP, $v$ , $t_s$ , GS, S	Thermal history	RNN
Zhang [58]	DED	Nickel-718	BP, $v$ , $T_s$ , $l_t$ , $l_w$	Thermal history	xGBoost, LSTM
Singh et al. [256]	SLM	Bronze	BP, $v$ , $h$	$\rho$	MLP
Tapia et al. [257]	SLM	SS316L	BP, $v$	Depth of MP	GP
Caiazzo and Caggiano [258]	DED	2020 Al alloy	BP, $v$ , PFR	MP dimensions	ANNs
Lu et al. [259]	DED	SS316	BP, $v$ PFR	Depositionheight	ANNs, LS-SVM
Aoyagi et al. [27]	EBM	COCr	BP, $v$	Porosity	SVM
Khanzadeh et al. [16]	DED	Ti-6Al-4 V	Thermal history	Porosity	DT, KNN, SVM, DA
Jafari-Mardani et al. [260]	DED	Ti-6Al-4 V	Thermal history	Porosity	KNN, NN, SOEDNN
Kappes et al. [261]	SLM	Inconel 718	PP, PO, FRP	Porosity	RFN
Ren et al. [221]	DED	-	TS, $t_s$ , geometry shape	Thermal history	RNN-DNN
Ren et al. [162]	DED	SS316L	TS	Thermal history	RNN
Smoqi et al. [229]	SLM	ATI 718Plus	MP dimensions, T	Porosity	KNN, SVM, LR, CNN
Pham et al. [212]	DED	M4 high-speed steel	BP, t	Thermal history	FFNN
Fetni et al. [213]	DED	316L SS	$x, y, t, x_L, y_L, d_x, d_y$	Thermal history	FFNN
Roy et al. [214]	FFF		$d, L_g$	Thermal history	ANN
Ren et al. [217]	SLM	Inconel 625	BP, Thermal history	MP dimensions	GPR
Zhu et al. [218]	-	Inconel 625	BP, $v$	MP dimensions, Thermal history	NN
Yang et al. [231]	SLM	Inconel 625	TS	MP dimensins	CNN
Kwon et al. [235]	SLM	SUS316L	MP images	$\rho$	ANN
Ye et al. [208]	DED	SS316	BP, $v$ , PFR, W, T	MP depth and height	ANN
Yuan et al. [230]	DED	SS316	Melt pool shapes	MP state detection	DenseNet
Mahmoudi et al. [222]	LPBF	SS	Thermal history	Anomaly detection	GP
Gaja et al. [224]	LMD	Ti-6Al-4 V	Acoustic emissions	Defect detection	LR, ANN
Gobert et al. [228]	SLM	SS GP-1	Layerwise optical images	Defect detection	SVM
Seifi et al. [223]	DED	Ti-6AL-4 V	Thermal history	Anomaly detection	SVM
Ye et al. [227]	SLM	SS 304L	Acoustic emissions	Defect detection	SVM
Hertlein et al. [236]	SLM	316L	$P, V, h, l_t$	$\rho$ , hardness, roughness, ultimate tensile strength	BN
Shevchik et al. [225]	SLM	SS 316L	Acoustic emissions	Anomaly detection	CNNs, SCNNs
Liu et al. [237]	SLM	Inconel 718	LED, LR, PI	Porosity	LR, GPR, SVR

Powder layer thickness ( $l_t$ ), beam power (BP), melt pool width (W), distance (d), hatch spacing (h), length of geometry ( $L_g$ ) scan speed (v), interval time ( $t_s$ ), surroundings temperature ( $T_s$ ), Temperature (T), and scanning mode (F), laser spot size (LSS), laser type (LT), powder material (PM), powder size distribution (PSD), depth of melt pool (DMP), remelted depth (RD), melt pool dimensions (MPD), material shrinkage (MS), cross-sectional bead image (CSI), Pressure intensity PI, laser radiation (LR), absorptivity ( $\eta$ ), toolpath strategy (TS), geometric size (GS), geometric shape (S), spread of the ejecta (SE), layer width ( $l_w$ ), density ( $\rho$ ), wire/powder feed rate (P/WFR), arc voltage (AV), nozzle to plate distance (NPD), Energy density (E), part position (PP), part orientation (PO), fraction recycled powder (FRP), laser position ( $x_L, y_L$ ).

### 3.2. Unsupervised learning

Unsupervised learning is employed to identify underlying patterns in the input data [166] with minimal human supervision. Developing in-situ monitoring technologies is critical for better understanding defect formation, assessing the process performance, and assuring the quality, integrity, and safety of AM parts. Unsupervised learning methods along with in-process monitoring provide the capability of early detection of defect formation. Unsupervised learning eliminates the need for person-hours to label the data, but this approach may still need classification after clustering. Table 4 summarized a list of unsupervised ML algorithms used for detecting defects using data clustering.

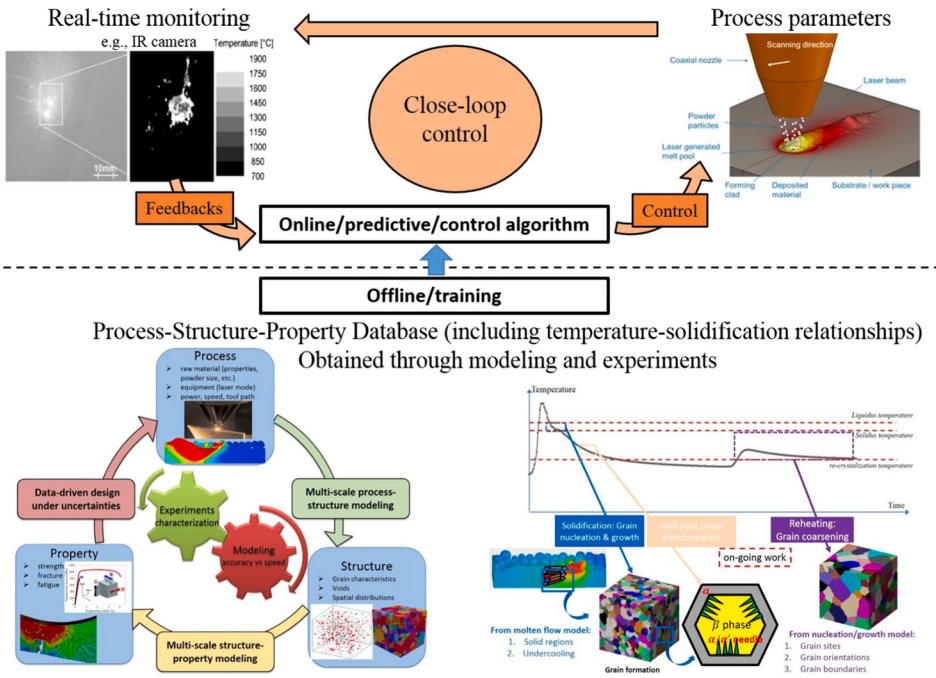


**Fig. 32.** Framework for achieving high-performance parts using online PIML methods suggest by Yan et al. [220].

**Table 4**  
Unsupervised learning.

Reference	AM process	Materials	Input	Output	ML method
Donegan et al. [285]	SLM	Ti-6Al-4	Thermal history	Process history	KMC
Tan et al. [286]	SLS	-	IR images	Anomaly detection	EDS
Scime and Beuth [49]	SLM	Inconel 718	IR images	Anomaly detection	KMC
Scime and Beuth [279]	SLM	-	powder bed images	Anomaly detection	KMC
Wu et al. [200]	-	-	Optical image	Anomaly detection	Not specified
Pagan et al. [287]	-	IN625	Diffraction images	Anomaly detection	LLE
Grasso et al. [273]	SLM	AISI	Optical images	Defect detection	PCA
Khanzadeh et al. [62]	DED	Ti-6Al-4 V	Thermal history	Porosity	SOM
Scime and Beuth [49]	DED	Inconel 718	Thermal history	Porosity and balling	BoW
Senill et al. [272]	SLM	Ti-6Al-4 V, Inconel 718, Haynes 282	2D and 3D pores	Porosity type	KMC
Taheri et al. [265]	DED	Ti-6Al-4 V	AE	Process conditions	KMC
Gaja et al. [263]	DED	Ti-6Al-4 V and H13 tool steel	AE	Crack, porosity	KMC
Ren et al. [247]	DED	Al7075 alloy	BP, v, PFR	Porosity	KMC
Ye et al. [248]	SLM	SS 304	AE	Defect pattern	DBN
Ye et al. [249]	SLM	SS 304	NIR image	Defect pattern	DBN
Gracia-Moreno et al. [274]	DED	Al-5083	Optical microscope images	Defect pattern	SOM

### 3.2.1. Clustering

One of the significant challenges in the AM processes is the lack of a systematic classification of defects, effective characterization of process conditions during manufacturing, and the unavailability of an appropriate approach to link the variations in the processing parameters to these defects [262]. One way to evaluate the quality of the 3D-printed parts is to obtain acoustic emissions during manufacturing. In one attempt [263], the acoustic emission was recorded during layer-by-layer material deposition and the silhouette value [264] was calculated for different numbers of clusters. It was found that the largest silhouette value can be obtained if the number of clusters is set to two, which indicates two classes of defects (i.e., porosity and crack) exist in the data. Then, the KMC algorithm, which aims to minimize the distances between all the vectors of a cluster and its center and maximize the distance between the centers of the clusters, was employed to analyze the AE signals and predict the defect type, as indicated in a flowchart in Fig. 33. More defect patterns were included in a model developed by Ye et al. [248] by gathering the acoustic signals from different defect patterns (i.e., balling, slight balling, normal, slight overheating, and overheating) formed during manufacturing at various energy densities. The relationship and hierarchical information of the raw acoustic signals were extracted using this approach with no need for preprocessing and feature extraction from the signals. Taheri et al. [265] analyzed the relationship between the process conditions (i.e., normal, low powder, and powder spray process conditions) and the acoustic emissions through in-situ monitoring of the DED process and classification of acoustic emission data using KMC. Although the model can fairly accurately correlate the processing

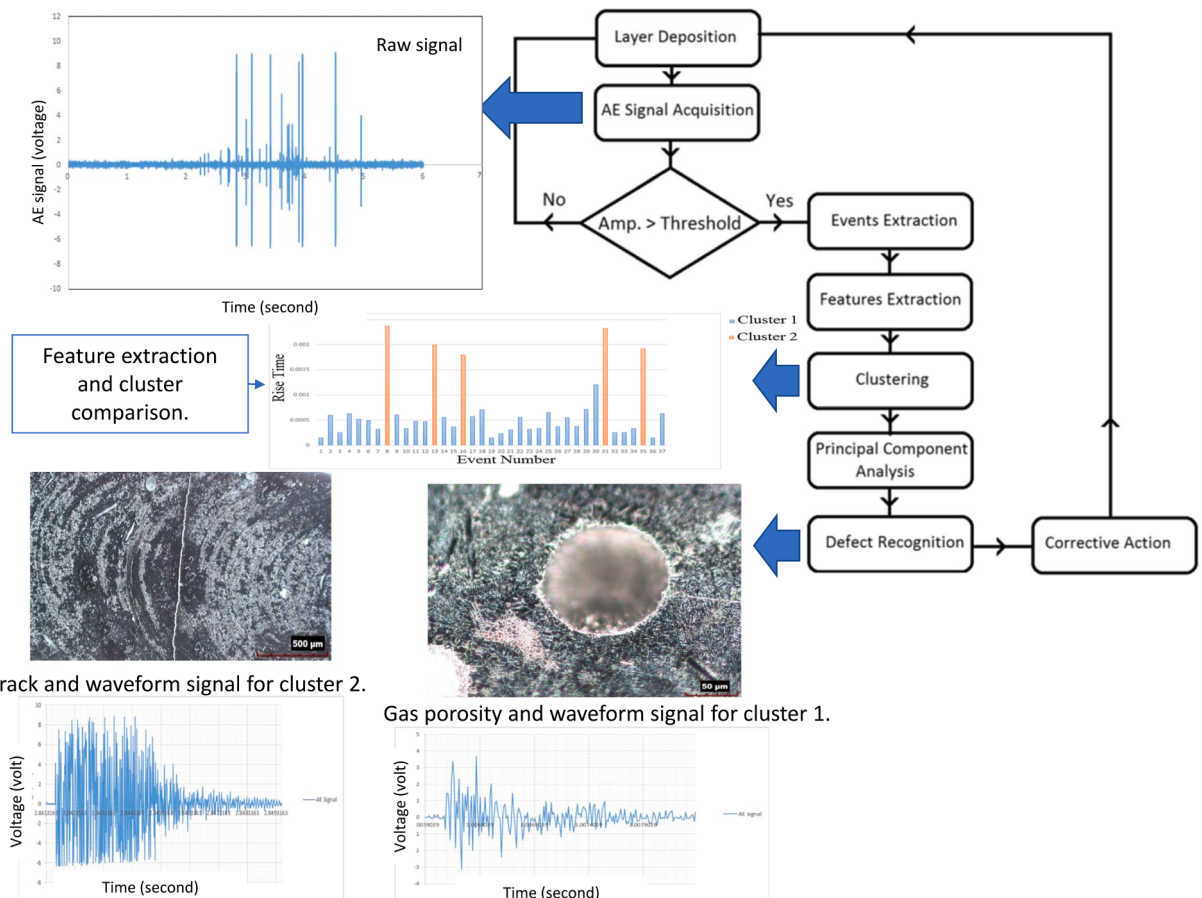


**Fig. 33.** Step-by-step operations used to perform acoustic emission analysis in a study by Gaja and Liou [263].

conditions to the acoustic emissions, the lowest classification accuracy occurred at low beam power process conditions. Different behavior of acoustic patterns due to the complexity of thermal behavior could be one reason for low classification accuracy at low beam power.

The inputs used in the clustering approaches could also be in the form of spectra emissions, linking the process parameters to the quality of the 3D-printed parts. The intensity and shape of spectra emissions indicate the concentration and plasma condition are directly related to the process parameters and the quality of 3D-printed parts. For instance, the spectra emissions were collected during the manufacturing process for the parts printed at varying laser power, scan speed, and powder delivery rate, and the spectra features were extracted using an LSTM-autoencoder. These features were then employed to classify the quality of the part based on the processing parameters using a KMC model [247].

One of the most popular data types used to train and develop an unsupervised ML model is optical measurements, which have been employed to collect the temperature field, image of the powder bed, and molten pool in the AM process [266,267]. The authors [248] previously developed a DBN model to detect defect type through acoustic signals and applied the same approach in another study [249] to correlate the plume and spatter near-infrared (NIR) images obtained during manufacturing with the melted state and energy density. The accuracy of the model developed using acoustic emission data in ref. [248] was reported higher than the accuracy of the model developed using the NIR images reported in ref. [249].

A convolutional autoencoder (CAE) model [268] (a subset of convolutional neural networks) and an auto decoder [269], which was often used to convert high-dimensional data obtained from images into a simplified reconstructed output, was employed in a study by Silbermann et al. [270] to classify the quality of the 3D-printed parts produced at different processing parameters. To do this, a large number of optical images were segmented and fed into a CAE model and were clustered based on the best gap value technique using a so-called gap statistic method [271]. The clusters were manually scored to represent the lowest to the highest quality, and then these results were applied to the original images to optimize the processing parameters. Although the model indicated the potential of scoring the quality of the part and the traditional parameter optimization, disparities exist between the ML model and the traditional optimization process. This disparity could be due to the limited diversity in the data employed in the image classification.

A rapid pore classification KMC model was developed using two different sources of data, namely 3D pore data collected using the XCT technique and 2D pore data collected using the optical microscopy technique by Snell [272]. The results revealed that KMC is not

suitable to analyze the 2D pore data. Although a fair starting point for 2D pore data clustering was established, more information is needed to reliably classify the data. KMC was found suitable more for analyzing 3D pores (i.e., lack-of-fusion and keyhole pores), as 3D pore data provided more information than 2D pores. KMC was also employed to automatically detect defect onset and spatially identify defects during the in-situ SLM process by identifying the molten areas with different behavior from other sections of the same layer [273]. The proposed approach considered the defects formed due to overheating and could be further extended by considering other defect scenarios. SOM, a neural network-based model (Fig. 34), was employed in a study by Gracia-Moreno [274] to develop an automatic porosity classification method based on the size, distribution, and origin of pores. Porosity formation was also predicted by Khanzadeh et al. [275,62] in the parts using the thermal profile of the melt pools. The authors basically identified pores from thermal profile images by categorizing melt pools into normal and porosity (abnormal) clusters. Porosity cluster includes the melt pools with low or high temperature and irregular shapes, as indicated in Fig. 35. They also compared the results with their previous study [276] considering morphological features of melt pools (e.g., length, width, area, etc.). They concluded that SOM clustering based on morphological features fails to properly distinguish different clusters. This means that the basic features of melt pools may not be sufficient for the identification of defects, and this detection could be performed better by considering the thermal distribution of melt pools as input. Although the authors utilized SOM to differentiate melt pool morphologies, the descriptor of the melt pool shape chosen in their studies was neither scale invariant nor capable of including spatter or vapor plume information. This gap was addressed in a study by Scime and Beuth [49] by incorporating the information about the shape of the melt pool, spatter, and vapor plume to improve the difference between in-situ morphologies. The authors combined the morphology of the melt pools previously collected by the authors [96] with fundamental knowledge of the space process [277]. The space process was analyzed using contemporary computer vision (CV) feature extraction methods [278], which were used to classify anomalies (i.e., recoater streaking, recoater hopping, debris, super-elevation, part failure, incomplete spreading) at the powder spreading [279] and powder characterization [280] stages. Scale Invariant Feature Transforms (SIFT) [281] and Bag-of-Words [192] unsupervised ML techniques linked these data to processing defects previously reported by the authors in ref. [96] using a multi-class SVM model. A flowchart of this methodology is shown in Fig. 36. Several other studies [282,283] evaluated the effect of temperature on the relative density and revealed a relationship between single melt pool events and defect formation. However, little to no studies monitored melt pools over multiple slices, revealing hidden patterns in noisy data. A recent study by Voigt et al. [284] employed photodiode on-axis signal to monitor melt pool condition over multiple slices and concluded density enhancement of the melt pool signal at the edges. This observation, which was obtained by clustering time-series sequences into three classes using unsupervised machine learning revealed that melt pool condition changes particularly close to the edges during the manufacturing of a slice.

According to the studies reviewed in this section, the role of laws of physics in the unsupervised methods is less pronounced, as the inputs of these unsupervised models are mainly categorized into acoustic emissions, spectra emissions, and images. Two first inputs may not be producible through common available numerical methods (e.g., FEM). However, laws of physics, for example, can contribute to developing dimensionless numbers that could be used as the input of an ML model predicting acoustic signals. Also, image-based data can also be generated using laws of physics and fed into PIML models. Working toward developing image-based data with the aid of laws of physics and employing these data to develop unsupervised PIML models could be a promising avenue of research. Also, other types of PIML models (i.e., PIMT, PIMC, PIMA, and PIMO) could still be employed to develop unsupervised PIML models, which could be another promising avenue of research in the field of AM.

### 3.3. Semi-supervised learning

As mentioned, supervised learning ML models require a great number of data labeled for training. Labeling these data is prohibitively time-consuming and costly, particularly when the size of the dataset is massive. More importantly, labeling data is a manual task, which increases the possibility of mislabeling due to human bias. In unsupervised ML models, the data are not required to be labeled. However, unsupervised machine learning is computationally expensive, as all the possibilities are evaluated to find the best pattern among the data. Unsupervised learning ML models are less accurate than supervised learning models, and the user needs to

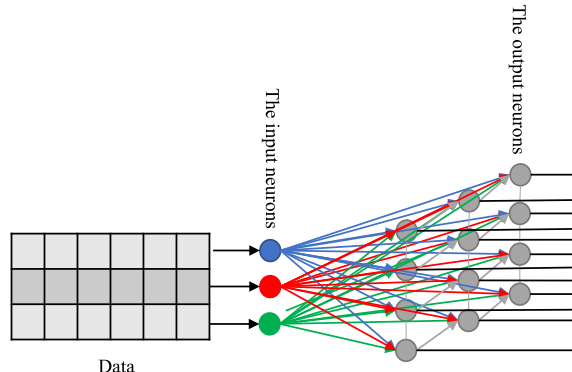
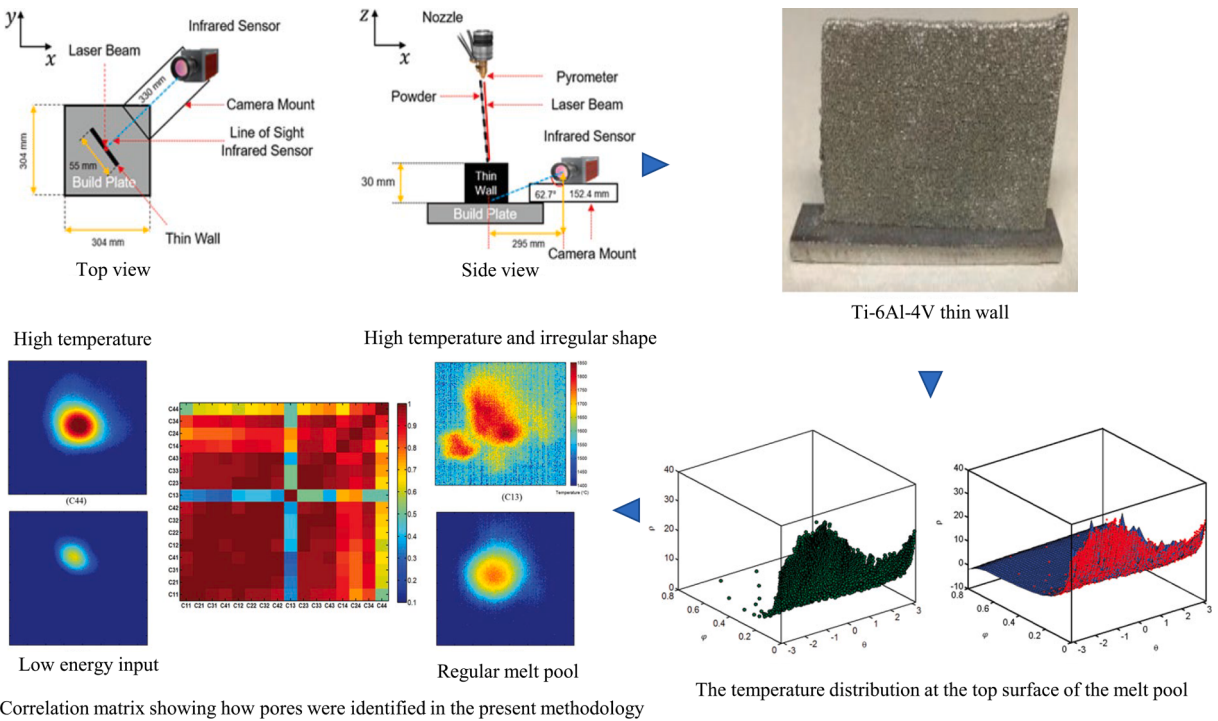


Fig. 34. A sample SOM network.



**Fig. 35.** Predicting pores from thermal profiles [62].

interpret the clusters at the end [166]. To resolve the issues mentioned for both supervised and unsupervised ML models, semi-supervised models are employed. In semi-supervised ML models, a supervised ML model is trained using a small labeled dataset supported by unlabeled data. By adding cheap and abundant unlabeled data along with labeled data in a semi-supervised ML model, the model will no longer have the limits mentioned in both supervised and unsupervised ML algorithms [288].

Despite the great practical value of semi-supervised ML models, These models have been less frequently used in the AM field. In the AM field, it is difficult to collect labeled data, though it is relatively easy to gather unlabeled data. The models developed using the semi-supervised ML approach have mostly been used in defect detection problems. To evaluate the quality of an AM part, a Gaussian mixture model was developed to automatically detect faults in the AM products in a study by Okaro et al. [250]. In their work, a large photodiode dataset was developed to extract key features. The monitoring system set up in their work includes in-situ monitoring and ex-situ labeling methods. To label the ex-situ data as faulty or acceptable, ultimate tensile strength tests were conducted. It was found that the semi-supervised model developed in this study can capture the benchmark results more closely than those obtained using the supervised approach as depicted in Fig. 37. A combination of supervised and unsupervised ML models (i.e., KNN) was also employed as a semi-supervised ML model to classify the printed layers into either drift (hotspot in the layer) or no drift (no hot spot in the layer) in a study by Yadav et al. [289]. Larsen et al. [290] modeled the laser dynamics of the SLM process directly from high-speed images, and the model was tested on various porosity levels and successfully differentiated the optimal processing and defective materials. Semi-supervised CNN was also employed to categorize the quality of the parts into under-melt, beautiful-weld, and over-melt in a study conducted by Li et al. [291]. The model revealed a promising performance using limited low-quality (i.e., noisy and blurred images) labeled data. In another study [251], the in-situ monitoring data in the form of video records were gathered during the printing of the part to predict the average width of the tracks and the quality of the part (track continuity) using CNN supervised and semi-supervised models. No rule exists regarding the number of labeled data required to train a semi-supervised model. Different labeled data sizes were chosen to evaluate the effect of the number of labeled data on the performance of the semi-supervised model. They reported that the semi-supervised CNN model outperformed the fully supervised method in both regression and classification problems. Comparing the results obtained using the semi-supervised method with the same results obtained using an unsupervised CNN model could be a great continuation of this work to further evaluate the semi-supervised performance. A summary of the semi-supervised models reviewed here is listed in Table 5.

### 3.4. Reinforced learning

Reinforced learning is a separate framework inspired by human cognitive capabilities of learning in its surrounding world [167]. RL is a different training process, which focuses on training agents, which interact with the environment to maximize the reward [167]. For example, Mozaffar et al. [292] proposed a framework for the toolpath design by employing PPO, DQN, and SAC algorithms. Wasmer et al. [293] classified the quality of a 3D-printed cuboid shape fabricated at different laser speeds using in-situ acoustic

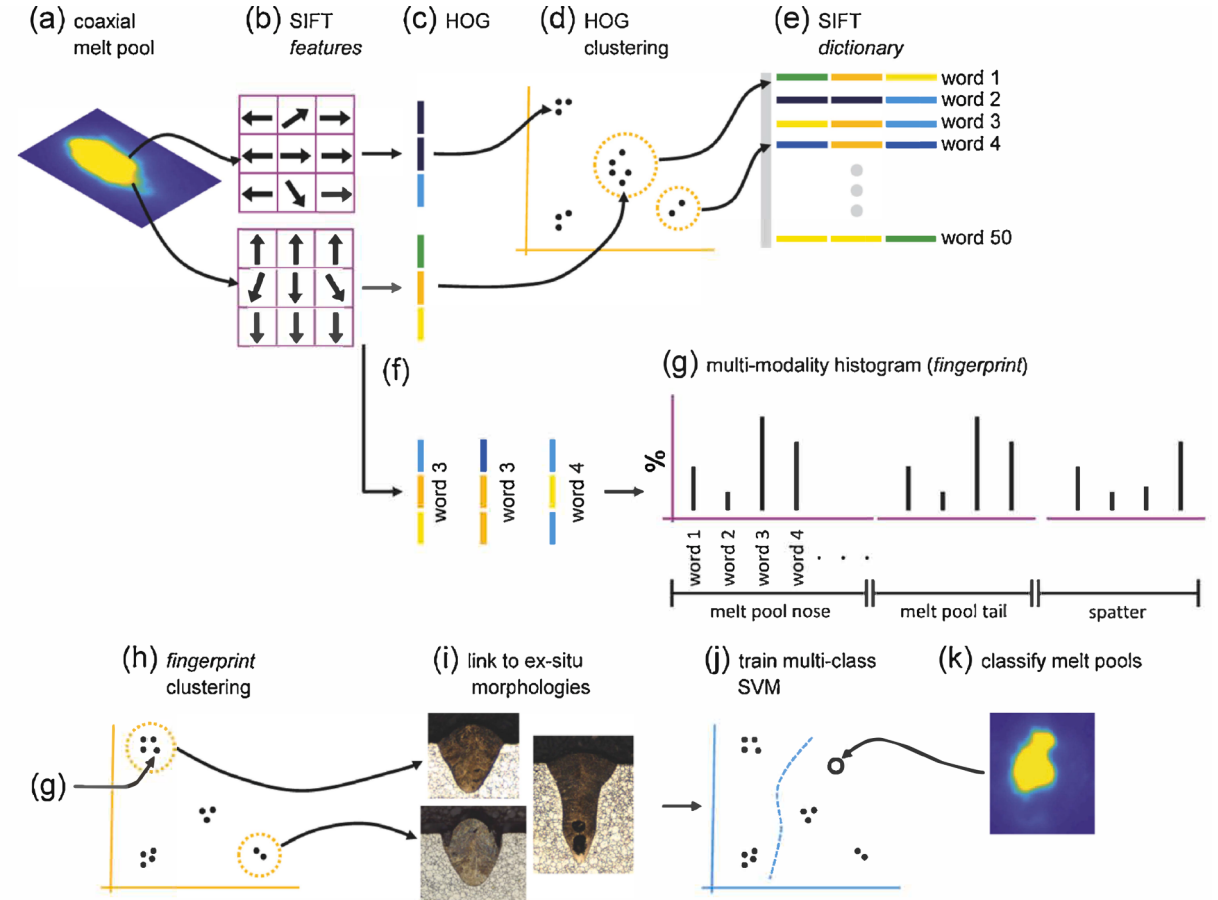


**Fig. 36.** Developing a hybrid supervised and unsupervised model to classify melt pools [49]. (a)-(f) feature extraction process using CV and BoW (g) fingerprints representation used to describe melt pool morphologies, (h)-(i) linking in-situ and ex-situ results (the micrographs shown in step (i) were collected from [96], and (j)-(k) training of the classification algorithm and classifying new data.

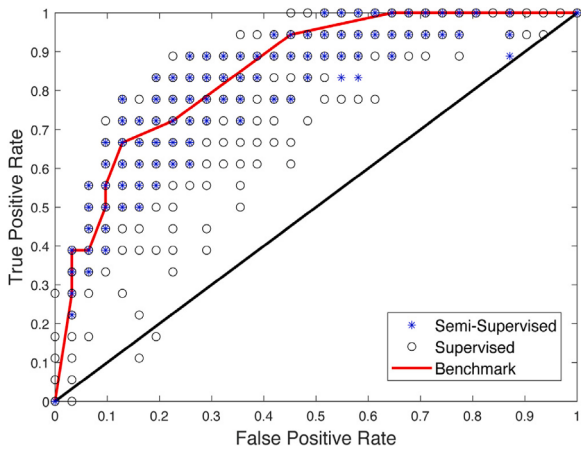


**Fig. 37.** Receiver operating characteristic curves for the ensemble of experiments in a study conducted by Okaro et al. [250]. The red line indicates the benchmark result (supervised learning when all 49 points are labeled).

**Table 5**  
Semi-supervised learning.

Reference	AM process	Materials	Input	Output	ML method
Okaro et al. [250]	SLM	IN718	PD	Faulty/acceptable	GMM
Larsen and Hooper [290]	SLM	-	HSI	Anomaly detection	VRNN
Li et al. [291]	LBAM	ASTM F75 I CoCrMo	Micrograph image	Defect detection	CNN
Yuan et al. [251]	SLM	SS316	Video data	Track width and continuity	CNN
Yadav et al. [289]	SLM	AlSi10Mg	Optical tomography image	hot spot detection	A combination of KMC and KNN

emissions and RL. Deep learning was also combined with reinforced learning to create a subset of deep reinforced learning (DRL) employed in a study by Ogoke and Farimani [168] to generate a control policy for managing the melt pool depth by controlling either the scan speed or power of the laser during the melting process. In the traditional 3D-printed cases where the processing parameters (e.g., scan speed) are kept unchanged throughout the entire trajectory, the melt pool noticeably becomes deeper at the locations at which the laser changes its direction. The growth in the melt pool dept at the spots where the laser changes its direction is due to heat accumulation. With the aid of DRL, the learned control policy is capable of achieving a considerably smaller melt pool depth variation than the constant process parameter scenario. The model proposed in the study by Ogoke and Farimani [168] was developed based on the numerical data and could be further extended using experimental data with necessary modifications. For example, due to the lag time between the order and execution of an action, controlling the scan speed might be difficult, particularly at high scan speeds. Also, some modifications in the printing process are required to change the processing parameters during manufacturing. A summary of the reinforced learning models reviewed here is listed in Table 6.

#### 4. Challenges and opportunities

The ultimate goal of finding the relationships between various types of input and response parameters of 3D-printed parts is to manufacture the parts in high quality regardless of the algorithms, input, and output data used during the manufacturing. The studies reviewed here linked the processing parameters to the defects formed during manufacturing in various ways. However, some challenges exist, which may lead to opportunities in the AM field. To discuss the challenges and suggest opportunities based on these challenges, two strategies have been executed; 1) the most frequent challenges directly discussed in the research papers reviewed here are summarized and echoed; 2) the challenges, gaps, and possible contributions to the AM field are identified based on reviewing the literature. In this section, three aspects of challenges are summarized based on the previous literature review. Also, four research directions and opportunities are suggested for future research and development of ML in the AM field.

##### 4.1. Challenges

###### 4.1.1. Standardization

One main challenge of the application of ML in the AM field is the lack of standardization, which hinders the real-world adaptation of ML in the prediction of the quality of the 3D-printed part. No comprehensive and accessible database, which includes different materials and printing processes, exists. Also, despite employing numerous criteria to evaluate the quality of 3D-printed parts, no specific measuring criteria have been defined to judge the quality of the 3D-printed parts. Due to a lack of standardization, the majority of studies reviewed earlier focused on the detection of defects rather than the detection and evaluation of the impact of defects. Developing binary defect classification ML models may help get a rough idea regarding the presence of defects and the quality of 3D-printed parts. However, defects need to be classified into more categories from negligible to severe defects. Developing such an ML model might be more challenging due to a lack of standardization and dataset size.

###### 4.1.2. Data availability and model interpretation

One of the challenges of developing ML models in the AM field is to develop a large dataset. Although small datasets sometimes have been used to train ML models, the performance of these models highly depends on the size of the dataset. Also, the size of dataset required to develop an ML model depends on the number of input parameters and the range of these input parameters. Apparently, if the number of input parameters increases or a wide range for each input parameter is studied, a larger dataset is required to develop the model. This issue has been mostly neglected in the articles reviewed earlier. Also, interpretability and traceability of the results yielded

**Table 6**  
Reinforced learning.

Reference	AM process	Materials	Input	Output	ML method
Wasmer et al. [293]	SLM	SS 316L	AE	Porosity type	RL
Ogoke et al. [168]	SLM	-	P, v	MPD	DRL
Mozafar et al. [292]	DED	-	2D sections	TP	PPO, DQN, SAC

by ML models is another issue that should be addressed to assist the decision-makers in better understanding the defect formation and its impact on the quality of the AM part. ML models are also lacking transferability [294], which limits the application of ML in the AM field.

#### 4.1.3. Physics-informed Models

Laws of physics could help decision-makers reach a better understanding of the relationship that exist between the PSPP steps of manufacturing, but these rules impose some limitations. Many studies focused on the accuracy of the data-driven models used to predict the quality of the 3D-printed parts. However, these models eventually provide the output for which they were trained. One solution for this drawback is to employ both data-driven and laws of physics while developing a model. However, physical modeling techniques may not be accurate enough, as they are still limited by many assumptions, simplifications, and approximations [295].

### 4.2. Opportunities

#### 4.2.1. Moving toward PIML models

One solution for many challenges listed above is to move toward PIML models. Compared to many ML models developed in the AM field, very few PIML models have been developed. The physics-informed ML models become more and more essential for overcoming these challenges. By incorporating the laws of physics into the model, the model variability can be minimized. The physics used in the PIML model could help develop models with a smaller dataset and more input parameters with a wider range [296]. Although physics-based models may not accurately predict the output due to many assumptions, simplifications, and approximations considered to develop the models, these models are still able to shed the light on the hidden knowledge of the AM problems. Also, finding the physical relationships between different parameters could be used within the PIML model. The processing parameters, for example, can turn into a set of dimensionless numbers, which describe the physics of the problem. When the physics of the problem is understood, the validity of these dimensionless numbers can be derived in a certain range, which makes the model valid beyond the range of the processing parameters employed to generate the dataset. This means that the ML model developed using this technique incorporates a higher number and a wider range of processing parameters with a smaller dataset size. More importantly, the PIMI models have been mainly developed in the AM field, as PIMI is the most convenient type of PIML model among all models introduced. Developing a different type of PIML (e.g., PIMT, PIMA, and PIMO) other than PIMI or even developing PIML models using more than one definition of PIML model is an underdeveloped and underexplored research area, which could be investigated.

#### 4.2.2. Employing different types of inputs

Developing machine learning models using different types of input parameters could be a promising avenue of research. Most existing machine learning models consider one type of input parameter to develop an ML model. This means that all other types of data (e.g., image-based data, acoustic data, dimensions of melt pools, etc.) are wasted and the model accuracy is just based on one type of data. Hybrid algorithms need to be developed with the ability to handle more than one type of data. Acoustic emission data, for example, could be linked to image-based data to develop a more robust machine learning model. With the development of such models, the application of ML in AM could become more and more practical.

#### 4.2.3. Developing practical models

In the AM field, developing machine learning models should become less costly and laborious. During the manufacturing of 3D-printed parts, a part of the data could be captured using in-situ monitoring techniques. The ML models developed in the AM field are mainly based on offline machine learning techniques, and this real-time data cannot be used in this type of ML model. With offline ML models, the chance of training and modifying the quality of the part during manufacturing is missing. However, the real-time data could be used to develop online ML models. Less effort is required to capture the data during manufacturing and also more data could be obtained with much less labor job. Due to these benefits of online learning, it is expected that more online learning models are employed for future studies in the AM field.

Also, one laborious task of collecting and preparing data for analysis is to label the data. Employing supervised techniques requires labeled data, and unsupervised techniques are not as accurate as supervised techniques. One way to reduce the cost and effort of preparing data is to use semi-supervised techniques. Despite the high capability of semi-supervised techniques in predicting the quality of the 3D-printed parts, they have been less employed in the AM field.

#### 4.2.4. Length scales

Developing ML models at different length scales could reach a better understanding of the problem and improve the accuracy of the developed model. The models developed in the AM field mostly fall on the macro-scale. More attention should be paid to the microstructure of the 3D-printed parts by developing micro-scale ML models. Also, developing ML models linking microscales to meso or macro scale could be another interesting topic in the AM field.

## 5. Summary and concluding thoughts

This paper reviewed recent AM publications with a focus on the application of machine learning in predicting the quality of 3D-printed parts. The common input and response parameters employed in the ML models to evaluate the quality of the 3D-printed parts were introduced along with different machine learning models used in the AM field. The articles reviewed here elucidate some key

points, which are listed as follow:

- Supervised machine learning approaches are the most popular algorithms among ML algorithms in the defect detection and quality evaluation of 3D-printed parts. However, data preparation for supervised machine learning algorithms is costly and time-consuming, which may make these approaches less practical in the AM field.
- Although unsupervised and semi-supervised techniques are more suitable for AM problems due to the cost of labeling data, these approaches have been less frequently used in the AM field.
- Future work in the AM field is envisioned to move towards semi-supervised and reinforcement learning algorithms. Semi-supervised machine learning models have demonstrated a high potential to be widely used in the AM field, as they fully satisfy the issues with supervised and unsupervised machine learning algorithms.
- Developing PIML models in the AM field is in its infancy, as the majority of the ML models developed to detect defects and evaluate the quality of 3D-printed parts ignored the physics of the problem and focused more on different methods of ML models and their accuracy.
- Among these PIML models, PIMT, PIMC, PIMA, and PIMO models have been left underexplored in detecting defects and analyzing the quality of 3D-printed parts, while more attention needs to be paid to PIMI models. Investigating the benefits of simultaneously employing more than one of these methods is believed to be unexplored.

According to the literature, machine learning algorithms seem to be a great solution to the continued challenges in the AM field and persistent quality issues of 3D-printed parts. The next generation of machine learning models will be physics-informed, online, and with less training and supervision needs.

### Declaration of Competing Interest

The authors declare that they have no known competing financial interests or personal relationships that could have appeared to influence the work reported in this paper.

### Data availability

Data will be made available on request.

### Acknowledgements

The authors acknowledge the infrastructure and support of the Center for Agile and Adaptive and Additive Manufacturing (CAAAM) funded through State of Texas Appropriation: 190405–105-805008–220.

### References

- [1] Hague R, Dickens P, Hopkinson N. *Rapid manufacturing: an industrial revolution for the digital age*. John Wiley & Sons; 2006.
- [2] Levy G, Schindel R. Overview of layer manufacturing technologies, opportunities, options and applications for rapid tooling. *Proc Inst Mech Eng, Part B: J Eng Manuf* 2002;216(12):1621–34.
- [3] Beaman JJ, Barlow JW, Bourell DL, Crawford RH, Marcus HL, McAlea KP. Solid freeform fabrication: a new direction in manufacturing. *Kluwer Academic Publishers*, Norwell, MA 1997;2061:25–49.
- [4] Kruth J-P, Leu M-C, Nakagawa T. Progress in additive manufacturing and rapid prototyping. *Cirp Annals* 1998;47(2):525–40.
- [5] Shahrbudin N, Lee TC, Ramian R. An overview on 3d printing technology: technological, materials, and applications. *Proc Manuf* 2019;35:1286–96.
- [6] K.M. Taminger, R.A. Hafley, Electron beam freeform fabrication for cost effective near-net shape manufacturing, in: NATO/RTO AVT-139 Specialists' Meeting on Cost Effective Manufacture via Net Shape Processing, 2006.
- [7] Xing Y, Luo C, Wu Z, Zhang K, Liu L. Fabrication and properties of micro-additive manufactured ni-based composite coatings by short-pulsed laser. *Optics & Laser Technol* 2022;150:107973.
- [8] Z. Doubrovský, J.C. Verlinden, J.M. Geraedts, Optimal design for additive manufacturing: opportunities and challenges, in: International design engineering technical conferences and computers and information in engineering conference, Vol. 54860, 2011, pp. 635–646.
- [9] Gao W, Zhang Y, Ramanujan D, Ramanan K, Chen Y, Williams CB, Wang CC, Shin YC, Zhang S, Zavattieri PD. The status, challenges, and future of additive manufacturing in engineering. *Comput Aided Des* 2015;69:65–89.
- [10] A.C.F. on Additive Manufacturing Technologies, A.C.F. on Additive Manufacturing Technologies. Subcommittee F42. 91 on Terminology, Standard terminology for additive manufacturing technologies, Astm International, 2012.
- [11] Chatham CA, Long TE, Williams CB. A review of the process physics and material screening methods for polymer powder bed fusion additive manufacturing. *Prog Polym Sci* 2019;93:68–95.
- [12] Kladovasilakis N, Charalampous P, Kostavelis I, Tzetzis D, Tzovaras D. Impact of metal additive manufacturing parameters on the powder bed fusion and direct energy deposition processes: a comprehensive review. *Prog Addit Manuf* 2021;6(3):349–65.
- [13] Kerschbaumer G, Ernst G. Hybrid manufacturing process for rapid high performance tooling combining high speed milling and laser cladding. *Proc 23rd Int Congr Appl Lasers Electro-Optics (ICALEO)* 2004:1710–20.
- [14] P. Ninpitch, P. Kotiwatwangkul, S. Mahathanabodee, P. Chalermkarnnon, P. Ratanadecho, A review of computer simulations of metal 3d printing, in: AIP Conference Proceedings, Vol. 2279, AIP Publishing LLC, 2020, p. 050002.
- [15] Brzeski D, Hia IL, Chauvette J-F, Farahani RD, Piccirilli N, Ross A, Therriault D. Design of thermoset composites for high-speed additive manufacturing of lightweight sound absorbing micro-scaffolds. *Addit Manuf* 2021;47:102245. <https://doi.org/10.1016/j.addma.2021.102245>. URL <https://www.sciencedirect.com/science/article/pii/S221486042100405X>.
- [16] Khanzadeh M, Chowdhury S, Marufuzzaman M, Tschopp MA, Bian L. Porosity prediction: Supervised-learning of thermal history for direct laser deposition. *J Manuf Syst* 2018;47:69–82. <https://doi.org/10.1016/j.jmsy.2018.04.001>. URL <https://www.sciencedirect.com/science/article/pii/S0278612518300402>.

- [17] Li L, McGuan R, Isaac R, Kavehpour P, Candler R. Improving precision of material extrusion 3d printing by in-situ monitoring & predicting 3d geometric deviation using conditional adversarial networks. *Addit Manuf* 2021;38:101695. <https://doi.org/10.1016/j.addma.2020.101695>. URL <https://www.sciencedirect.com/science/article/pii/S2214860420310678>.
- [18] Kawalkar R, Dubey HK, Lokhande SP. A review for advancements in standardization for additive manufacturing. *Materials Today: Proceedings* 2022;50: 1983–90.
- [19] Bandyopadhyay A, Zhang Y, Bose S. Recent developments in metal additive manufacturing. *Current opinion in chemical engineering* 2020;28:96–104.
- [20] Rashid AA, Khan SA, Al-Ghamdi SG, Koç M. Additive manufacturing of polymer nanocomposites: Needs and challenges in materials, processes, and applications. *Journal of Materials Research and Technology* 2021;14:910–41. <https://doi.org/10.1016/j.jmrt.2021.07.016>. URL <https://www.sciencedirect.com/science/article/pii/S2238785421006797>.
- [21] Nasiri S, Khosrovani MR. Machine learning in predicting mechanical behavior of additively manufactured parts. *Journal of Materials Research and Technology* 2021;14:1137–53. <https://doi.org/10.1016/j.jmrt.2021.07.004>. URL <https://www.sciencedirect.com/science/article/pii/S2238785421006670>.
- [22] D.L. Bourell, M.C. Leu, D.W. Rosen, Roadmap for additive manufacturing identifying the future of freeform processing (2009).
- [23] Measurement science roadmap for metal-based additive manufacturing (2013).
- [24] Qu M, Guo Q, Escano LI, Nabaa A, Hojjatzaadeh SMH, Young ZA, Chen L. Controlling process instability for defect lean metal additive manufacturing. *Nat Commun* 2022;13(1):1–8.
- [25] Gong H, Raff K, Gu H, Starr T, Stucker B. Analysis of defect generation in ti-6al-4v parts made using powder bed fusion additive manufacturing processes. *Addit Manuf* 2014;1:4–87–98. <https://doi.org/10.1016/J.ADDMA.2014.08.002>.
- [26] Bauereiß A, Scharowsky T, Körner C. Defect generation and propagation mechanism during additive manufacturing by selective beam melting. *J. Mater. Process. Technol.* 2014;214:2522–8. <https://doi.org/10.1016/J.JMATPROTEC.2014.05.002>.
- [27] Aoyagi K, Wang H, Sudo H, Chiba A. Simple method to construct process maps for additive manufacturing using a support vector machine. *Addit Manuf* 2019; 27:353–62.
- [28] Yadroitsev I. Direct manufacturing of 3d objects by selective laser melting of metal powders. Ph.D. thesis. Saint-Etienne; 2008.
- [29] Kamath C. Data mining and statistical inference in selective laser melting. *Int. J. Adv. Manuf. Technol.* 2016;86:1659–77. <https://doi.org/10.1007/s00170-015-8289-2>.
- [30] Johnson N, Vulimiri P, To A, Zhang X, Brice C, Kappes B, Stebner A. Invited review: Machine learning for materials developments in metals additive manufacturing. *Addit Manuf* 2020;36:101641.
- [31] Zhu K, Fuh JYH, Lin X. Metal-based additive manufacturing condition monitoring: A review on machine learning based approaches. *IEEE/ASME Trans. Mechatron.* 2021.
- [32] Tercan H, Meisen T. Machine learning and deep learning based predictive quality in manufacturing: a systematic review. *J Intell Manuf* 2022;1–27.
- [33] Fu Y, Downey AR, Yuan L, Zhang T, Pratt A, Balogun Y. Machine learning algorithms for defect detection in metal laser-based additive manufacturing: a review. *Journal of Manufacturing Processes* 2022;75:693–710.
- [34] Nasiri S, Khosrovani MR. Applications of data-driven approaches in prediction of fatigue and fracture. *Materials Today Communications* 2022;33:104437.
- [35] Wang C, Tan XP, Tor SB, Lim CS. Machine learning in additive manufacturing: State-of-the-art and perspectives. *Addit Manuf* 2020;36:101538. <https://doi.org/10.1016/j.addma.2020.101538>.
- [36] Qin J, Hu F, Liu Y, Witherell P, Wang CC, Rosen DW, Simpson T, Lu Y, Tang Q. Research and application of machine learning for additive manufacturing. *Addit Manuf* 2022;102691.
- [37] Tian C, Li T, Bustillos J, Bhattacharya S, Turnham T, Yeo J, Moridi A. Data-driven approaches toward smarter additive manufacturing. *Advanced Intelligent Systems* 2021;3(12):2100014.
- [38] Kumar S, Gopi T, Harikeerthana N, Gupta MK, Gaur V, Krolczyk GM, Wu C. Machine learning techniques in additive manufacturing: a state of the art review on design, processes and production control. *J Intell Manuf* 2022;1–35.
- [39] Guo S, Agarwal M, Cooper C, Tian Q, Gao RX, Grace WG, Guo Y. Machine learning for metal additive manufacturing: Towards a physics-informed data-driven paradigm. *Journal of Manufacturing Systems* 2022;62:145–63.
- [40] Fink A. Conducting research literature reviews: From the internet to paper. Sage publications; 2019.
- [41] Chowdhary K. Natural language processing. *Fundamentals of artificial intelligence* 2020:603–49.
- [42] Bird S. NLTK: the natural language toolkit. In: *Proceedings of the COLING/ACL 2006 Interactive Presentation Sessions*; 2006. p. 69–72.
- [43] Jones KS. A statistical interpretation of term specificity and its application in retrieval. *Journal of documentation* 1972.
- [44] Rousseeuw PJ. Silhouettes: a graphical aid to the interpretation and validation of cluster analysis. *Journal of computational and applied mathematics* 1987;20: 53–65.
- [45] Higuchi K. Kh coder 3 reference manual. Kioto (Japan): Ritsumeikan University; 2016.
- [46] Bayat M, Dong W, Thorborg J, To AC, Hattel JH. A review of multi-scale and multi-physics simulations of metal additive manufacturing processes with focus on modeling strategies. *Addit Manuf* 2021;47:102278.
- [47] Khosrovani MR, Reinicke T. On the use of x-ray computed tomography in assessment of 3d-printed components. *J. Nondestr. Eval.* 2020;39(4):1–17.
- [48] Du Plessis A, Yadroitsev I, Yadroitseva I, Le Roux SG. X-ray microcomputed tomography in additive manufacturing: a review of the current technology and applications. *3D Printing and Additive Manufacturing* 2018;5(3):227–47.
- [49] Scime L, Beuth J. Using machine learning to identify in-situ melt pool signatures indicative of flaw formation in a laser powder bed fusion additive manufacturing process. *Addit Manuf* 2019;25:151–65.
- [50] Criales LE, Ariso Y, Lane B, Moylan S, Donmez A, Öznel T. Laser powder bed fusion of nickel alloy 625: experimental investigations of effects of process parameters on melt pool size and shape with spatter analysis. *Int. J. Mach. Tools Manuf* 2017;121:22–36.
- [51] Dilip J, Zhang S, Teng C, Zeng K, Robinson C, Pal D, Stucker B. Influence of processing parameters on the evolution of melt pool, porosity, and microstructures in ti-6al-4v alloy parts fabricated by selective laser melting. *Progress in Additive Manufacturing* 2017;2(3):157–67.
- [52] Keshavarzermani A, Marzbanrad E, Esmailizadeh R, Mahmoodkhani Y, Ali U, Enrique PD, Zhou NY, Bonakdar A, Toyserkani E. An investigation into the effect of process parameters on melt pool geometry, cell spacing, and grain refinement during laser powder bed fusion. *Optics & Laser Technology* 2019;116: 83–91.
- [53] Yu G, Gu D, Dai D, Xia M, Ma C, Chang K. Influence of processing parameters on laser penetration depth and melting/re-melting densification during selective laser melting of aluminum alloy. *Appl. Phys. A* 2016;122(10):1–12.
- [54] Khosrovani MR, Reinicke T. Fracture behavior of intact and defected 3d-printed parts. *Procedia Structural Integrity* 2021;31:105–10.
- [55] Yasa E, Kruth JP, Deckers J. Manufacturing by combining selective laser melting and selective laser erosion/laser re-melting. *CIRP Ann.* 2011;60:263–6. <https://doi.org/10.1016/J.CIRP.2011.03.063>.
- [56] Yadroitsev I, Gusarov A, Yadroitseva I, Smurov I. Single track formation in selective laser melting of metal powders. *J. Mater. Process. Technol.* 2010;210: 1624–31. <https://doi.org/10.1016/J.JMATPROTEC.2010.05.010>.
- [57] A. Laohaprapanon, P. Jeamwathanachai, M. Wongcumchang, N. Chantarapanich, S. Chantaweroad, K. Sitthisiripratip, S. Wisutmethangoon, Optimal scanning condition of selective laser melting processing with stainless steel 316l powder, in: *Advanced Materials Research*, Vol. 341, Trans Tech Publ, 2012, pp. 816–820.
- [58] Zhang Z, Liu Z, Wu D. Prediction of melt pool temperature in directed energy deposition using machine learning. *Addit Manuf* 2021;37:101692.
- [59] Olleak A, Xi Z. Calibration and validation framework for selective laser melting process based on multi-fidelity models and limited experiment data. *J. Mech. Des.* 2020;142(8):081701.
- [60] Luo Z, Zhao Y. A survey of finite element analysis of temperature and thermal stress fields in powder bed fusion additive manufacturing. *Addit Manuf* 2018;21: 318–32.

- [61] Mohammadpour P, Plotkowski A, Phillion AB. Revisiting solidification microstructure selection maps in the frame of additive manufacturing. *Addit Manuf* 2020;31:100936.
- [62] Khanzadeh M, Chowdhury S, Tschopp MA, Doude HR, Marufuzzaman M, Bian L. In-situ monitoring of melt pool images for porosity prediction in directed energy deposition processes. *IISE Transactions* 2019;51(5):437–55.
- [63] Shamsaei N, Yadollahi A, Bian L, Thompson SM. An overview of direct laser deposition for additive manufacturing; part ii: Mechanical behavior, process parameter optimization and control. *Additive Manufacturing* 2015;8:12–35. <https://doi.org/10.1016/J.ADDMA.2015.07.002>.
- [64] Mozaffar M, Paul A, Al-Bahrani R, Wolff S, Choudhary A, Agrawal A, Ehmann K, Cao J. Data-driven prediction of the high-dimensional thermal history in directed energy deposition processes via recurrent neural networks. *Manufacturing letters* 2018;18:35–9.
- [65] Montgomery DC, Runger GC. Applied statistics and probability for engineers. John Wiley & Sons; 2010.
- [66] Wang C, Tan X, Du Z, Chandra S, Sun Z, Lim C, Tor S, Lim C, Wong C. Additive manufacturing of nitinol shape memory alloys using pre-mixed powders. *J. Mater. Process. Technol.* 2019;271:152–61.
- [67] Wang C, Tan X, Liu E, Tor SB. Process parameter optimization and mechanical properties for additively manufactured stainless steel 316L parts by selective electron beam melting. *Materials & Design* 2018;147:157–66.
- [68] Zhang Y, Zhang J. Modeling of solidification microstructure evolution in laser powder bed fusion fabricated 316L stainless steel using combined computational fluid dynamics and cellular automata. *Addit Manuf* 2019;28:750–65.
- [69] Soomro AA, Mokhtar AA, Kurnia JC, Lashari N, Lu H, Sambo C. Integrity assessment of corroded oil and gas pipelines using machine learning: A systematic review. *Eng. Fail. Anal.* 2022;131:105810. <https://doi.org/10.1016/j.englfailanal.2021.105810>. URL <https://www.sciencedirect.com/science/article/pii/S1350630721006713>.
- [70] Patnaik A, Satapathy A, Chand N, Barkoula NM, Biswas S. Solid particle erosion wear characteristics of fiber and particulate filled polymer composites: A review. *Wear* 2010;268:249–63. <https://doi.org/10.1016/j.wear.2009.07.021>. URL <https://www.sciencedirect.com/science/article/pii/S004316480900475X>.
- [71] Huang DJ, Li H. A machine learning guided investigation of quality repeatability in metal laser powder bed fusion additive manufacturing. *Materials & Design* 2021;203:109606.
- [72] He P, Liu Q, Krusic JJ, Li X. Machine-learning assisted additive manufacturing of a TiCN reinforced AlSi10Mg composite with tailororable mechanical properties. *Mater. Lett.* 2022;307:131018.
- [73] Wang C, Tan X, Tor S, Lim C. Machine learning in additive manufacturing: State-of-the-art and perspectives. *Addit Manuf* 2020;36:101538.
- [74] Druzgalski C, Ashby A, Guse G, King W, Roehling TT, Matthews MJ. Process optimization of complex geometries using feed forward control for laser powder bed fusion additive manufacturing. *Addit Manuf* 2020;34:101169.
- [75] Ball P. Using artificial intelligence to accelerate materials development. *MRS Bull.* 2019;44(5):335–44.
- [76] Ward L, Agrawal A, Choudhary A, Wolverton C. A general-purpose machine learning framework for predicting properties of inorganic materials. *npj Computational Materials* 2016;2(1):1–7.
- [77] S.S. Razvi, S. Feng, A. Narayanan, Y.-T.T. Lee, P. Witherell, A review of machine learning applications in additive manufacturing (8 2019). doi:10.1115/DETC2019-98415. doi: 10.1115/DETC2019-98415.
- [78] Meng L, McWilliams B, Jarosinski W, Park H-Y, Jung Y-G, Lee J, Zhang J. Machine learning in additive manufacturing: A review. *JOM* 2020;72:2363–77. <https://doi.org/10.1007/s11837-020-04155-y>.
- [79] Jiang J, Xiong Y, Zhang Z, Rosen DW. Machine learning integrated design for additive manufacturing. *J. Intell. Manuf.* 2020. <https://doi.org/10.1007/s10845-020-01715-6>.
- [80] Razvi SS, Feng S, Narayanan A, Lee Y-TT, Witherell P. In: A review of machine learning applications in additive manufacturing, Vol. 59179. in: International Design Engineering Technical Conferences and Computers and Information in Engineering Conference, American Society of Mechanical Engineers; 2019. V001T02A040.
- [81] Jin Z, Zhang Z, Demir K, Gu GX. Machine learning for advanced additive manufacturing. *Matter* 2020;3(5):1541–56.
- [82] DebRoy T, Wei HL, Zuback JS, Mukherjee T, Elmer JW, Milewski JO, Beese AM, de Wilson-Heid A, De A, Zhang W. Additive manufacturing of metallic components—process, structure and properties. *Prog. Mater. Sci.* 2018;92:112–224.
- [83] Yang J, Han J, Yu H, Yin J, Gao M, Wang Z, Zeng X. Role of molten pool mode on formability, microstructure and mechanical properties of selective laser melted Ti-6Al-4V alloy. *Materials & Design* 2016;110:558–70. <https://doi.org/10.1016/J.MATDES.2016.08.036>.
- [84] Thompson SM, Bian L, Shamsaei N, Yadollahi A. An overview of direct laser deposition for additive manufacturing; part i: Transport phenomena, modeling and diagnostics. *Addit Manuf* 2015;8:36–62.
- [85] Bauereiß A, Schärowsky T, Körner C. Defect generation and propagation mechanism during additive manufacturing by selective beam melting. *J. Mater. Process. Technol.* 2014;214(11):2522–8. <https://doi.org/10.1016/j.jmatprotec.2014.05.002>. URL <https://www.sciencedirect.com/science/article/pii/S0924013614001691>.
- [86] Dadbakhsh S, Hao L. Effect of Al alloys on selective laser melting behaviour and microstructure of in situ formed particle reinforced composites. *Journal of alloys and compounds* 2012;541:328–34.
- [87] Yasa E, Kruth J-P. Microstructural investigation of selective laser melting 316L stainless steel parts exposed to laser re-melting. *Procedia Engineering* 2011;19:389–95.
- [88] Clark D, Bache M, Whittaker MT. Shaped metal deposition of a nickel alloy for aero engine applications. *Journal of materials processing technology* 2008;203 (1–3):439–48.
- [89] Yusuf SM, Gao N. Influence of energy density on metallurgy and properties in metal additive manufacturing. *Mater. Sci. Technol.* 2017;33(11):1269–89.
- [90] Darvish K, Chen Z, Pasang T. Reducing lack of fusion during selective laser melting of CoCrMo alloy: Effect of laser power on geometrical features of tracks. *Materials & Design* 2016;112:357–66.
- [91] Promopatnum P, Yao S-C. Analytical evaluation of defect generation for selective laser melting of metals. *The International Journal of Advanced Manufacturing Technology* 2019;103(1):1185–98.
- [92] King WE, Barth HD, Castillo VM, Gallegos GF, Gibbs JW, Hahn DE, Kamath C, Rubenchik AM. Observation of keyhole-mode laser melting in laser powder-bed fusion additive manufacturing. *J. Mater. Process. Technol.* 2014;214(12):2915–25.
- [93] Khairallah SA, Anderson AT, Rubenchik A, King WE. Laser powder-bed fusion additive manufacturing: Physics of complex melt flow and formation mechanisms of pores, spatter, and denudation zones. *Acta Mater.* 2016;108:36–45. <https://doi.org/10.1016/J.ACTAMAT.2016.02.014>.
- [94] Sibilano T, Ancona A, Berardi V, Schingaro E, Basile G, Lugarà P. Optical detection of conduction/keyhole mode transition in laser welding. *J. Mater. Process. Technol.* 2007;191(1–3):364–7.
- [95] Lee JY, Ko SH, Farson DF, Yoo CD. Mechanism of keyhole formation and stability in stationary laser welding. *J. Phys. D: Appl. Phys.* 2002;35(13):1570.
- [96] Scime L, Beuth J. Melt pool geometry and morphology variability for the inconel 718 alloy in a laser powder bed fusion additive manufacturing process. *Addit Manuf* 2019;29:100830. <https://doi.org/10.1016/j.addma.2019.100830>. URL <https://www.sciencedirect.com/science/article/pii/S2214860419306104>.
- [97] JadHAV SD, Goossens LR, Kinds Y, Van Hooreweder B, Vanmeensel K. Laser-based powder bed fusion additive manufacturing of pure copper. *Addit Manuf* 2021;42:101990.
- [98] Tang C, Tan JL, Wong CH. A numerical investigation on the physical mechanisms of single track defects in selective laser melting. *Int. J. Heat Mass Transf.* 2018;126:957–68. <https://doi.org/10.1016/J.IJHEATMASSTRANSFER.2018.06.073>.
- [99] Kruth JP, Froyen L, Vaerenbergh JV, Mercelis P, Rombouts M, Lauwers B. Selective laser melting of iron-based powder. *J. Mater. Process. Technol.* 2004;149:616–22. <https://doi.org/10.1016/J.JMATPROTEC.2003.11.051>.
- [100] Tapia G, Elwany AH, Sang H. Prediction of porosity in metal-based additive manufacturing using spatial gaussian process models. *Addit Manuf* 2016;12:282–90. <https://doi.org/10.1016/j.addma.2016.05.009>.

- [101] Akbari P, Ogoke F, Kao N-Y, Meidani K, Yeh C-Y, Lee W, Farimani AB. Meltpoolnet: Melt pool characteristic prediction in metal additive manufacturing using machine learning. *Addit Manuf* 2022;55:102817.
- [102] Vilaro T, Colin C, Bartout J-D. As-fabricated and heat-treated microstructures of the ti-6al-4v alloy processed by selective laser melting. *Metallurgical and materials transactions A* 2011;42(10):3190–9.
- [103] Wang S, Ning J, Zhu L, Yang Z, Yan W, Dun Y, Xie P, Xu P, Bose S, Bandyopadhyay A. Role of porosity defects in metal 3d printing: Formation mechanisms, impacts on properties and mitigation strategies. *Mater. Today* 2022.
- [104] Sola A, Nouri A. Microstructural porosity in additive manufacturing: The formation and detection of pores in metal parts fabricated by powder bed fusion. *Journal of Advanced Manufacturing and Processing* 2019;1(3):e10021.
- [105] Paul R, Anand S, Gerner F. Effect of thermal deformation on part errors in metal powder based additive manufacturing processes. *Journal of manufacturing science and Engineering* 2014;136(3).
- [106] Wang R-J, Wang L, Zhao L, Liu Z. Influence of process parameters on part shrinkage in sls. *The International Journal of Advanced Manufacturing Technology* 2007;33(5):498–504.
- [107] Paul R. Modeling and optimization of powder based additive manufacturing (AM) processes. University of Cincinnati; 2013.
- [108] Li C, Liu Z, Fang X, Guo Y. Residual stress in metal additive manufacturing. *Procedia Cirp* 2018;71:348–53.
- [109] Gu D, Hagedorn Y-C, Meiners W, Meng G, Batista RJS, Wissenbach K, Poprawe R. Densification behavior, microstructure evolution, and wear performance of selective laser melting processed commercially pure titanium. *Acta Mater.* 2012;60(9):3849–60.
- [110] P. Mercelis, J.-P. Kruth, Residual stresses in selective laser sintering and selective laser melting, *Rapid prototyping journal* (2006).
- [111] King WE, Anderson AT, Ferencz RM, Hodge NE, Kamath C, Khairallah SA, Rubenchik AM. Laser powder bed fusion additive manufacturing of metals; physics, computational, and materials challenges. *Applied Physics Reviews* 2015;2(4):041304.
- [112] Zhu H, Lu L, Fuh J. Study on shrinkage behaviour of direct laser sintering metallic powder. *Proc. Inst. Mech. Eng., Part B: J. Eng. Manuf.* 2006;220(2):183–90.
- [113] Wang S, Zhu L, Dun Y, Yang Z, Fuh JYH, Yan W. Multi-physics modeling of direct energy deposition process of thin-walled structures: defect analysis. *Comput. Mech.* 2021;67(4):1229–42.
- [114] Raghunath N, Pandey PM. Improving accuracy through shrinkage modelling by using taguchi method in selective laser sintering. *Int. J. Mach. Tools Manuf* 2007;47(6):985–95. <https://doi.org/10.1016/j.ijmachtools.2006.07.001>. URL <https://www.sciencedirect.com/science/article/pii/S0890695506001775>.
- [115] Yang Wp, Tarny Y. Design optimization of cutting parameters for turning operations based on the taguchi method. *Journal of materials processing technology* 1998;84(1–3):122–9.
- [116] Zheng H, Zhang J, Lu S, Wang G, Xu Z. Effect of core–shell composite particles on the sintering behavior and properties of nano-al<sub>2</sub>O<sub>3</sub>/polystyrene composite prepared by sls. *Mater. Lett.* 2006;60(9–10):1219–23.
- [117] Klingbeil NW, Beuth JL, Chin R, Amon C. Residual stress-induced warping in direct metal solid freeform fabrication. *Int. J. Mech. Sci.* 2002;44(1):57–77.
- [118] M. Zaeh, G. Branner, T. Krol, A three dimensional fe-model for the investigation of transient physical effects in selective laser melting, in: Fourth International Conference on Advanced Research in Virtual and Rapid Prototyping: Innovative Development in Design and Manufacturing-Advanced Research in Virtual and Rapid Prototyping, Leiria, Portugal (Taylor & Francis, London, 2009), 2009, pp. 415–424.
- [119] W. Rong-Ji, L. Xin-Hua, W. Qing-Ding, W. LingLing, Optimizing process parameters for selective laser sintering based on neural network and genetic algorithm, *The International Journal of Advanced Manufacturing Technology* 2008 42:11 42 (2008) 1035–1042. doi:10.1007/S00170-008-1669-0. <https://link.springer.com/article/10.1007/S00170-008-1669-0>.
- [120] Williams JD, Deckard CR. Advances in modeling the effects of selected parameters on the sls process. *Rapid Prototyping Journal* 1998;4:90–100. <https://doi.org/10.1108/13552549810210257/FULL.XML>.
- [121] Bai Y, Wagner G, Williams CB. Effect of particle size distribution on powder packing and sintering in binder jetting additive manufacturing of metals. *J. Manuf. Sci. Eng.* 2017;139(8).
- [122] Lee S, Peng J, Shin D, Choi YS. Data analytics approach for melt-pool geometries in metal additive manufacturing. *Sci. Technol. Adv. Mater.* 2019;20:972–8. <https://doi.org/10.1080/14686996.2019.1671140>.
- [123] Johnson L, Mahmoudi M, Zhang B, Seede R, Huang X, Maier JT, Maier HJ, Karaman I, Elwany A, Arróyave R. Assessing printability maps in additive manufacturing of metal alloys. *Acta Mater.* 2019;176:199–210. <https://doi.org/10.1016/j.jactamat.2019.07.005>.
- [124] Clijsters S, Craeghs T, Buls S, Kempen K, Kruth J-P. In situ quality control of the selective laser melting process using a high-speed, real-time melt pool monitoring system. *The International Journal of Advanced Manufacturing Technology* 2014;75(5):1089–101.
- [125] Heigl JC, Lane BM. Measurement of the melt pool length during single scan tracks in a commercial laser powder bed fusion process. *J. Manuf. Sci. Eng.* 2018;140(5).
- [126] Tan W, Shin YC. Analysis of multi-phase interaction and its effects on keyhole dynamics with a multi-physics numerical model. *J. Phys. D: Appl. Phys.* 2014;47(34):34501.
- [127] Hann D, Iammi J, Folkes J. A simple methodology for predicting laser-weld properties from material and laser parameters. *J. Phys. D: Appl. Phys.* 2011;44(44):445401.
- [128] Fabro R, Dal M, Peyre P, Coste F, Schneider M, Gunenthiram V. Analysis and possible estimation of keyhole depths evolution, using laser operating parameters and material properties. *Journal of Laser Applications* 2018;30(3):032410.
- [129] Goossens LR, Van Hooreweder B. A virtual sensing approach for monitoring melt-pool dimensions using high speed coaxial imaging during laser powder bed fusion of metals. *Addit Manuf* 2021;40:101923.
- [130] Ye J, Khairallah SA, Rubenchik AM, Crumb MF, Guss G, Belak J, Matthews MJ. Energy coupling mechanisms and scaling behavior associated with laser powder bed fusion additive manufacturing. *Adv. Eng. Mater.* 2019;21(7):1900185.
- [131] Pinkerton AJ, Li L. Modelling the geometry of a moving laser melt pool and deposition track via energy and mass balances. *J. Phys. D: Appl. Phys.* 2004;37(14):1885.
- [132] Zhuang J-R, Lee Y-T, Hsieh W-H, Yang A-S. Determination of melt pool dimensions using doe-fem and rsm with process window during slm of ti6al4v powder. *Optics & Laser Technology* 2018;103:59–76.
- [133] Sun Z, Guo W, Li L. In-process measurement of melt pool cross-sectional geometry and grain orientation in a laser directed energy deposition additive manufacturing process. *Optics & Laser Technology* 2020;129:106280.
- [134] Pinkerton AJ, Li L. Multiple-layer cladding of stainless steel using a high-powered diode laser: an experimental investigation of the process characteristics and material properties. *Thin Solid Films* 2004;453:471–6.
- [135] Majumdar JD, Pinkerton A, Liu Z, Manna I, Li L. Microstructure characterisation and process optimization of laser assisted rapid fabrication of 316l stainless steel. *Appl. Surf. Sci.* 2005;247(1–4):320–7.
- [136] Yahata T, Ikeda T, Maeda M. Deoxidation of molten titanium by electron-beam remelting technique. *Metall. Trans. B* 1993;24(4):599–604.
- [137] Van Den Avyle JA, Brooks JA, Powell AC. Reducing defects in remelting processes for high-performance alloys. *Jom* 1998;50(3):22–5.
- [138] Sun Y, Moroz A, Alrabey K. Sliding wear characteristics and corrosion behaviour of selective laser melted 316l stainless steel. *Journal of materials engineering and performance* 2014;23(2):518–26.
- [139] Fang X, Du J, Wei Z, Wang X, He P, Bai H, Wang B, Chen J, Geng R, Lu B. Study on metal deposit in the fused-coating based additive manufacturing. *Procedia Cirp* 2016;55:115–21.
- [140] Li Y, Gu D. Parametric analysis of thermal behavior during selective laser melting additive manufacturing of aluminum alloy powder. *Materials & design* 2014;63:856–67.
- [141] Hao S, Zhang X, Mei X, Grosdidier T, Dong C. Surface treatment of dz4 directionally solidified nickel-based superalloy by high current pulsed electron beam. *Materials letters* 2008;62(3):414–7.
- [142] Das S. Physical aspects of process control in selective laser sintering of metals. *Adv. Eng. Mater.* 2003;5(10):701–11.
- [143] Charles C. Modelling microstructure evolution of weld deposited ti-6al-4v. Luleå tekniska universitet; 2008. Ph.D. thesis.

- [144] Huang F, Jiang Z, Liu X, Lian J, Chen L. Microstructure and properties of thin wall by laser cladding forming. *J. Mater. Process. Technol.* 2009;209(11):4970–6.
- [145] Vastola G, Zhang G, Pei Q, Zhang Y-W. Modeling and control of remelting in high-energy beam additive manufacturing. *Addit Manuf* 2015;7:57–63.
- [146] Zhang G, Lu X, Li J, Chen J, Lin X, Wang M, Tan H, Huang W. In-situ grain structure control in directed energy deposition of ti6al4v. *Addit Manuf* 2022; 102865.
- [147] Ren K, Chew Y, Fuh J, Zhang Y, Bi G. Thermo-mechanical analyses for optimized path planning in laser aided additive manufacturing processes. *Materials & Design* 2019;162:80–93.
- [148] Tang L, Landers RG. Melt pool temperature control for laser metal deposition processes-part i: Online temperature control. *Journal of Manufacturing Science and Engineering, Transactions of the ASME* 2010;132:0110101–9. <https://doi.org/10.1115/1.4000882/468568>. URL <https://asmedigitalcollection.asme.org/manufacturingscience/article/132/1/011010/468568/Melt-Pool-Temperature-Control-for-Laser-Metal>.
- [149] Fisher BA, Lane B, Yeung H, Beuth J. Toward determining melt pool quality metrics via coaxial monitoring in laser powder bed fusion. *Manufacturing Letters* 2018;15:119–21. <https://doi.org/10.1016/J.MFGLET.2018.02.009>.
- [150] Masoomi M, Thompson SM, Shamsaei N. Laser powder bed fusion of ti-6al-4v parts: Thermal modeling and mechanical implications. *Int. J. Mach. Tools Manuf* 2017;118:73–90.
- [151] Tang M, Pistorius PC, Beuth JL. Prediction of lack-of-fusion porosity for powder bed fusion. *Addit Manuf* 2017;14:39–48.
- [152] Zheng B, Zhou Y, Smugeresky J, Schoenung J, Lavernia E. Thermal behavior and microstructural evolution during laser deposition with laser-engineered net shaping: Part i numerical calculations. *Metallurgical and materials transactions A* 2008;39(9):2228–36.
- [153] Khairallah SA, Anderson AT, Rubenchik A, King WE. Laser powder-bed fusion additive manufacturing: Physics of complex melt flow and formation mechanisms of pores, spatter, and denudation zones. *Acta Mater.* 2016;108:36–45.
- [154] Yadollahi A, Shamsaei N. Additive manufacturing of fatigue resistant materials: Challenges and opportunities. *Int. J. Fatigue* 2017;98:14–31.
- [155] Wolff S, Lee T, Fairson E, Ehmann K, Cao J. Anisotropic properties of directed energy deposition (ded)-processed ti-6al-4v. *Journal of Manufacturing Processes* 2016;24:397–405. <https://doi.org/10.1016/J.JMAPRO.2016.06.020>.
- [156] Keicher DM, Smugeresky JE. The laser forming of metallic components using particulate materials. *Jom* 1997;49(5):51–4.
- [157] Ren K, Chew Y, Zhang Y, Bi G, Fuh J. Thermal analyses for optimal scanning pattern evaluation in laser aided additive manufacturing. *J. Mater. Process. Technol.* 2019;271:178–88.
- [158] Hua T, Jing C, Xin L, Fengying Z, Weidong H. Research on molten pool temperature in the process of laser rapid forming, *journal of materials processing technology* 2008;198(1–3):454–62.
- [159] Islam M, Purtonen T, Piili H, Salminen A, Nyrhilä O. Temperature profile and imaging analysis of laser additive manufacturing of stainless steel. *Physics Procedia* 2013;41:835–42.
- [160] Liu Z, Kim H, Liu W, Cong W, Jiang Q, Zhang H. Influence of energy density on macro/micro structures and mechanical properties of as-deposited inconel 718 parts fabricated by laser engineered net shaping. *Journal of manufacturing processes* 2019;42:96–105.
- [161] Paulson NH, Gould B, Wolff SJ, Stan M, Greco AC. Correlations between thermal history and keyhole porosity in laser powder bed fusion. *Addit Manuf* 2020; 34:101213.
- [162] Ren K, Chew Y, Liu N, Zhang Y, Fuh J, Bi G. Integrated numerical modelling and deep learning for multi-layer cube deposition planning in laser aided additive manufacturing. *Virtual and Physical Prototyping* 2021;16(3):318–32.
- [163] Francis J, Bian L. Deep learning for distortion prediction in laser-based additive manufacturing using big data. *Manufacturing Letters* 2019;20:10–4.
- [164] Rakita A, Nikolić N, Mildner M, Matiasek J, Elbe-Bürger A. Re-epithelialization and immune cell behaviour in an ex vivo human skin model. *Scientific reports* 2020;10(1):1–11.
- [165] Fantz U. Basics of plasma spectroscopy. *Plasma sources science and technology* 2006;15(4):S137.
- [166] A. Géron, Hands-on Machine Learning with Scikit-Learn, Keras & TensorFlow, second edi Edition, 2019.
- [167] Sutton RS, Barto AG. Reinforcement learning: An introduction. MIT press; 2018.
- [168] Ogoke F, Farimani AB. Thermal control of laser powder bed fusion using deep reinforcement learning. *Addit Manuf* 2021;46:102033.
- [169] Zhou Z-H. Machine learning. Springer Nature; 2021.
- [170] Zhu X, Goldberg AB. Introduction to semi-supervised learning. *Synthesis lectures on artificial intelligence and machine learning* 2009;3(1):1–130.
- [171] Breiman L. Random forests. *Machine learning* 2001;45(1):5–32.
- [172] Cortes C, Vapnik V. Support-vector networks. *Machine learning* 1995;20(3):273–97.
- [173] Rasmussen CE. Gaussian processes in machine learning. In: Summer school on machine learning. Springer; 2003. p. 63–71.
- [174] Hoerl AE, Kennard RW. Ridge regression: Biased estimation for nonorthogonal problems. *Technometrics* 1970;12(1):55–67.
- [175] Hinton GE, Osindero S, Teh Y-W. A fast learning algorithm for deep belief nets. *Neural computation* 2006;18(7):1527–54.
- [176] Sewak M, Karim MR, Pujari P. Practical convolutional neural networks: implement advanced deep learning models using Python. Packt Publishing Ltd; 2018.
- [177] T. Chen, C. Guestrin, Xgboost: A scalable tree boosting system, in: Proceedings of the 22nd international conference on knowledge discovery and data mining, 2016, pp. 785–794.
- [178] Friedman J, Hastie T, Tibshirani R. Additive logistic regression: a statistical view of boosting (with discussion and a rejoinder by the authors). *The annals of statistics* 2000;28(2):337–407.
- [179] Friedman JH. Greedy function approximation: a gradient boosting machine. *Annals of statistics* 2001:1189–232.
- [180] Tibshirani R. Regression shrinkage and selection via the lasso. *J. Roy. Stat. Soc.: Ser. B (Methodol.)* 1996;58(1):267–88.
- [181] O. Kramer, K-nearest neighbors, in: Dimensionality reduction with unsupervised nearest neighbors, Springer, 2013, pp. 13–23.
- [182] G. Huang, Z. Liu, L. Van Der Maaten, K.Q. Weinberger, Densely connected convolutional networks, in: Proceedings of the IEEE conference on computer vision and pattern recognition, 2017, pp. 4700–4708.
- [183] Kohonen T. Self-organizing maps, ser. *Information Sciences*. Berlin: Springer 2001;30.
- [184] Jafari-Marandi R, Khanzadeh M, Smith BK, Bian L. Self-organizing and error driven (soed) artificial neural network for smarter classifications. *Journal of Computational Design and Engineering* 2017;4(4):282–304.
- [185] Lee JA, Verleysen M. Nonlinear dimensionality reduction, Vol. 1. Springer; 2007.
- [186] Lu H, Plataniotis KN, Venetsanopoulos AN. Multilinear principal component analysis of tensor objects for recognition. In: in: 18th International Conference on Pattern Recognition (ICPR'06), Vol. 2. IEEE; 2006. p. 776–9.
- [187] S. Mika, G. Ratsch, J. Weston, B. Scholkopf, K.-R. Mullers, Fisher discriminant analysis with kernels, in: Neural networks for signal processing IX: Proceedings of the 1999 IEEE signal processing society workshop (cat. no. 98tbh8468), Ieee, 1999, pp. 41–48.
- [188] B. Becker, R. Kohavi, D. Sommerfield, Visualizing the simple bayesian classifier (1997).
- [189] J.-C. Vialatte, V. Gripon, G. Mercier, Generalizing the convolution operator to extend cnns to irregular domains, arXiv preprint arXiv:1606.01166 (2016).
- [190] M. Awad, R. Khanna, Support vector regression, in: Efficient learning machines, Springer, 2015, pp. 67–80.
- [191] L.K. Saul, S.T. Roweis, An introduction to locally linear embedding, unpublished. Available at: <http://www.cs.toronto.edu/~roweis/lle/publications.html> (2000).
- [192] Csurka G, Dance C, Fan L, Willamowski J, Bray C. Visual categorization with bags of keypoints. In: *Workshop on statistical learning in computer vision, ECCV, Prague, Vol. 1*; 2004. p. 1–2.
- [193] Likas A, Vlassis N, Verbeek JJ. The global k-means clustering algorithm. *Pattern recognition* 2003;36(2):451–61.
- [194] Le Roux N, Bengio Y. Representational power of restricted boltzmann machines and deep belief networks. *Neural computation* 2008;20(6):1631–49.
- [195] Bishop CM, Nasrabadi NM. *Pattern recognition and machine learning*, Vol. 4. Springer; 2006.
- [196] J. Schulman, F. Wolski, P. Dhariwal, A. Radford, O. Klimov, Proximal policy optimization algorithms, arXiv preprint arXiv:1707.06347 (2017).
- [197] V. Mnih, A.P. Badia, M. Mirza, A. Graves, T. Lillicrap, T. Harley, D. Silver, K. Kavukcuoglu, Asynchronous methods for deep reinforcement learning, in: International conference on machine learning, PMLR, 2016, pp. 1928–1937.

- [198] T. Haarnoja, A. Zhou, K. Hartikainen, G. Tucker, S. Ha, J. Tan, V. Kumar, H. Zhu, A. Gupta, P. Abbeel, et al., Soft actor-critic algorithms and applications, arXiv preprint arXiv:1812.05905 (2018).
- [199] Wan H, Chen G, Li C, Qi X, Zhang G. Data-driven evaluation of fatigue performance of additive manufactured parts using miniature specimens. *Journal of Materials Science & Technology* 2019;35(6):1137–46.
- [200] Wu M, Phoha VV, Moon YB, Belman AK. Detecting malicious defects in 3d printing process using machine learning and image classification. In: ASME International Mechanical Engineering Congress and Exposition, Vol. 50688. American Society of Mechanical Engineers; 2016. V014T07A004.
- [201] Xie X, Bennett J, Saha S, Lu Y, Cao J, Liu WK, Gan Z. Mechanistic data-driven prediction of as-built mechanical properties in metal additive manufacturing. *npj Computational Materials* 2021;7(1):1–12.
- [202] Yan R, Gao RX. Base wavelet selection for bearing vibration signal analysis. *Int. J. Wavelets Multiresolut. Inf. Process.* 2009;7(04):411–26.
- [203] Inyang-Udoh U, Mishra S. A learning-based approach to modeling and control of inkjet 3d printing. 2020 American Control Conference (ACC). IEEE; 2020. p. 460–6.
- [204] Inyang-Udoh U, Mishra S. A physics-guided neural network dynamical model for droplet-based additive manufacturing. *IEEE Trans. Control Syst. Technol.* 2021.
- [205] T. Li, Z. Zhao, C. Sun, L. Cheng, X. Chen, R. Yan, R.X. Gao, Waveletkernelnet: An interpretable deep neural network for industrial intelligent diagnosis, *IEEE Transactions on Systems, Man, and Cybernetics: Systems* (2021).
- [206] Grezmak J, Wang P, Sun C, Gao RX. Explainable convolutional neural network for gearbox fault diagnosis. *Procedia CIRP* 2019;80:476–81.
- [207] Bach S, Binder A, Montavon G, Klauschen F, Müller K-R, Samek W. On pixel-wise explanations for non-linear classifier decisions by layer-wise relevance propagation. *PLoS one* 2015;10(7):e0130140.
- [208] Ye J, Bab-Hadiashar A, Hoseinnezhad R, Alam N, Vargas-Usategui A, Patel M, Cole I. Predictions of in-situ melt pool geometric signatures via machine learning techniques for laser metal deposition. *Int. J. Comput. Integr. Manuf.* 2022;1–17.
- [209] C. Spearman, The proof and measurement of association between two things. (1961).
- [210] Yuan B, Guss GM, Wilson AC, Hau-Rige SP, DePond PJ, McMains S, Matthews MJ, Giera B. Machine-learning-based monitoring of laser powder bed fusion. *Advanced Materials Technologies* 2018;3(12):1800136.
- [211] Chowdhury S, Anand S. Artificial neural network based geometric compensation for thermal deformation in additive manufacturing processes. In: International Manufacturing Science and Engineering Conference, Vol. 49910. American Society of Mechanical Engineers; 2016. V003T08A006.
- [212] T.Q.D. Pham, T.V. Hoang, Q.T. Pham, T.P. Huynh, V.X. Tran, S. Fetni, L. Duchêne, H.S. Tran, A.M. Habraken, Data-driven prediction of temperature evolution in metallic additive manufacturing process (2021).
- [213] S. Fetni, Q.D.T. Pham, V.X. Tran, L. Duchêne, H.S. Tran, A.M. Habraken, Thermal field prediction in ded manufacturing process using artificial neural network (2021).
- [214] Roy M, Wodo O. Data-driven modeling of thermal history in additive manufacturing. *Addit Manuf* 2020;32:101017.
- [215] Kozjek D, Carter III FM, Porter C, Mogonye J-E, Ehmann K, Cao J. Data-driven prediction of next-layer melt pool temperatures in laser powder bed fusion based on co-axial high-resolution planar thermometry measurements. *Journal of Manufacturing Processes* 2022;79:81–90.
- [216] Ren Y, Wang Q, Michaleris PP. A physics-informed two-level machine-learning model for predicting melt-pool size in laser powder bed fusion. *J. Dyn. Syst. Meas. Contr.* 2021;143(12).
- [217] Ren Y, Wang Q. Gaussian-process based modeling and optimal control of melt-pool geometry in laser powder bed fusion. *J. Intell. Manuf.* 2021;1–18.
- [218] Zhu Q, Liu Z, Yan J. Machine learning for metal additive manufacturing: Predicting temperature and melt pool fluid dynamics using physics-informed neural networks. *Comput. Mech.* 2021;67(2):619–35.
- [219] Yan J, Yan W, Lin S, Wagner G. A fully coupled finite element formulation for liquid-solid-gas thermo-fluid flow with melting and solidification. *Comput. Methods Appl. Mech. Eng.* 2018;336:444–70.
- [220] Yan W, Lin S, Kafka OL, Lian Y, Yu C, Liu Z, Yan J, Wolff S, Wu H, Ndip-Agbor E, et al. Data-driven multi-scale multi-physics models to derive process-structure-property relationships for additive manufacturing. *Comput. Mech.* 2018;61(5):521–41.
- [221] Ren K, Chew Y, Zhang Y, Fuh J, Bi G. Thermal field prediction for laser scanning paths in laser aided additive manufacturing by physics-based machine learning. *Comput. Methods Appl. Mech. Eng.* 2020;362:112734.
- [222] Mahmoudi M, Ezzat AA, Elwany A. Layerwise anomaly detection in laser powder-bed fusion metal additive manufacturing. *J. Manuf. Sci. Eng.* 2019;141(3).
- [223] Seifi SH, Tian W, Doude H, Tschopp MA, Bian L. Layer-wise modeling and anomaly detection for laser-based additive manufacturing. *J. Manuf. Sci. Eng.* 2019;141(8):081013.
- [224] Gaja H, Liou F. Defect classification of laser metal deposition using logistic regression and artificial neural networks for pattern recognition. *The International Journal of Advanced Manufacturing Technology* 2018;94(1):315–26.
- [225] Shevchik SA, Kenel C, Leinenbach C, Wasmer K. Acoustic emission for in situ quality monitoring in additive manufacturing using spectral convolutional neural networks. *Addit Manuf* 2018;21:598–604.
- [226] J. Bruna, W. Zaremba, A. Szlam, Y. LeCun, Spectral networks and locally connected networks on graphs, arXiv preprint arXiv:1312.6203 (2013).
- [227] Ye DS, Fuh Y, Zhang Y, Hong G, Zhu KP. Defects recognition in selective laser melting with acoustic signals by svm based on feature reduction. In: IOP Conference Series: Materials Science and Engineering, Vol. 436. IOP Publishing; 2018. p. 012020.
- [228] Goertzel C, Reutzel EW, Petrich J, Nassar AR, Phoha S. Application of supervised machine learning for defect detection during metallic powder bed fusion additive manufacturing using high resolution imaging. *Addit Manuf* 2018;21:517–28.
- [229] Smoqi Z, Gaikwad A, Bevans B, Kobir MH, Craig J, Abul-Haj A, Peralta A, Rao P. Monitoring and prediction of porosity in laser powder bed fusion using physics-informed meltpool signatures and machine learning. *J. Mater. Process. Technol.* 2022;304:117550.
- [230] Yuan J, Liu H, Liu W, Wang F, Peng S. A method for melt pool state monitoring in laser-based direct energy deposition based on densenet. *Measurement* 2022;195:111146.
- [231] Yang Z, Lu Y, Yeung H, Krishnamurthy S. Investigation of deep learning for real-time melt pool classification in additive manufacturing. 2019 IEEE 15th international conference on automation science and engineering (CASE). IEEE; 2019. p. 640–7.
- [232] Khan MF, Alam A, Siddiqui MA, Alam MS, Rafat Y, Salik N, Al-Saidan I. Real-time defect detection in 3d printing using machine learning. *Materials Today: Proceedings* 2021;42:521–8.
- [233] Valizadeh M, Wolff SJ. Convolutional neural network applications in additive manufacturing: A review, *Advances in Industrial and Manufacturing Engineering* 2022;100072.
- [234] Imani F, Gaikwad A, Montazeri M, Rao P, Yang H, Reutzel E. Process mapping and in-process monitoring of porosity in laser powder bed fusion using layerwise optical imaging. *J. Manuf. Sci. Eng.* 2018;140(10).
- [235] Kwon O, Kim HG, Ham MJ, Kim W, Kim G-H, Cho J-H, Kim NI, Kim K. A deep neural network for classification of melt-pool images in metal additive manufacturing. *J. Intell. Manuf.* 2020;31(2):375–86.
- [236] Hertlein N, Deshpande S, Venugopal V, Kumar M, Anand S. Prediction of selective laser melting part quality using hybrid bayesian network. *Addit Manuf* 2020;32:101089.
- [237] Liu R, Liu S, Zhang X. A physics-informed machine learning model for porosity analysis in laser powder bed fusion additive manufacturing. *The International Journal of Advanced Manufacturing Technology* 2021;113(7):1943–58.
- [238] DebRoy T, Wei H, Zuback J, Mukherjee T, Elmer J, Milewski J, Beese AM, Wilson-Heid Ad, De A, Zhang W. Additive manufacturing of metallic components-process, structure and properties. *Prog. Mater Sci.* 2018;92:112–224.
- [239] Wei H, Mukherjee T, Zhang W, Zuback J, Knapp G, De A, DebRoy T. Mechanistic models for additive manufacturing of metallic components. *Prog. Mater Sci.* 2021;116:100703.
- [240] Du Y, Mukherjee T, DebRoy T. Physics-informed machine learning and mechanistic modeling of additive manufacturing to reduce defects. *Applied Materials Today* 2021;24:101123.

- [241] Ness KL, Paul A, Sun L, Zhang Z. Towards a generic physics-based machine learning model for geometry invariant thermal history prediction in additive manufacturing. *J. Mater. Process. Technol.* 2022;302:117472.
- [242] Liu S, Stebner AP, Kappes BB, Zhang X. Machine learning for knowledge transfer across multiple metals additive manufacturing printers. *Addit Manuf* 2021;39:101877.
- [243] Gunasegaram D, Murphy A, Barnard A, DebRoy T, Matthews M, Ladani L, Gu D. Towards developing multiscale-multiphysics models and their surrogates for digital twins of metal additive manufacturing. *Addit Manuf* 2021;46:102089.
- [244] Mani M, Lane BM, Donmez MA, Feng SC, Moylan SP. A review on measurement science needs for real-time control of additive manufacturing metal powder bed fusion processes. *Int. J. Prod. Res.* 2017;55(5):1400–18.
- [245] Yavari R, Riensche A, Tekerek E, Jacquemetton L, Halliday H, Vandever M, Tenequer A, Perumal V, Kontos A, Smoqi Z, et al. Digitally twinned additive manufacturing: Detecting flaws in laser powder bed fusion by combining thermal simulations with in-situ meltpool sensor data. *Materials & Design* 2021;211:110167.
- [246] Chen L, Yao X, Xu P, Moon SK, Bi G. Rapid surface defect identification for additive manufacturing with in-situ point cloud processing and machine learning. *Virtual and Physical Prototyping* 2021;16(1):50–67.
- [247] Ren W, Wen G, Zhang Z, Mazumder J. Quality monitoring in additive manufacturing using emission spectroscopy and unsupervised deep learning. *Mater. Manuf. Processes* 2021;1–8.
- [248] Ye D, Hong GS, Zhang Y, Zhu K, Fuh JYH. Defect detection in selective laser melting technology by acoustic signals with deep belief networks. *The International Journal of Advanced Manufacturing Technology* 2018;96(5):2791–801.
- [249] Ye D, Fuh JYH, Zhang Y, Hong GS, Zhu K. In situ monitoring of selective laser melting using plume and spatter signatures by deep belief networks. *ISA transactions* 2018;81:96–104.
- [250] Okaro IA, Jayasinghe S, Sutcliffe C, Black K, Paoletti P, Green PL. Automatic fault detection for laser powder-bed fusion using semi-supervised machine learning. *Addit Manuf* 2019;27:42–53.
- [251] Yuan B, Giera B, Guss G, Matthews I, McMains S. Semi-supervised convolutional neural networks for in-situ video monitoring of selective laser melting. 2019 IEEE winter conference on applications of computer vision (WACV). IEEE; 2019. p. 744–53.
- [252] Tran HC, Lo YL. Systematic approach for determining optimal processing parameters to produce parts with high density in selective laser melting process. *Int. J. Adv. Manuf. Technol.* 2019;105:4443–60. <https://doi.org/10.1007/s00170-019-04517-0>.
- [253] Schmid S, Krabusch J, Schromm T, Jieqing S, Ziegelmeier S, Grosse CU, Schleifenbaum JH. A new approach for automated measuring of the melt pool geometry in laser-powder bed fusion. *Prog Addit Manuf* 2021;6:269–79. <https://doi.org/10.1007/s40964-021-00173-7>.
- [254] Chen Y, Wang H, Wu Y, Wang H. Predicting the printability in selective laser melting with a supervised machine learning method. *Materials* 2020;13(22):5063.
- [255] Meng L, Zhang J. Process design of laser powder bed fusion of stainless steel using a gaussian process-based machine learning model. *JOM* 2020;72(1):420–8.
- [256] A. Singh, D. Cooper, N. Blundell, G. Gibbons, D. Pratihar, Modelling of direct metal laser sintering of eos dm20 bronze using neural networks and genetic algorithms, in: Proceedings of the 37th international MATADOR conference, Springer Science & Business Media, 2012, pp. 395–398.
- [257] Tapia G, Khairallah S, Matthews M, King WE, Elwany A. Gaussian process-based surrogate modeling framework for process planning in laser powder-bed fusion additive manufacturing of 316l stainless steel. *The International Journal of Advanced Manufacturing Technology* 2018;94(9):3591–603.
- [258] Caiazzo F, Caggiano A. Laser direct metal deposition of 2024 al alloy: trace geometry prediction via machine learning. *Materials* 2018;11:444.
- [259] Lu Z, Li D, Lu B, Zhang A, Zhu G, Pi G. The prediction of the building precision in the laser engineered net shaping process using advanced networks. *Opt. Lasers Eng.* 2010;48(5):519–25.
- [260] Jafari-Marandi R, Khanzadeh M, Tian W, Smith B, Bian L. From in-situ monitoring toward high-throughput process control: cost-driven decision-making framework for laser-based additive manufacturing. *Journal of Manufacturing Systems* 2019;51:29–41.
- [261] B. Kappes, S. Moorthy, D. Drake, H. Geerlings, A. Stebner, Machine learning to optimize additive manufacturing parameters for laser powder bed fusion of inconel 718, in: Proceedings of the 9th international symposium on superalloy 718 & derivatives: Energy, aerospace, and industrial applications, Springer, 2018, pp. 595–610.
- [262] Malekipour E, El-Mounayri H. Defects, process parameters and signatures for online monitoring and control in powder-based additive manufacturing. In: *Mechanics of Additive and Advanced Manufacturing*, Volume 9. Springer; 2018. p. 83–90.
- [263] Gaja H, Liou F. Defects monitoring of laser metal deposition using acoustic emission sensor. *The International Journal of Advanced Manufacturing Technology* 2017;90(1):561–74.
- [264] Gutkin R, Green C, Vangrattanachai S, Pinho S, Robinson P, Curtis P. On acoustic emission for failure investigation in cfrp: Pattern recognition and peak frequency analyses. *Mechanical systems and signal processing* 2011;25(4):1393–407.
- [265] Taheri H, Koester LW, Bigelow TA, Fairson EL, Bond LJ. In situ additive manufacturing process monitoring with an acoustic technique: clustering performance evaluation using k-means algorithm. *J. Manuf. Sci. Eng.* 2019;141(4).
- [266] Tapia G, Elwany A. A review on process monitoring and control in metal-based additive manufacturing. *J. Manuf. Sci. Eng.* 2014;136(6).
- [267] Zhang Y, Fuh JY, Ye D, Hong GS. In-situ monitoring of laser-based pbf via off-axis vision and image processing approaches. *Addit Manuf* 2019;25:263–74.
- [268] Guo X, Liu X, Zhu E, Yin J. Deep clustering with convolutional autoencoders. In: *International conference on neural information processing*. Springer; 2017. p. 373–82.
- [269] Hinton GE, Salakhutdinov RR. Reducing the dimensionality of data with neural networks, *science* 2006;313(5786):504–7.
- [270] Silbernagel C, Aremu A, Ashcroft I. Using machine learning to aid in the parameter optimisation process for metal-based additive manufacturing. *Rapid Prototyping Journal* 2020.
- [271] Tibshirani R, Walther G, Hastie T. Estimating the number of clusters in a data set via the gap statistic. *Journal of the Royal Statistical Society: Series B (Statistical Methodology)* 2001;63(2):411–23.
- [272] Snell R, Tammas-Williams S, Chechik L, Lyle A, Hernández-Nava E, Boig C, Panoutsos G, Todd I. Methods for rapid pore classification in metal additive manufacturing. *Jom* 2020;72(1):101–9.
- [273] Grasso M, Laguzza V, Semeraro Q, Colosimo BM. In-process monitoring of selective laser melting: spatial detection of defects via image data analysis. *J. Manuf. Sci. Eng.* 2017;139(5).
- [274] García-Moreno A-I. Automatic quantification of porosity using an intelligent classifier. *The International Journal of Advanced Manufacturing Technology* 2019;105(5):1883–99.
- [275] Khanzadeh M, Chowdhury S, Bian L, Tschopp MA. A methodology for predicting porosity from thermal imaging of melt pools in additive manufacturing thin wall sections. In: *International Manufacturing Science and Engineering Conference*, Vol. 50732. American Society of Mechanical Engineers; 2017. V002T01A044.
- [276] Khanzadeh M, Bian L, Shamsaei N, Thompson SM. Porosity detection of laser based additive manufacturing using melt pool morphology clustering. In: in: 2016 International Solid Freeform Fabrication Symposium. University of Texas at Austin; 2016.
- [277] Beuth J, Fox J, Gockel J, Montgomery C, Yang R, Qiao H, Soylemez E, Reesewatt P, Anvari A, Narra S, et al. Process mapping for qualification across multiple direct metal additive manufacturing processes. In: in: 2013 International Solid Freeform Fabrication Symposium. University of Texas at Austin; 2013.
- [278] DeCost BL, Jain H, Rollett AD, Holm EA. Computer vision and machine learning for autonomous characterization of am powder feedstocks. *Jom* 2017;69(3):456–65.
- [279] Scime L, Beuth J. Anomaly detection and classification in a laser powder bed additive manufacturing process using a trained computer vision algorithm. *Addit Manuf* 2018;19:114–26.
- [280] DeCost BL, Holm EA. Characterizing powder materials using keypoint-based computer vision methods. *Comput. Mater. Sci.* 2017;126:438–45.
- [281] D.G. Lowe, Object recognition from local scale-invariant features, in: *Proceedings of the seventh IEEE international conference on computer vision*, Vol. 2, Ieee, 1999, pp. 1150–1157.

- [282] Bisht M, Ray N, Verbist F, Coeck S. Correlation of selective laser melting-melt pool events with the tensile properties of ti-6al-4v eli processed by laser powder bed fusion. *Addit Manuf* 2018;22:302–6.
- [283] Coeck S, Bisht M, Plas J, Verbist F. Prediction of lack of fusion porosity in selective laser melting based on melt pool monitoring data. *Addit Manuf* 2019;25: 347–56.
- [284] J. Voigt, T. Bock, U. Hilpert, R. Hellmann, M. Moeckel, Increased relative density and characteristic melt pool. signals at the edge in pbf-lb/m, *Additive Manufacturing* (2022) 102798.
- [285] Donegan SP, Schwalbach EJ, Goeber MA. Zoning additive manufacturing process histories using unsupervised machine learning. *Mater. Charact.* 2020;161. <https://doi.org/10.1016/j.matchar.2020.110123>.
- [286] Y. Tan, B. Jin, A. Nettekoven, Y. Chen, Y. Yue, U. Topcu, A. Sangiovanni-Vincentelli, An encoder-decoder based approach for anomaly detection with application in additive manufacturing, *Proceedings - 18th IEEE International Conference on Machine Learning and Applications, ICMLA 2019* (2019) 1008–1015. doi:10.1109/ICMLA.2019.000171.
- [287] Pagan DC, Phan TQ, Weaver JS, Benson AR, Beaudoin AJ. Unsupervised learning of dislocation motion. *Acta Mater.* 2019;181:510–8.
- [288] Singh A, Nowak R, Zhu J. Unlabeled data: Now it helps, now it doesn't. *Adv Neural Inform Process Syst* 2008;21.
- [289] Yadav P, Singh VK, Joffre T, Rigo O, Arvieu C, Le Guen E, Lacoste E. Inline drift detection using monitoring systems and machine learning in selective laser melting. *Adv. Eng. Mater.* 2020;22(12):2000660.
- [290] Larsen S, Hooper PA. Deep semi-supervised learning of dynamics for anomaly detection in laser powder bed fusion. *J Intell Manuf* 2022;33(2):457–71.
- [291] Li X, Jia X, Yang Q, Lee J. Quality analysis in metal additive manufacturing with deep learning. *J Intell Manuf* 2020;31(8):2003–17.
- [292] Mozaffar M, Ebrahimi A, Cao J. Toolpath design for additive manufacturing using deep reinforcement learning, arXiv preprint arXiv:2009.14365; 2020.
- [293] Wasmer K, Le-Quang T, Meylan B, Shevchik SA. In situ quality monitoring in am using acoustic emission: A reinforcement learning approach. *J. Mater. Eng. Perform.* 2019;28(2):666–72.
- [294] Weiss K, Khoshgoftaar TM, Wang D. A survey of transfer learning. *J Big data* 2016;3(1):1–40.
- [295] Teng C, Gong H, Szabo A, Dilip J, Ashby K, Zhang S, Patil N, Pal D, Stucker B. Simulating melt pool shape and lack of fusion porosity for selective laser melting of cobalt chromium components. *J Manuf Sci Eng* 2017;139(1).
- [296] Karniadakis GE, Kevrekidis IG, Lu L, Perdikaris P, Wang S, Yang L. Physics-informed machine learning. *Nat Rev Phys* 2021;3(6):422–40.